SEISMIC RESERVOIR CHARACTERIZATION AND 3D MODELLING OF OY FIELD, OFFSHORE NIGER DELTA

BY

ADEBOYE OLUWATOFUNMI JEREMIAH

18010401001

A THESIS SUBMITTED TO THE DEPARTMENT OF GEOSCIENCES, COLLEGE OF BASIC AND APPLIED SCIENCES, MOUNTAIN TOP UNIVERSITY, PRAYER CITY, OGUN STATE, NIGERIA

IN PARTIAL FULFILMENT OF THE REQUIREMENTS FOR THE AWARD OF A BACHELOR OF SCIENCE (B. Sc.) DEGREE IN APPLIED GEOPHYSICS

AUGUST, 2022

DECLARATION

I hereby declare that this project has been written by me and is a record of my own research work. It has not been presented in any previous application for a higher degree of this or any other University. All citations and sources of information are clearly acknowledged by means of reference.

_____

ADEBOYE, Oluwatofunmi Jeremiah

CERTIFICATION

I hereby certify that this research titled **"Seismic Reservoir Characterization and 3D Modelling of OY Field, Offshore Niger Delta"** was completed and submitted by ADEBOYE, Oluwatofunmi Jeremiah with matriculation number 18010401001, in partial fulfilment of the requirements for the award of BACHELOR OF SCIENCE (B.Sc.) DEGREE IN APPLIED GEOPHYSICS. The original research work was carried out by him under my supervision and is hereby accepted.

Dr. A.E. JONATHAN _____

Supervisor I *(Signature and date)*

Mr. R.P AKINWALE _____

Supervisor II *(Signature and date)*

DR. O. B BALOGUN _____

Head of Department *(Signature and date)*

DEDICATION

This project is dedicated to the glory of Almighty God, THE FATHER, THE SON and THE HOLY SPIRIT, who has made this program a success. Also, a special thanks to my wonderful and supportive parents, Mr. and Mrs. Olugbenga Adeboye, as well as my siblings, Tomi, Tobi and Tolu.

ACKNOWLEDGEMENT

Except the Lord builds the house, they labour in vain that build it..." Indeed without the involvement of the Almighty God - Omnipotent, Omniscient, Omnipresent, this work would not have been a success. Great is thy faithfulness O Lord!

Also, I appreciate the Chancellor, Dr. D. K. Olukoya for his financial and spiritual support during my period of study. I also express my profound gratitude to the Vice Chancellor, Professor E. A. Ayolabi for is unwavering support and guidance throughout my four years programme. I sincerely appreciate the efforts of my supervisors, Dr. A.E Jonathan and Mr. R P. Akinwale for their support and contributions towards the success of this project research. Their endurance, patience and constructive criticism and correction saw me through the various phases of this project work. I also appreciate Professor A. I. Olayinka. I appreciate the advice and professional support provided by the Head of Department, Dr. O. B. Balogun throughout the course of this research. Also, I appreciate the other members of staff of Department of Geosciences, Mr Alao, Dr. M. O. Okunubi and Mr Dayo.

I appreciate my Dad, Pastor Olugbenga Adeboye, and Mum, Mrs. Adeola Adeboye, and my dear siblings, Tomi, Tobi and Tolu, for all their unquantifiable love and financial support throughout my period of study at Mountain Top University.

My gratitude goes to Dr. A. O. Young who has significantly contributed to my success in Mountain Top University. He has indeed been a source of encouragement and has also been very supportive.

Also, I won't fail to acknowledge the American Association of Petroleum Geologist (AAPG) Foundation who supported the funding of this research work through the L. Austin Weeks Undergraduate Grant Program.

I would also like to thank all my friends who made substantial impact in my life throughout the course of this programme. I Love you all.

I would not forget to remember all the students in the Department of Geosciences, for making my stay a worthwhile, I say Thank you and God bless you all.

TABLE OF CONTENTS

LIST OF TABLES

LIST OF FIGURES

ABBREVIATIONS

3D: Three Dimension.

RMS: Root Mean Square.

GOR: Gas Oil Ratio.

VSP: Vertical Seismic Profiling

LWD: Logging While Drilling.

MWD: Measurements While Drilling.

TWT: Two Way Time.

GR: Gamma Ray.

TD: Total depth.

TDR: Time Depth Relationship.

NTG: Net to Gross.

SGS: Sequential Gaussian Simulation.

GIIP: Gas Initially In Place.

OOIP: Original Oil Initially In Place.

STOIIP: Stock Tank Oil Initially In Place.

STB: Stock Tank Barrel.

SCF: Standard Cubic Foot.

FDP: Field Development Plan.

GWC: Gas Water Contact.

OWC: Oil Water Contact.

ABSTRACT

As exploration and production move further offshore, a better understanding of the Niger Delta reservoir system is necessary. In order to quantify reserves, eliminate uncertainty, and find the best strategy for optimum recovery of hydrocarbon, it is critical to model the reservoir as accurately as possible.

3D reservoir modelling and characterization was carried out on the OY Field, which is a shallow offshore hydrocarbon field situated in the north-western Niger Delta region of Nigeria. The dataset used for this study were 3D migrated seismic data, composite well logs and check shot. The Petrel E&P software was used for reservoir correlation, petrophysical analysis, 3D seismic interpretation and reservoir modelling.

The methods adopted involved the well log analysis, generation of synthetic seismograms, surface attribute analysis and the 3D static modelling. In the well log analysis, five hydrocarbon bearing reservoir (Sand A, B, C, D and E) were delineated. The five horizons were mapped on the 3D seismic data and the time and depth maps generated, showed fault dependent closure, four assisted closure and four-way closure. Attributes analysis were carried out to enhance data interpretation and high anomalies were observed around the closure drilled on the field. The 3D petrophysical models of the reservoir have shown the prominence of good porosity distribution with porosity varying from 0.3 - 0.4, the net to gross model reveals good net to gross within the well area varying from 0.5 - 1.0 and the 3D water saturation model shows the hydrocarbon zone region with water saturation value varying from 0.1 - 0.5.

The 3D petrophysical model have enhanced a better understanding of the distribution of the petrophysical properties and can guide an optimal field development plan (FDP), well planning and production of hydrocarbon on the field.

Keyword: 3D Reservoir Modelling, Offshore, Niger Delta.

CHAPTER ONE

INTRODUCTION

1.1 Introduction

Niger Delta is a prolific petroleum habitat with reserves estimate of 34 billion barrels of oil and 93 trillion cubic feet of gas. The estimated production at present is 2 million barrels (320,000 m^3) per day (Wikipedia, 2022). To increase production rate, new fields must be discovered and more hydrocarbon recovered from currently producing fields. Early water breakthrough, high Gas to Oil Ratio (GOR) and sand production are some of the challenges encountered in Niger Delta Fields.

Besides solving production problems, an improved understanding of petroleum reservoirs is necessary in Field Development Planning (FDP). FDP requires constructing a reservoir model from static to flow simulation. Necessary input from the reservoir studies to the FDP are estimates of the hydrocarbon-initially-in-place (HIIP), producible volumes of hydrocarbon (reserves), production file and reservoir behaviour.

Globally, exploration and production are shifting from the traditional and conventional to the unconventional. Unconventional reservoirs – high temperature and pressure, ultra-deep offshore environment, high waxy oil, low API gravity oil, high sulphur content, etc. demand an advanced knowledge of the workings of petroleum reservoirs.

In Nigeria, oil is a major primary source of revenue in Nigeria for the country's development, and as such greater efforts are demanded from both the Government and the research institutions to ensure that this non-renewable resource is adequately tapped. Reservoir characterization has long been identified as the main process employed in the detailed description of any reservoir to properly study and analyse the reserve as well as to optimally place the wells for optimal production of the reservoir. The goal of any reservoir characterization or reservoir modelling is to easily understand the reservoir connectivity in static and dynamic conditions by integrating data from different sources, therefore, it is important to accurately incorporate the uncertainty associated with not knowing a reservoir's uniqueness while developing a geologic representation of what it is most likely to be. (Odai et al., 2010). It has been difficult to effectively characterize the Niger Delta's stratigraphic architecture and subsurface reservoir by conventional stand-alone data set (Okpogo et al., 2018). Reservoir characterization is essential for a second petroleum

management purpose of improving the estimation of reserves and making decisions regarding the development of the field. Characterizing the reservoir is a process that describes various properties in reservoirs using all the available data in order to accurately predict a reservoir's performance (Shofiqul et al., 2013). To eliminate ambiguity and uncertainty in the description of reservoir systems and their economic feasibility, it is required to integrate well log data as analogous and depositional constraints that are capable of capturing anisotropy and non-homogeneity.

1.2 Statement of the Problem

As exploration and production move further offshore, a better understanding of the Niger Delta reservoir system is necessary. It is essential to model the reservoir as accurately as possible to reduce uncertainty, calculate reserves and determine the most effective way for optimum recovery. Therefore, this research has integrated all available data (3D migrated Seismic, well logs and Time-Depth-Relationship information) to develop property models of the mapped reservoirs for a better understanding of the field.

1.3 Aim and Objectives of the Study

1.3.1 Aim

The aim of this research is to characterize hydrocarbon reservoir and generate a 3D reservoir property model of the OY field to understand the 3D architecture and reservoir property distribution of the field to be used for optimal field development and enhanced oil recovery of the field.

1.3.2 Objectives

The following are the specific objectives of the research

i. Correlation of well logs.
ii. Determination of hydrocarbon fluid type in the reservoir and petrophysical evaluation.
iii. 3D seismic interpretation; faults and horizons mapping to understand the structural framework and trapping mechanisms in the field.
iv. Estimate the hydrocarbon volumes in the identified reservoir zones.
v. 3D petrophysical property modelling of the reservoirs.

1.4 Significance of Study

The result of this study will enhance our understanding of the hydrocarbon producibility of the reservoir of the study area.

1.5 Description of the Study Area

The study area is the “OY” field which is located in the north-western Niger Delta region of Nigeria. It is a shallow offshore field which is located 13 km offshore Sapele. The new name is given to the field and the well which is strictly restricted for this research work as shown in Figure 1.1.

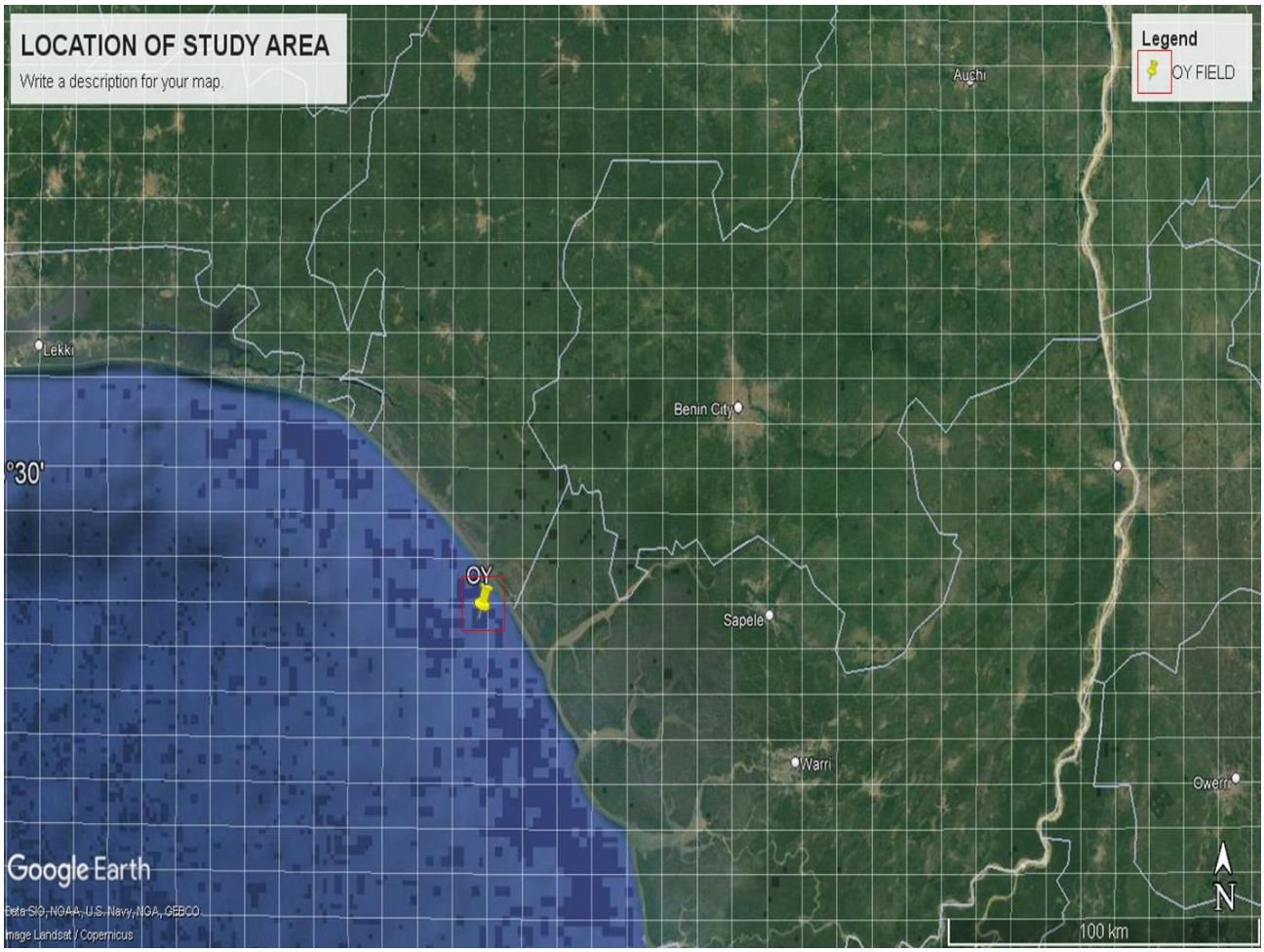

Figure 1.1: Google Earth Map of Niger-Delta indicating where the study area OY field is located.

CHAPTER TWO

LITERATURE REVIEW

2.1 Review of Related Previous Works

In the past, several authors have carried out studies on seismic reservoir characterization. Several studies include;

Edigbue et al. (2014) carried out reservoir characterization of "Keke" Field, Niger Delta by integrating 3D migrated seismic and petrophysical data to evaluate the hydrocarbon reservoir potentials in this field. Seismic structural attribute (variance) was used to delineate six major faults in the field. Time and Depth maps were produced for the top and base of the horizons from which isopach map were generated. The acquired seismic and petrophysical data were used to compute the amount of hydrocarbon in-place, which revealed the reservoirs' potential. S1 and S2 are the defined sand units characterized by hydrocarbon saturation of 65% and 81.8% respectively. Isopach map shows thicker sediments in the central and southern parts of the field ranging from 70ft to 90ft, isochron and is depth revealed structural high (anticlines) at the field's central block, which is wedged between the growth faults and has possibly accumulated hydrocarbon. The results indicate the "Keke" field's mechanism and the determined Petrophysical parameters which are significantly to the build-up of hydrocarbons. The estimated reserves are adequate for subsequent exploratory work.

Osinowo et al. (2018) characterised and described the Eni Field offshore Niger Delta reservoir in southern Nigeria. The Eni field, which has been experiencing production decline with an increase in water output, has been studied using a combination of stratigraphic analyses, integration of structural and horizon mapping of 3D migrated seismic volume, reservoir property modelling and petrophysical analyses of sixty (60) wireline logs, and production data. The built reservoir structural framework and spatial distribution of the reservoir properties have proven helpful in determining the optimal placement of proposed wells in providing the necessary information of the best production plan that would guarantee effective oil drainage from the defined reservoir compartments.

Hossain et al. (2021) evaluated the Srikail gas field to characterize reservoirs and discovering of new prospects by integrating 2D seismic data and wireline logs. The research focuses on

identifying gas zones, estimating reserves, and discovering of new prospects in the Bengal Basin's eastern fold belt's Srikail gas field. The reservoir characterization of the Srikail gas field reveals the presence of seven hydrocarbon-bearing zones (A, B, C, D, E, F, and G) identified from well log data within the measured depth range 2429.5 – 3501 m. Ranges of the reservoir's properties are as follows: effective porosity 12.3 and 24.9%, hydrocarbon saturation 53.1 and 75.1%, water saturation 24.9 and 46.9%, shale volume varies between 8 and 38%, and the net-to-gross ratio of 10 and 56% which shows a good level of hydrocarbon in the zones. Seismic sequence analysis points out that all the gas zones occur between SB-2 and SB-3. Carrying out the combined analyses provides important reservoir parameters and potential sequences which are critical for identifying new prospects as well as fully understanding the potential reservoir zones.

Abdullah et al. (2022) applied 3D static modelling in reservoir characterization of the Qishn Formation reservoir at the Sharyoof oil field in the Masila Basin. The seismic structural interpretation was employed to start the investigation, which was then followed by the construction of a 3D structural framework and the analysis of well log data. The Qishn Fm. is made up of 43.83% limestone, 21.53% shale, 21.26% sandstone, 13.21% siltstone, and 0.17% dolomite, per the facies models. In contrast to the Upper Qishn Clastics S1A and C, which have high reservoir quality, and S1B, which have fair reservoir quality, the Qishn Carbonates Member has low porosity values, making it a possible seal for the underlying reservoirs. While the Lower Qishn Clastics zone has high reservoir quality, the Upper Qishn Clastics S2 and S3 also have fair reservoir quality. The water saturation increases in the north and south and drops in the west and east. The S1A, S1C, and S2 zones of the Upper Qishn clastics contain 106 million STB of original oil still in situ (OOIP).

Adagunodo et al. (2022) carried carried out a depositional analysis and reservoir characterization of the shallow offshore JP Field in Nigeria's Niger Delta Basin. For this study, well log analyses were done. This was done to evaluate the JP Field's deposition environment and describe the reservoirs using estimated petrophysical characteristics. In the JP Field, seven reservoirs were identified and correlated among the four drilled wells. Across the four drilled wells in JP Field, seven reservoirs were identified and correlated. Estimates were made for petrophysical properties such as porosity, shale volume, water saturation, and hydrocarbon saturation. Additionally, based

on the gamma-ray responses, the depositional environments of each reservoir in the JP Field were identified. It is discovered that JP Field has significant oil hydrocarbon saturation and porosity ranges from good to very good. JP Field is located in the marginal marine depositional habitat, according to the research.

2.2 Geology of the study area.

The Niger Delta is located in the Gulf of Guinea of West Africa as illustrated in figure 2.1 and contains the Tertiary Niger Delta Petroleum System. The Niger Delta covers approximately around 75,000 km^2 and extends more than 300 km from apex to mouth. The Niger Delta province is located in the south of Nigeria; it is bordered to the North by the Benin flank and to the south by the Atlantic Ocean. It extends from longitudes 3°E-9°E and latitudes 4°30′N - 5°20′N.

2.2.1 Stratigraphy of the Niger Delta

The stratigraphic sequence (see figure 2.2) of the Niger Delta comprises three broad lithostratigraphic units namely;

1. The Continental Sands (Benin Formation).
2. The Paralic Clastics (Agbada Formation).
3. The Marine Shale (Akata Formation).

Benin Formation

According to Short and Stable (1967), this unit is made up primarily of continental fluvial sands, which are typical of southern Nigeria and cover a large region around Benin City. The estimated thickness of these sands is 3050 m. The Continental Sands, which constitute the upper layer of the Niger Delta depositional series and are the shallowest portion of the sequence, are characterized by a high sand content (70–100%). The massive sands were deposited in a continental setting that included the upper delta plains braided and meandering river channels. Also involved are the lagoonal, deltaic, estuarine, and fluviolacustrine sub-environments. Although some marine shale breaks have been identified within the formation, the bulk of the belt facies (Allen, 1965a; Dessauvagie, 1972). The formation is hydrocarbon bearing in some of the Mobil fields, contrary to the situation elsewhere where it is solely water bearing.

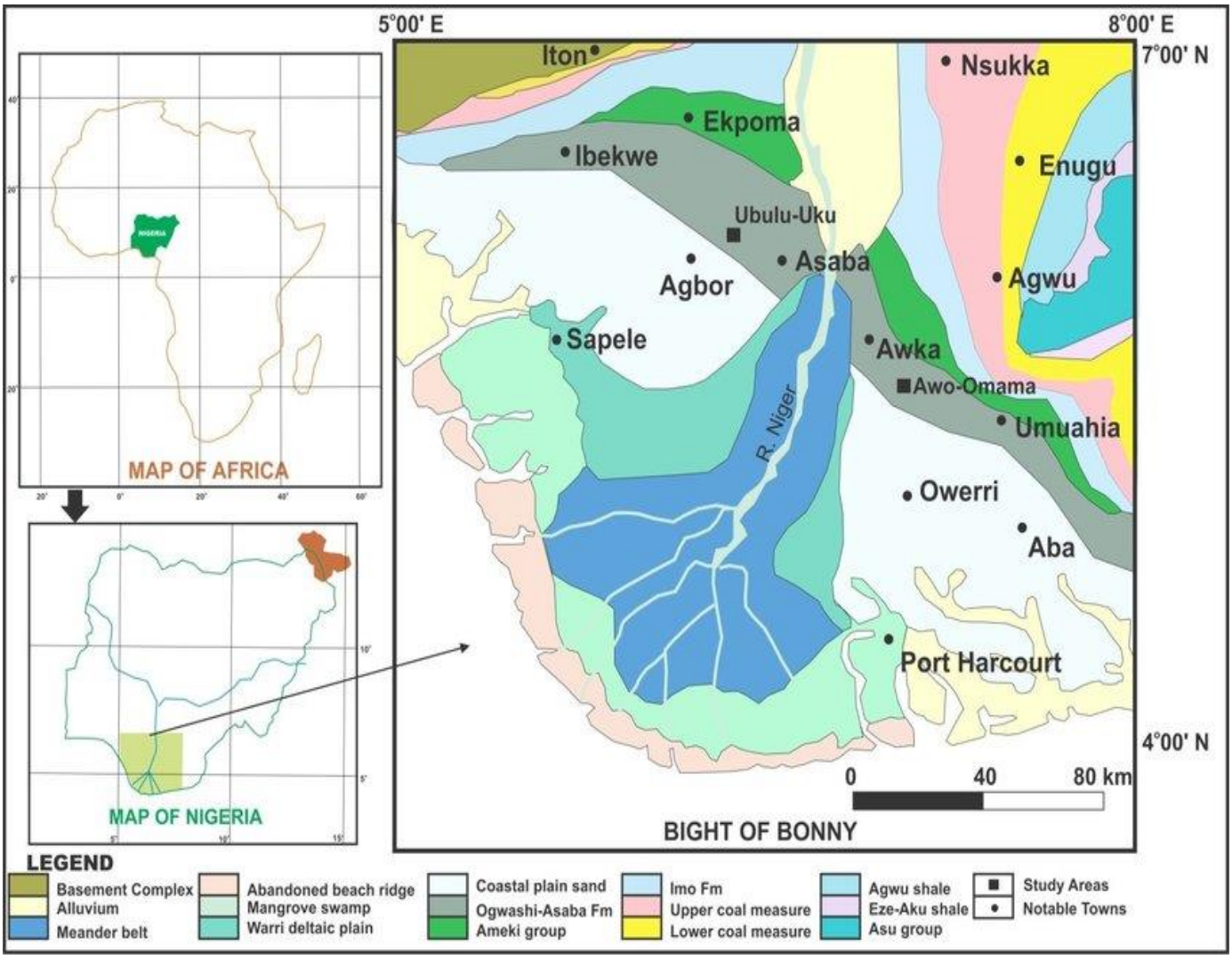

Figure 2. 1: Geologic Map of Niger Delta (after Nwajide 2013).

In several parts of the subsurface Niger Delta, within the Agbada and Benin /Formations, deep and relatively extensive erosional canyons are found filled with clays and subordinate sands. They are found in the eastern and western re-entrants of the delta but are more common on the eastern side. Their location has been attributed to ocean current action at the re-entrants of the Nigerian coastline. The canyons are said to represent erosional processes during relative sea level falls, followed by canyon filling during the subsequent relative sea level rises. At those low stands of the sea, the Niger Delta built pronouncedly seaward and became a shelf edge delta with sediment debouching as turbidity flows that nourished deep sea fans.

Agbada Formation

The Agbada Formation (Figure 2.2) forms the hydrocarbon-prospective sequence in the Niger delta basin. It is composed of alternating layers of sands, slits, and shales in varying quantities and thicknesses that indicate sediments from the transitional habitat that includes the lower delta plain (mangrove, swamp, floodplain, and marsh), as well as the coastal barrier and fluviomarine regions. The formation, which dates from the Eocene to the present, is very diachronous. The current delta's mangrove swamp to coastal barriers and fluviomarine zones make up the surface exposure of recent age. The Agbada Formation contains between 30 and 70% sand, which is the consequence of several depositional off-lap cycles. Most exploration wells in the Niger delta have bottomed in these lithofacies, which reach a maximum thickness of more than 3000 m.

Akata Formation

The Akata Formation (Figure 2.2) is the base of the sequence in each depobelts and ranges from Paleocene to Holocene in age and consists of mainly marine mud facies with turbidite sands and continental slope channel fills. The environments where the sediments were deposited were prodelta. Here, sand makes up typically less than 30% of the total. Although the exact thickness of this sequence is unknown, it may exceed 7000 m at the delta's centre. The Imo Shale, which is part of the Akata formation, is found onshore in the northern part of the delta and offshore in diapirs along the continental slope. Typically, the marine shale is under pressure.

2.2.2 Tectonics

Cretaceous fracture zones represented as trenches and ridges in the deep Atlantic are in control of the tectonic framework of the continental margin along the West Coast of equatorial Africa. The Cretaceous Benue-Abakaliki trough, which penetrates deeply into the West African shield, is divided into distinct basins by the fracture zone ridges, which also serve as the boundary faults of the trough in Nigeria. A failed rift triple junction connected to the opening of the South Atlantic is represented by the trough. Rifting began in this area in the Late Jurassic and continued until the Middle Cretaceous (Lehner and De Ruiter, 1977). Rifting completely stopped occurring in the Late Cretaceous in the Niger Delta area. Gravity tectonics took over as the main deformational activity once rifting stopped. Internal deformation was driven by shale mobility and resulted from two mechanisms (Kulke, 1995). Shale diapirs first developed as a result of greater density delta-front sands loading poorly compacted, over-pressured delta slope clays (Akata Formation) (Agbada Formation.). Second, slope instability resulted from the delta-slope clays' inability to provide lateral, basin-ward support (Akata Formation.) Gravity tectonics, which was finished before the Benin Formation was deposited, is expressed in complex structures, such as shale diapirs, roll-over anticlines, collapsed growth fault crests, back-to-back features, and steeply dipping, closely spaced flank faults, for any given deposition (Evamy et al.,1978; Xiao and Suppe, 1992). Near the top of the Akata Formation, these faults flatten into detachment planes and mostly offset various Agbada Formation layers. According to the tectonic framework mentioned above, the Niger Delta's onshore, continental shelf, and deep-water terrains share three groups of structural patterns.

2.2.3 Depobelts

Each one of the five off-lapping siliciclastic sedimentation cycles that make up the Niger Delta resulted in the deposition of one of the three formations. These cycles (depobelts) are characterized by synsedimentary faulting that took place in response to varying rates of subsidence and sediment input, and they prograde south-westward 250 kilometres over oceanic crust into the Gulf of Guinea (Stacher, 1995). (Doust and Omatsola, 1990). When additional crustal sinking of the basin could no longer be tolerated, the concentration of sediment deposition migrated seaward, establishing a new depobelt. This was the outcome of the interaction between subsidence and supply rates (Doust and Omatsola, 1990).

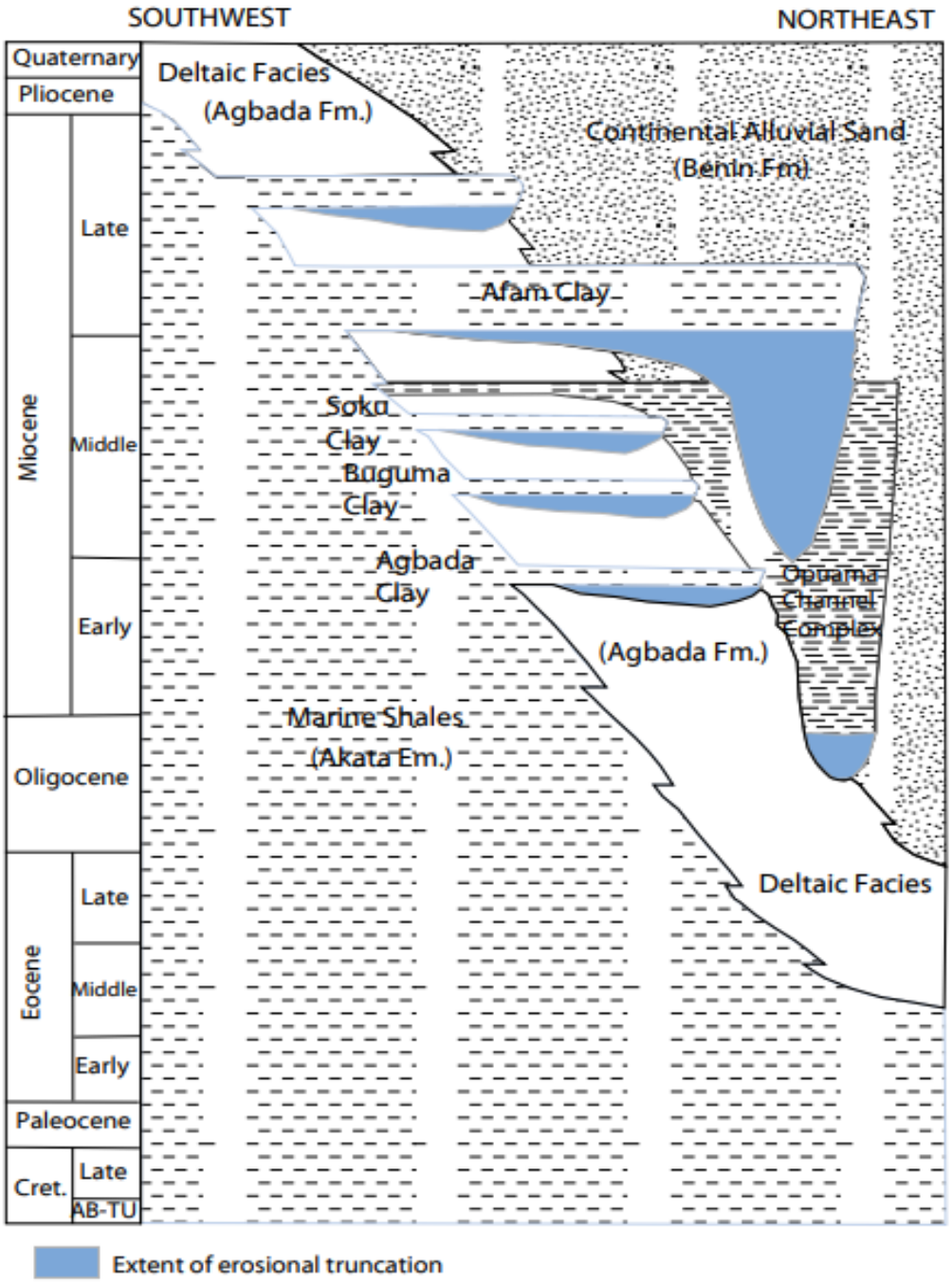

Figure 2.2: Stratigraphic column showing the three formations of the Niger Delta. Modified from Shannon and Naylor (1989) and Doust and Omatsola (1990).

Each depobelt is a distinct unit that corresponds to a discontinuity in the delta's regional dip. It is bordered on the landward side by growth faults and the seaward side by major counter-regional faults or the growth fault of the subsequent seaward belt (Evamy et al., 1978; Doust and Omatsola, 1990). There are five well-known main depobelts, each with unique sedimentation, deformation, and petroleum histories. Three depobelt provinces are described by Doust and Omatsola (1990) based on structure. The earliest growth faults, which are typically rotating, uniformly spaced, and increase in steepness toward the sea, are found in the northern delta province, which sits on top of a very shallow basement. The depobelts in the central delta province have distinct characteristics, such as rollover crests that get progressively deeper and move toward the sea for any particular growth fault. Due to internal gravity tectonics on the contemporary continental slope, the distal delta province has the most complicated structural characteristics (Figure 2.3).

2.2.4 Petroleum and its occurrence

2.2.4.1 Distribution of petroleum

However, several directional trends create an "oil-rich belt" with the largest field and lowest gas-to-oil ratio in the Agbada Formation of the Niger Delta, where petroleum is present throughout (Evamy et al., 1978; Ejedawe, 1981; Doust and Omatsola, 1990). In the area of Port Harcourt, the belt stretches along many north-south trends and from the northwest offshore area to the southeast offshore. Within the axis of greatest sedimentary thickness, it generally relates to the boundary between continental and oceanic crust. Initially, the timing of trap development in relation to petroleum migration was blamed for this hydrocarbon distribution (earlier landward structures trapped earlier migrating oil). However, Evamy et al. (1978) demonstrated that in many rollovers, movement on the structure-building fault and the subsequent growth continued and were gradually relayed southward into the younger part of the section by succeeding crestal faults, leading them to conclude that there was no relationship between growth along a fault and distribution of petroleum. According to Ejedawe (1981), the zone of the oil-rich regions inside the belt is related to five delta lobes supplied by four distinct rivers. According to him, the two decisive factors are an increase in geothermal gradient compared to the minimal gradient in the delta centre and the sediments in the band typically being older than those further out to sea. The sediments inside the belt have the maximum "maturity per unit depth" due to the interaction of these variables.

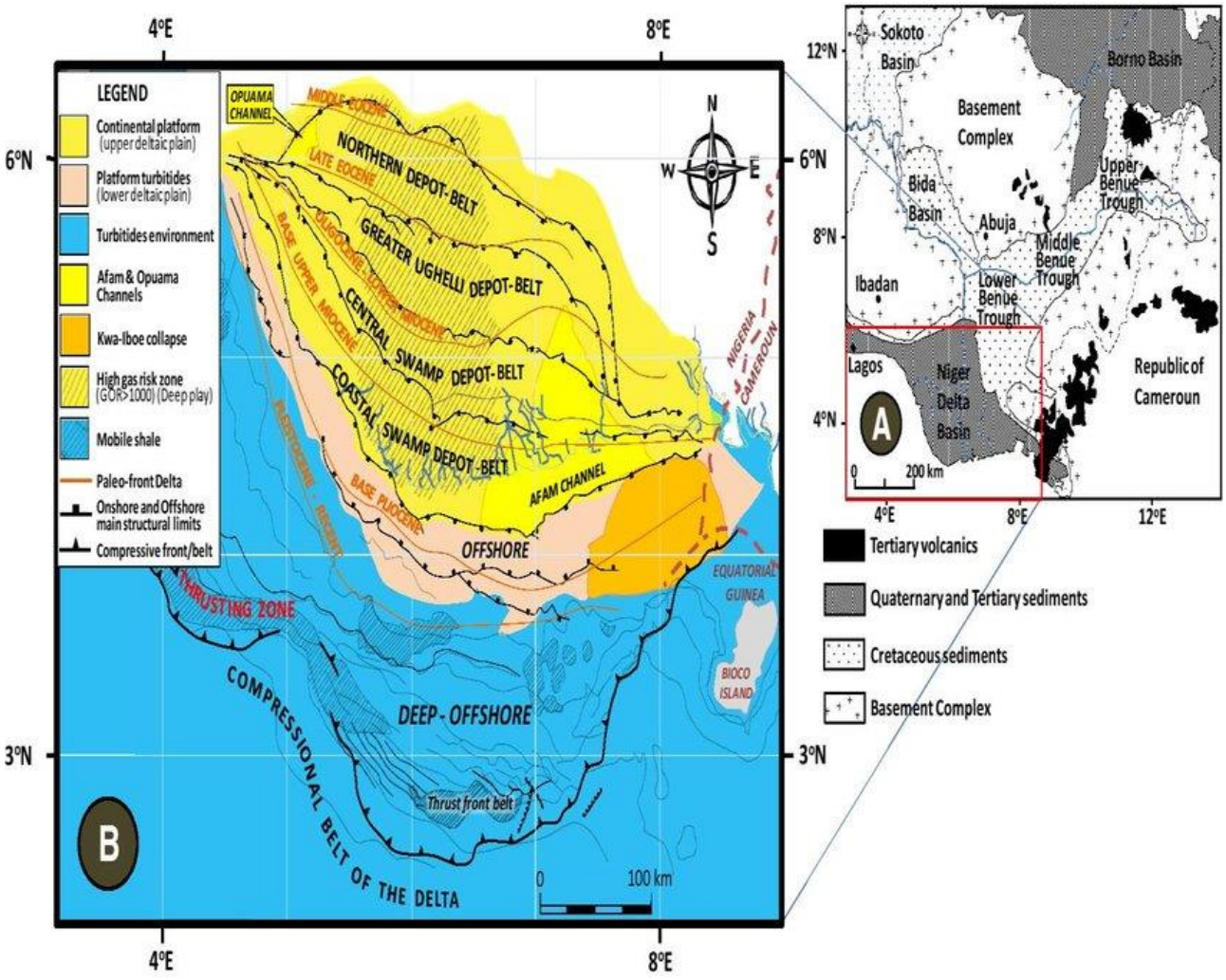

Figure 2.3: Geologic map of Nigeria showing the location of the Niger Delta Basin (a) (after Ebong et al. 2017) and sectional map of the Niger Delta depobelts and structural limits (b) (from Ebong et al. 2017).

According to Weber (1987), the oil-rich belt ("golden lane") is located across depobelts with a concentration of rollover structures but with short southern flanks and a limited paralic sequence to the south. Doust and Omatsola (1990) suggest that the distribution of petroleum is likely related to heterogeneity of source rock type (greater contribution from paralic sequences in the west) and/or segregation due to remigration. Haack and co-researchers (1997) link the location of the oil-rich belt to marine source rocks that were oil-prone when they were deposited around the delta lobes, and they hypothesise that the formation of these source rocks was regulated by pre-tertiary structural sub-basins connected to basement structures. The middle, eastern, and northernmost portions of the delta are considered to be the "oil-rich belt," while the gas-oil ratios (GOR) are high elsewhere. The GOR rises seaward and along strikes away from the depositional centers within each depobelt. GOR distribution may be due to remigration driven on by tilting during the later period of deposition inside the down-dip section of the depobelt, up-dip flushing of accumulations by gas produced at greater maturity, and/or heterogeneity of source rock type (Doust and Omatsola, 1990). Stacher (1995) developed a hydrocarbon habitat model for the Niger Delta using sequence stratigraphy (Figure 2.4). The Akata Formation (the presumed source rock) and the sand/shale units of the Agbada Formation (the reservoirs and seals) were deposited in the centre region of the delta, including portions of the oil-rich zone, and their deposition is related to sea level. Miocene Agbada sequence system tracts are found on top of Pre-Miocene Akata shale, which was laid down in deep water during lowstands. Third order lowstand system tracts were not developed, and the Agbada Formation in the delta's middle region best matches a shallow ramp model with highstand (hydrocarbon-bearing sands) and transgressive (sealing shale) system tracts. The Agbada Formation's faulting developed structural and stratigraphic traps that acted as channels for petroleum migration and deposited petroleum. Shale in the transgression 16 system tract improved clay smearing inside faults and served as a great seal above the sands (Figure 2.4). The order Stratigraphic map of the Niger Delta's centre region illustrating the relationship between the source rock, migration routes, and hydrocarbon traps connected to growth faults (Modified from Stacher, 1995).

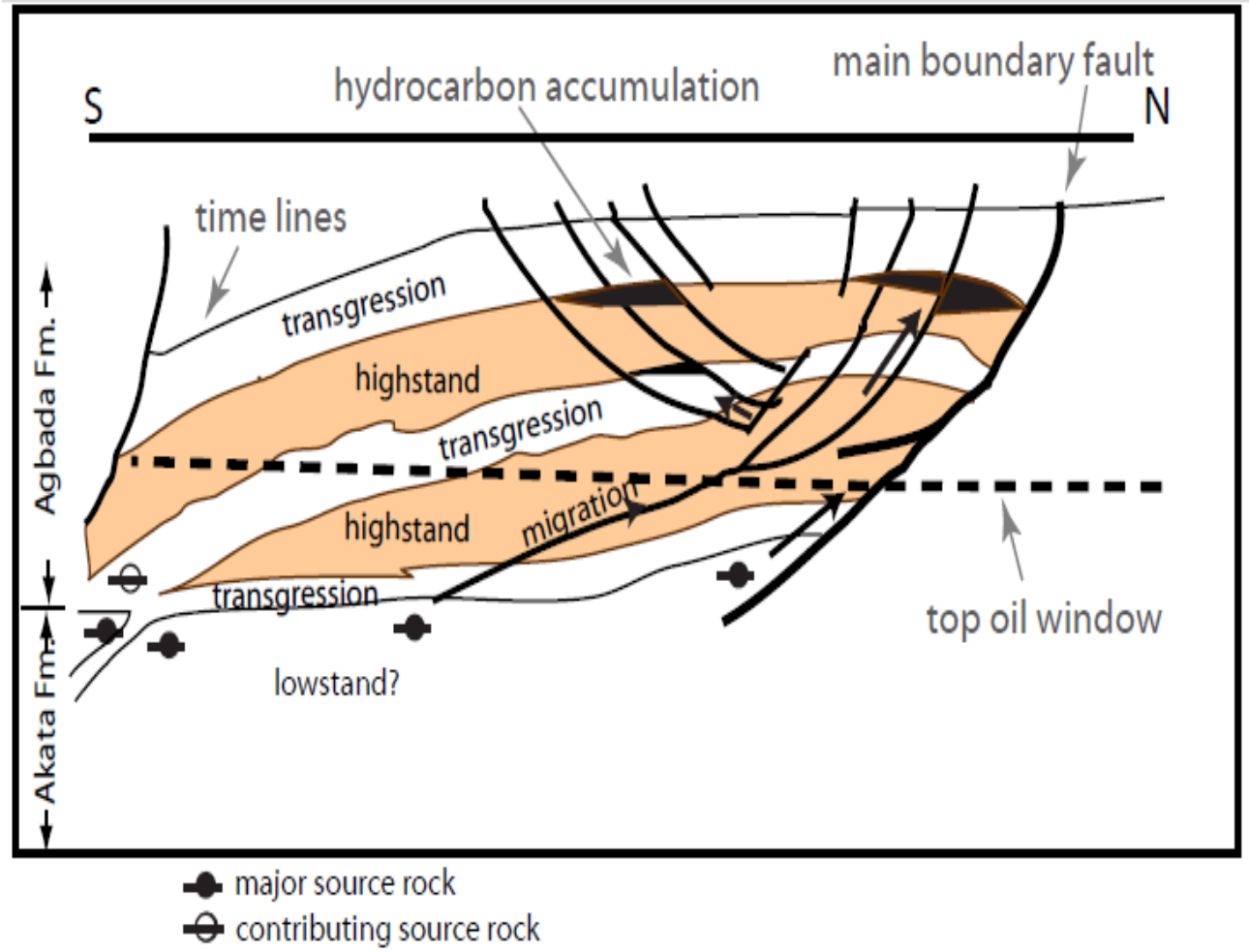

Figure 2.4: Sequence Stratigraphic model for the central portion of the Niger Delta showing the relation of source rock, migration pathways and hydrocarbon traps related to growth faults (Modified from Stacher, 1995).

2.2.4.2 Source rock

The Niger Delta's Akata formation is said to be the region where the hydrocarbons originally formed. It is the Niger Delta complex's basic lithologic unit. It is marine and mostly made up of shale, siltstone, and occasionally in-place turbidite. The formation is composed primarily of gray shales in the upper portion, however in certain places the top part is sandy or silty where it grades into the Agbada formation. Planktonic foraminifera make up the majority of the biofacies present in the pressurized Akata formation. The Akata formation dates from the Paleocene through the Holocene era (Reijers, 1996).

2.2.4.3 Reservoir rock

Sandstone and loose sands, mostly from the Agbada Formation, are used to generate petroleum in the Niger Delta. The depositional environment and depth of burial are the two factors that affect the properties of the reservoirs in the Agbada Formation. Dating from the Eocene to the Pliocene, known reservoir rocks are frequently stacked and range in thickness from less than 15 metres to 10% having more than 45 metres (Evamy and others, 1978). The thicker reservoirs probably consist of layered channel composite bodies (Doust and Omatsola, 1990). The most significant reservoir forms, according to Kulke (1995), are point bars of distributary channels and coastal barrier bars that are sporadically crossed by sand-filled channels. The primary Niger Delta reservoirs are described by Edwards and Santogrossi (1990) as 14 Miocene paralic sandstones with 40% porosity, 2 Darcy's permeability, and a thickness of 100 metres. Growth faults exert strong control over the lateral variation in reservoir thickness; the reservoir thickens toward the fault within the downthrown block (Weber and Daukoru, 1975). The reservoir sandstone has a very diverse range of grain sizes, with fluvial sandstones typically being coarser than their delta front counterparts, point bars fine upward, and barrier bars typically having the best grain sorting. Much of this sandstone is nearly unconsolidated, some with a minor component of argillo-silicic cement (Kulke, 1995). Porosity only slowly decreases with depth because of the young age of the sediment and the coolness of the delta complex.

2.2.4.4 Traps and Seals

Although stratigraphic traps are not infrequent, structural traps are the most common in Niger Delta fields (Figure 2.5). The structural traps formed while the Agbada paralic sequence underwent synsedimentary deformation (Evamy et al, 1978; Stacher, 1995). Because the under-compacted, overpressured shale becomes more unstable, structural complexity rises from the north (earlier formed depobelts) to the south (later formed depobelts). Several structural trapping elements are described by Doust and Omatsola (1990), including those connected to straightforward rollover structures, clay-filled channels, structures with several growth faults, structures with antithetic faults, and collapsed crest structures. Stratigraphic traps are probably just as significant on the delta's flanks as structural traps (Beka and Oti, 1995). Sandstone pockets can be seen in this area in between diapiric buildings. This alternating series of sandstone and shale progressively grades to main sandstone towards the delta toe (base of distal slope). Shale that is interbedded within the Agbada Formation is the main seal rock in the Niger Delta. Three different forms of seals are available in the shale: vertical seals, interbedded sealing units where reservoir sands are juxtaposed due to faulting, and clay smear along faults (Doust and Omatsola, 1990). Major erosional events in the early to middle Miocene produced clay-filled canyons on the delta's flanks. The top seals for several significant offshore oilfields are made of these clays (Doust and Omatsola, 1990).

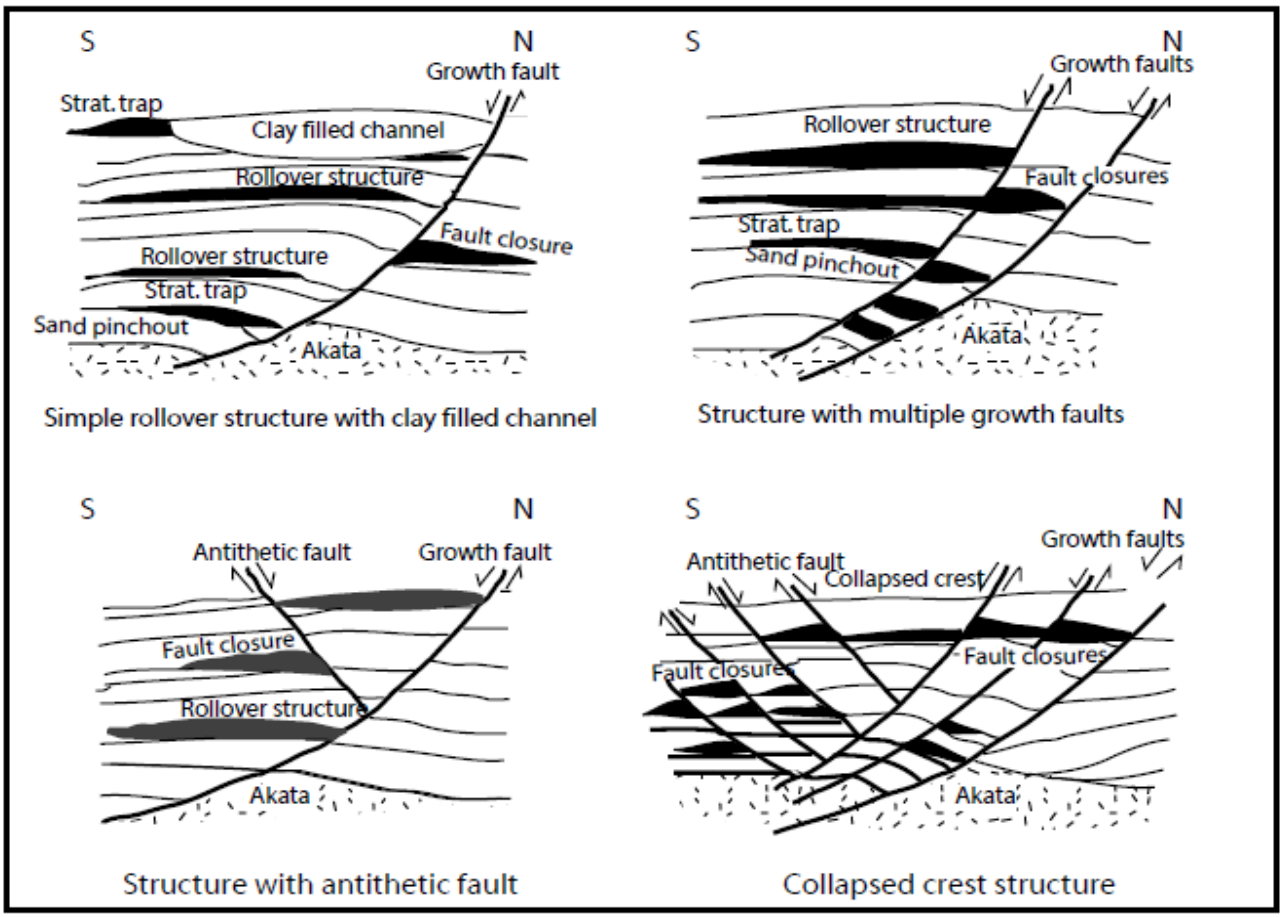

Figure 2.5: Examples of oil field structures in the Niger Delta and related trap types (Modified from Doust and Omatsola, 1990 and Stacher, 1995)

2.2.4.5 Petroleum Generation and Migration

The Niger Delta's current oil window's top temperature was estimated by Evamy et al. (1978) to be 240°F (115°C). The upper Akata Formation and the lower Agbada Formation are where the oil window (active source-rock interval) is located in the northwest corner of the delta. The apex of the oil window is lower stratigraphically to the southeast (up to 4000 below the upper Akata/lower Agbada sequence; Evamy et al., 1978). According to several studies' findings (Nwachukwu and Chukwura, 1986; Doust and Omatsola, 1990; Stacher, 1995), the overburden rock's thickness and sand/shale ratios are responsible for the distribution of the top of the oil window (Benin Fm. and variable proportions of the Agbada Fm.). The thermal gradient is lowest in the sandy continental sediment (Benin Fm.) and ranges from 1.3 to 1/8°C/100 m; it is intermediate in the paralic Agbada Formation (2.7°C/100 m); and highest in the marine, under-pressured Akata Formation (5.5°C/100 m) (Ejedawe et al., 1984). As a result, the depth to any temperature inside each depobelt depends on the overall distribution of sand and shale. The distant offshore subsurface temperatures would be higher because sand percentages are lower if sand/shale ratios were the only factor. Contrarily, it is projected that the depth of the hydrocarbon kitchen will be greater than that of the delta itself, as the depth of oil generation depends on a number of variables, including temperature, duration, and tectonic-related deformation (Beka and Oti, 1995). It's possible that migration from mature, over-pressured shales in the more distant part of the delta will depict that from shales in the Gulf of Mexico. Hunt (1990) connects the fracturing and resealing of the top seal of the over-pressured interval to the episodic expulsion of petroleum from abnormally pressured, mature source rocks. The fracturing/resealing cycle takes place at intervals of tens of thousands of years in basins that are quickly sinking, like the Gulf of Mexico. In the Niger Delta basin, where the Akata Formation is under excessive strain, this form of cyclic outflow is unquestionably plausible. Beka and Oti (1995) estimate that down-slope dilution of organic matter as well as differentiation linked to expulsion from over-pressured sources will lead to a bias towards lighter hydrocarbons (gas and condensate) from the over-pressured shale.

2.3 Basic Theory of Methods Used

2.3.1 Seismic Reflection Method

Seismic Reflection is a method of exploration geophysics that provides information subsurface geological structure which has obvious value towards the exploitation of hydrocarbons, the identification of certain sediment logical features which are important in petroleum exploration such as river channels, deltas, fans etc. The seismic method makes use of the properties of the velocity of sound. This velocity is different for different rocks and it is this difference which is exploited in the seismic method. When we create sound at or near the surface of the earth, some energy will be reflected back (bounced back).This is known as the two way travel time (TWT). They can be characterized as echoes. The two way travel time is the period for the seismic waves to travel down from the source until they meet a boundary between layers with a different seismic velocity (V), density (ρ) and acoustic impedance (Z) where they are reflected and then return to the surface. The contrast between acoustic impedance is called reflection coefficient (RC). At such interfaces, the seismic rays are partially refracted, partially transmitted and partially reflected back to the surface where they are detected by a group of receivers (Figure 2.6).

$$Z = \rho V$$

$$RC = \frac{Z_2 - Z_1}{Z_2 + Z_1}$$

2.3.1.1 Acquisition

To gather the seismic signals, many alternative receiver configurations are used in the acquisition process, such as towing hydrophones behind a marine seismic vessel and placing geophones or seismometers on the Earth's surface or the seafloor. A source, such as a vibrator, dynamite, or air pistol, produces acoustic or elastic vibrations that penetrate the Earth pass through strata that have various seismic responses and filtering effects, and then return to the surface to be captured as seismic data.

2.3.1.2 Processing

Seismic data are modified to reduce noise, improve the signal, and move seismic events to the proper location in space. Analysis of velocities and frequencies, static corrections, Deconvolution, normal moveout, dip moveout, stacking, and migration which may be done before or after stacking are typical processing processes. A better interpretation is made possible by seismic processing because subsurface features and reflection geometries are more visible.

2.3.1.3 Interpretation

Seismic interpretation & subsurface mapping are key skills that are used commonly in the oil industry. It is used to generate reasonable models and predictions about the properties and structures of the subsurface. Some of this interpretation process which involves

i. Loading the data into the software i.e. the seismic sections: (post stack data), available well data (well logs, deviation data and formation tops), velocity data of wells: from check-shot survey or vertical seismic profiling (VSP).
ii. Well Tie: To determine the precise location of the formation tops of the intersected horizon and to connect it to the seismic section, a synthetic seismogram is generated. Synthetic indicates also if the horizon response is peak or trough. From the well, we know the depth of the event (Formation tops). From plotting values of depths & times which came from the check-shot survey, we can extract the time value for a certain depth (to mark that depth on the seismic section). We repeat these steps with all wells to get the true depth of the horizon.
iii. Mapping of Horizon: Identifying wiggles from the same reflection that appear on different traces is required.
iv. Mapping of faults: Fault mapping on the seismic section, both on the crosslines and inlines.
v. Surface Generation: Maps are generated from the mapped horizons and faults.

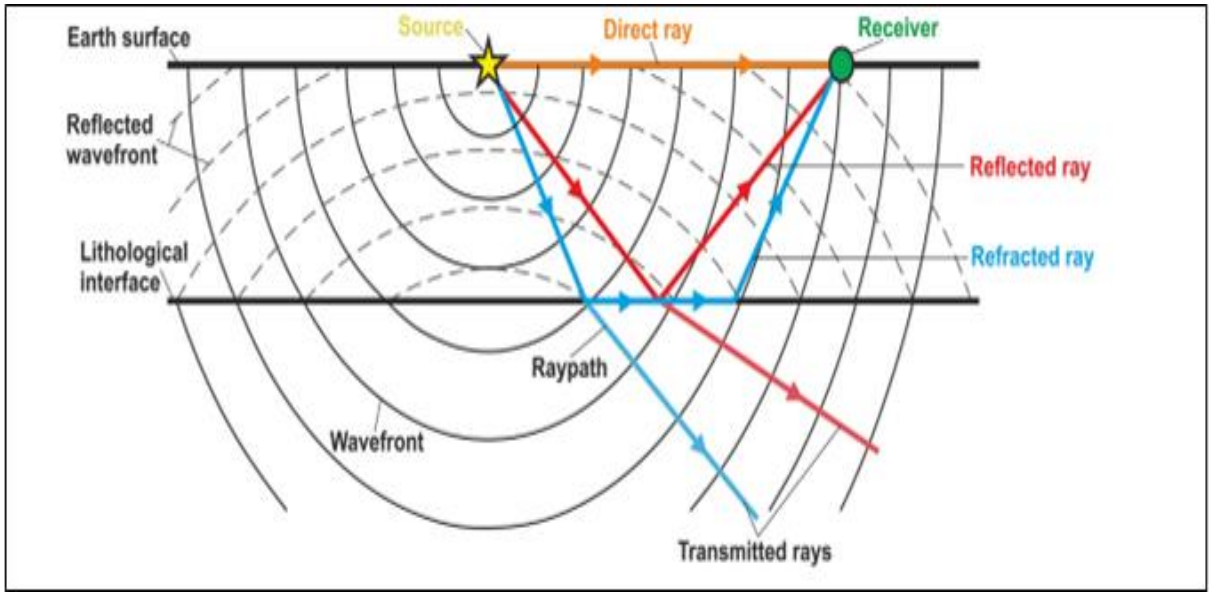

Figure 2.5: Diagram illustrating the seismic wave's travel direction, which is shown not only by ray paths but also by wavefronts, which reveal the wave's three-dimensional (3D) nature (Modified from Ashcroft, 2011).

2.3.2 Seismic Attributes

Any seismic data measure that aids in better visualizing or quantifying aspects relevant to interpretation is referred to as a seismic attribute. It could be considered a potent tool for enhancing the precision of predictions and interpretations in the discovery and production of hydrocarbons. Geoscientists can more quickly decipher the history of structural deformation by interpreting faults and channels, identifying depositional environments, and using seismic characteristics. In many cases, seismic characteristics group features into displays that offer enhanced pictures for either a human interpretation or for contemporary geostatistical or neural-network computer analysis. Seismic characteristics are susceptible to lateral changes in noise in addition to lateral changes in geology. Seismic attributes can be divided into two categories: those that quantify the reflectivity component of seismic data and those that quantify its morphological component. To identify faults, channels, fractures, diapirs, and carbonate buildups, the morphological features are used to extract data on reflector dip, azimuth, and terminations. To determine lithology, reservoir thickness, and the existence of hydrocarbons, the reflectivity attributes extract data on reflector amplitude, waveform, and variation with illumination angle. 3D seismic properties could be used in the reconnaissance mode to quickly characterise structural structures and depositional settings. The 3D seismic features are calibrated against actual and simulated well data in the reservoir characterization mode to assess hydrocarbon accumulations and compartmentalization. Taner et al. provided a thorough categorization of attributes into geometrical and physical categories. The geometrical qualities are sensitive to lateral variations in dip, azimuth, continuity, similarity, curvature, and energy and have the potential to improve the visibility of the geometrical properties of seismic occurrences. These are employed in stratigraphic interpretation as well as fault or structural interpretation. However, for lithological classification and reservoir characterization, the physical attributes improve the subsurface's physical parameters linked to lithology and stratigraphy. Seismic occurrences' amplitude, phase, and frequency are among them. The acoustic impedance contrast directly affects the size of the trace envelope, while frequencies are related to bed thickness, wave scattering, and absorption. Rock characteristics have a direct impact on both instantaneous and average velocities.

Table 2. 1: Some Seismic Attributes, description and applicability (Leonardo and Guerra, 2009)

Attribute Name	Description	Applicability
RMS Amplitude	The "root mean square" of the original amplitude within a user-defined window	Distinguish between lithological changes. RMS values that are high may indicate porous sands or sinuous channel belts. Isolated extreme values of this attribute may be a bright spot.
Apparent Polarity	The sign of f(t) at a local maximum of the Envelope attribute	Useful to track lateral changes in lithology and enhance reflectors continuity. May distinguish different kinds of bright spots.
Instantaneous Phase	Is the argument of the intricate seismic trace	Enhance reflectors continuity, discontinuities, faults and pinch-outs. Is useful in stratigraphic pattern interpretation.
Cosine of Instantaneous Phase	Is the cosine of the instantaneous phase attribute	Improves reflectors continuity and enhance discontinuities, faults and pinch-outs. Helps the stratigraphic interpretation process. Since it is invariant with amplitude is used conjugated with the instantaneous phase attribute.
Envelope	Is the complex seismic trace's modulus or total instantaneous energy	It distinguishes differences in stratigraphy, lithology, and fluid laterality inside a hydrocarbon reservoir, as well as significant lithological and sequence boundary modifications. It may detect bright spots as well as function as a DHI.
Local Structural Azimuth and Dip	Uses three methods to estimate the orientation of a bed. The gradient method calculates the gradient in 3 directions. The event uses the same approximation of the gradient method but with a different convention.	Evaluates a seismic reflector's azimuth, dip, and orientation.It is also used as an internal algorithm for other seismic attributes extraction
Structural Smoothing	Fast volumetric signal processing. Apply a 3D Gaussian filter honouring, or not, the estimated bed orientation.	Reduces spatial noise within the data, improving reflectors continuity. May also enhance edges.

Ant Tracking	Uses swarm intelligent concepts where virtual “ants” are deployed into an edge detection cube (e.g. variance) to automatically track and enhance faults and discontinuities with high level of detail.	The enhanced faults can be automatically extracted, using Petrel’s “Automatic Fault Extraction”, to be inserted in a hydrocarbon reservoir model.
Variance	It computes the normalized population variance with an optional weighted vertical smoothing.	Detect edges, such as faults and discontinuities. It sharply delineates a salt body and with a short vertical window, It is use for interpreting depositional elements.

2.3.3 Borehole geophysics (Well logs)

Electrical well logging was introduced to the oil industry over half a century ago. Since that time, many additional and improved logging devices have been developed and put into general use. As well logging science evolved, the art of interpreting the data also advanced. Today, the detailed analysis of a carefully chosen suite of wireline services provides a method of deriving or inferring accurate values for the hydrocarbon and water saturations, the porosity, the permeability index, and the lithology of the reservoir rock. The first oil field electrical log was recorded in 1927 in a well in the small field oil field of Pechelbronn, in Alsace, a province of north-eastern France. At regular intervals, the downhole measuring device (known as a sonde) was stopped in the borehole to take measurements. The computed resistivity was then manually plotted on a graph.

2.3.2.1 Measurements While Drilling (MWD)

Increasingly today, formation properties are being measured at the time the formation is drilled by use of special drill collars that house measuring devices. These measurement-while-drilling (MWD) tools (or logging while drilling LWD) are particularly valuable in deviated offshore wells where well bore path control is critical and where an immediate knowledge of the formation properties is vital for decision making on such matters as the choice of logging and casing points.

2.3.2.2 Open-hole logging and logging tools

The term open-hole refers to the condition of the borehole immediately after the drilling is completed or prior to casing of the borehole. There are modern equipment that can make measurements in cased holes. A continuous record of measurement versus depth of several formation properties is provided by open-hole logging. In particular, electrical resistivity, naturally occurring, bulk density, and artificially produced radioactivity, hydrogen concentration, and elastic modulus can all be recorded via wireline logs.

The open-hole logging tools include:

Formation Fluid Content Indicators

i. Induction.
ii. Laterolog.

iii. Microfocused (micro-resistivity).
iv. Pulsed neutron.
v. Inelastic gamma.

Porosity-Lithology Indicators

i. Sonic (acoustic).
ii. Density and lithologic density.
iii. Neutron.
iv. Natural gamma ray.
v. Spectral gamma ray.

Reservoir Geometry Indicators

i. Dipmeter.
ii. Borehole gravimeter.
iii. Ultralong spacing electric.

Formation Productivity Indicators

i. Spontaneous potential (SP) log.
ii. Caliper log.

2.3.2.2.1 Gamma Ray Log

The overall amount of natural gamma radiation coming from a formation is measured by the gamma ray log. The Uranium-Radium and Thorium series of isotopes, as well as potassium-40, are the sources of this gamma radiation. The symbol GR is frequently used for the gamma ray log. As a result of collisions with other atoms in the rock, the gamma rays gradually lose energy after being released by an isotope in the formation (Compton scattering). Compton scattering continues until the gamma ray's energy is so low that the formation entirely absorbs it. Therefore, the log's measurements of gamma ray intensity depend on:

i. The initial quantity of gamma ray emission, which is a result of the rock's elemental composition.
ii. The degree of Compton scattering that the gamma rays encounter, depends on both the material's density and the distance between the emitter and the detector.

Zone correlation and lithology identification are both possible using the gamma ray log. Low radioactive material concentrations and low gamma ray readings can be found in sandstones and carbonates that do not contain shale (Figure 2.7). Due to the quantity of radioactive elements in shale, the gamma ray log response rises as shale content does. However, if the sandstone contains potassium feldspars, micas, glauconite, or uranium-rich fluids, clean sandstone (i.e. low shale concentration) may also result in a strong gamma ray response.

Volume of Shale Calculation

Shale is more radioactive than sand or carbonate, therefore the volume of shale in porous reservoirs can be determined using gamma ray logs. The analysis of shaly sands can then be done using the volume of shale. To calculate the volume of shale from a gamma ray log, the gamma ray index must first be calculated (the following formula from Schlumberger, 1974).

$$I_{GR} = \frac{GR_{log} - GR_{min}}{GR_{max} - GR_{min}} \quad 2.1$$

Where:

I_{GR} = Gamma ray index

GR_{log} = Gamma ray reading of formation

GR_{min} = Low gamma ray (clean sand or carbonate)

GR_{max} = High gamma ray (shale)

The volume of shale is also calculated mathematically from the gamma ray index (I_{GR}) by the following Dresser Atlas (1979) formulas:

Older rocks, consolidated:

$$V_{sh} = 0.33\left[2^{(2\times I_{GR})} - 1.0\right] \quad 2.2$$

Tertiary rocks, unconsolidated:

$$V_{sh} = 0.083\left[2^{(3.7\times I_{GR})} - 1.0\right] \quad 2.3$$

Where:

V_{sh} = Volume of shale

I_{GR} = Gamma ray index

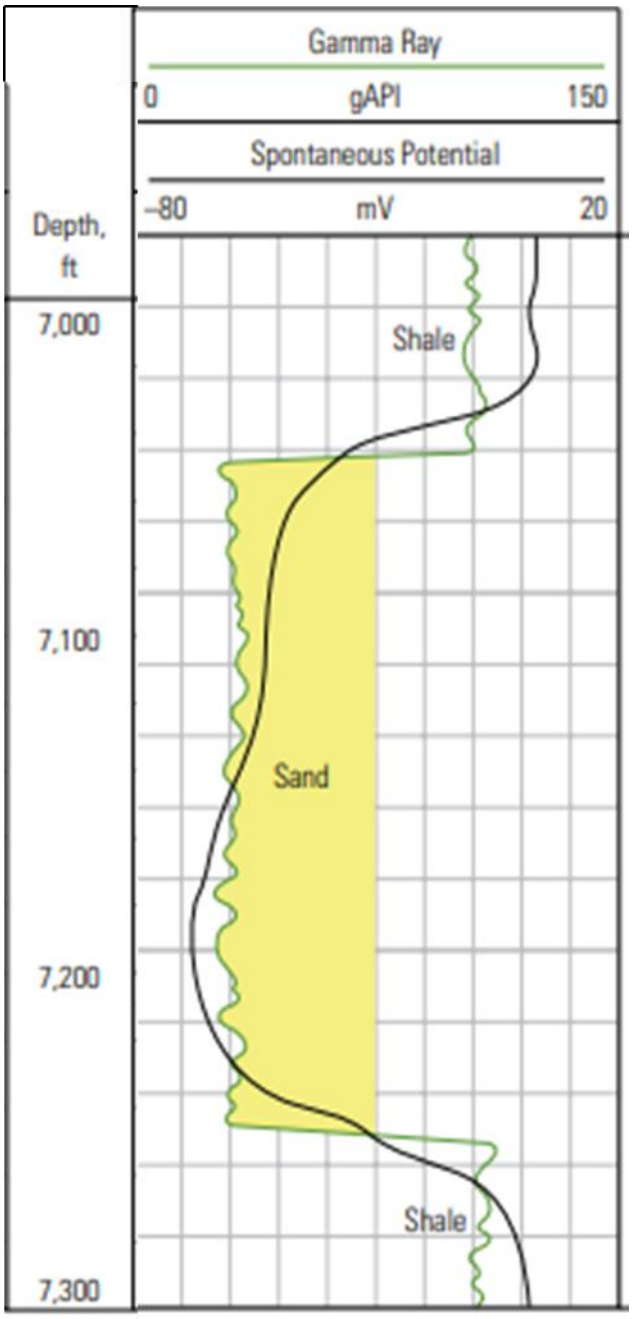

Figure 2.6: Typical gamma log (Modified from Varhaug, 2016).

2.3.2.2.2 Resistivity Log

Electric logs called resistivity logs are used to identify permeable zones, identify hydrocarbon-versus-water-bearing zones, and calculate resistivity porosity. Determining whether a zone is water or hydrocarbon-bearing is by far the most crucial application of resistivity logs (Figure 2.8). The ability of the rock to transfer a current is nearly completely a function of the water in the pores because the matrix or grains of the rock are not conductive. Since hydrocarbons are non-conductive, just like the matrix of the rock, the rock's resistance rises as the hydrocarbon saturation of the pores does. A geologist, by knowing a formation's water resistivity (R_w), its porosity (R_w), and a value for the cementation exponent (m) can determine a formation's water saturation (F) from Archie equation:

$$S_W = \left(\frac{F \times R_w}{R_t}\right)^{\frac{1}{m}}$$

2.4

$$F = \frac{a}{\phi^m}$$

2.5

Where:

S_W = Water Saturation.

F= Formation Factor.

R_w = Resistivity of formation water.

R_t = True formation resistivity as measured by a deep reading resistivity log.

a = Tortuosity factor.

m = Cementation exponent.

n = Saturation exponent (most commonly 2.0).

Resistivity Derived Porosity

Both the hydrocarbons in the pores and the minerals that make up the grains in the rock's matrix are non-conductive. Therefore, water in the pore space is almost solely responsible for the rock's ability to conduct an electrical current. Mud filtrate replaces formation water when drilling fluid invades a porous and permeable, water-bearing formation. Shallow resistivity (R_{xo}) and porosity in a water-bearing can be related by the following equations:

$$S_{xo} = \sqrt{F \times \frac{R_{mf}}{R_{xo}}} \quad 2.6$$

Where S_{xo} = 1.0 (100%) in water-bearing zones.

$$\phi = \left(\frac{a \times R_{mf}}{R_{xo}}\right)^{\frac{1}{m}} \quad 2.7$$

Where:

ϕ = Formation porosity

R_{mf} = Resistivity of mud filtrates at formation temperature

S_{XO} = Flushed zone water saturation

R_{XO} = Resistivity of flushed zone from Microlaterolog, Proximity Log, Laterolog-8, or Microspherically Focused Log values

a = Constant (1.0 for carbonates, 0.62 for unconsolidated sands and 0.81 for consolidated sands)

m = Constant (2.0 for consolidated sands and carbonates, and 2.15 for unconsolidated sands)

F = Formation factor

In hydrocarbon-bearing zones, the shallow resistivity (R_{XO}) is affected by the unflushed residual hydrocarbons left by the invading mud filtrate. These residual hydrocarbons will result in a value for shallow resistivity (R_{XO}) which is too high because hydrocarbons have a higher resistivity than formation water. Therefore, the calculated resistivity porosity in hydrocarbon-bearing zones

will be too low. To correct for residual hydrocarbons in the flushed zone, flushed zone water saturation (S_{XO}) must be known or estimated. The shallow resistivity (R_{XO}) of a formation can be related to porosity by the following:

$$\phi = \left[\frac{a(R_{mf}/R_{xo})}{{S_{xo}}^2}\right]^{\frac{1}{m}} \qquad 2.8$$

Where:

ϕ = formation porosity

R_{mf} = resistivity of mud filtrate at formation temperature.

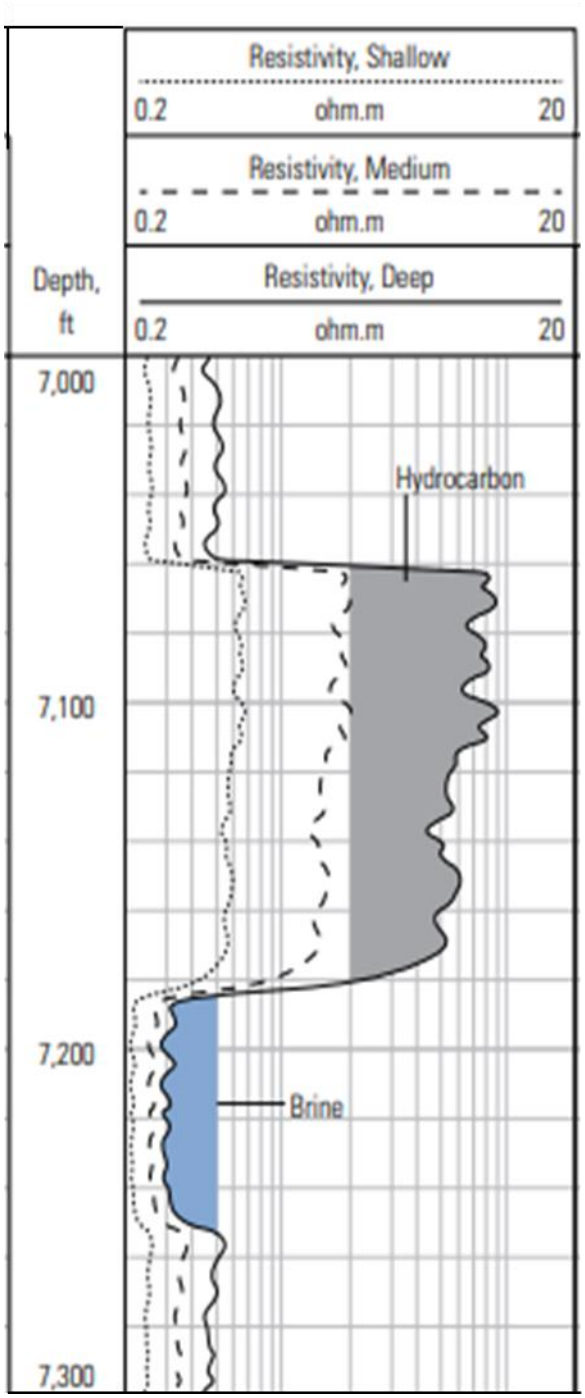

Figure 2.7: Typical resistivity log (Modified from Varhaug, 2016).

2.3.2.2.3 Sonic Log

The interval transit time of a compressional sound wave passing through a foot of formation is measured by the sonic log, a porosity log. One or more sound transmitters and two or more sound receivers make up the sonic log device. Sonic logs of today are borehole-adjusted tools (BHC). These tools significantly reduce errors brought on by sonic tool tilt as well as erroneous effects of borehole size variations (Kobesh and Blizard, 1959). (Schlumberger, 1972). The reciprocal of a compressional sound wave's velocity in feet per second is the interval transit time (Δt), which is measured in microseconds per foot. Lithology, porosity and interval transit time (Δt) are both affected by each other. Therefore, in order to determine the sonic porosity of a formation, its matrix velocity (Table 2.2) must be known. This can be done using a chart or the following formula (Wyllie etal, 1958):

$$\phi_{sonic} = \frac{\Delta t_{log} - \Delta t_{ma}}{\Delta t_f - \Delta t_{ma}} \qquad 2.9$$

Where:

ϕ_{sonic} = Sonic derived porosity

Δt_{ma} = Matrix interval transit time (Table 6)

Δt_{log}= Formation interval transit time

Δt_f= Well bore fluid interval transit time (fresh mud = 189; salt mud = 185)

Table 2.2: Sonic Velocities and Interval Transit Times for Different Matrices. The Sonic Porosity Formula uses these constants (after Schlumberger, 1972).

	V_{ma} (ft/sec)	Δt_{ma} ($\mu sec/ft$)	Δt_{ma} ($\mu sec/ft$) commonly used
Sandstone	18,000 - 19,500	55.5 -51.0	55.5 - 51.0
Limestone	21,000 - 23,000	47.6 - 43.5	47.6
Dolomite	23,000 - 26,000	43.5 - 38.5	43.5
Anhydrite	20,000	50	50
Salt	15,000	66.7	67
Casing (Iron)	17,500	57	57

Consolidated sandstones and carbonates having intergranular porosity (grain stones) or intercrystalline porosity can be utilised to calculate sonic porosity using the Wyllie et al. (1958) formula (sucrosic dolomites). However, the Wyllie formula will result in too low porosity estimates when used to compute the sonic porosities of carbonates with vuggy or fracture porosity. This will occur because the sonic log only records matrix porosity and not secondary porosity from fractures or vuggy porosity.

When determining porosity in unconsolidated sands with a sonic log, the following empirical compaction factor or should be included in the Wyllie et al (1958) equation:

$$\phi_{sonic} = \left(\frac{\Delta t_{log} - \Delta t_{ma}}{\Delta t_f - \Delta t_{ma}}\right) \times 1/C_p \quad 2.10$$

$$C_p = \frac{\Delta t_{sh} \times C}{100} \quad 2.11$$

Where

$C_p =$ Compaction factor

Δt_{sh} = interval transit time for adjacent shale

$C =$ Compaction factor

$C_p =$ Constant which is normally 1.0 (Hilchie, 1978).

The presence of hydrocarbons increases a formation's interval transit time (Δt). (i.e. hydrocarbon effect). If the hydrocarbon impact is not taken into account, the sonic-derived porosity will be excessive. The following empirical corrections for the hydrocarbon effect are suggested by Hilchie (1978).

$$\phi = \phi_{sonic} \times 0.7(gas) \quad 2.12$$

$$\phi = \phi_{sonic} \times 0.9\ (oil) \quad 2.13$$

2.3.2.2.4 Density Logs

A porosity log that measures electron density is called the formation density log (Figure 2.9). Evaporite minerals, gas-bearing zones, hydrocarbon density, evaluation of shaly sand reservoirs, and complex lithologies can all be done with its help (Schlumberger, 1972). A medium-energy gamma ray source that emits gamma rays into a formation constitutes the density recording device, a contact tool.Cobalt-60 or Cesium-137 is the gamma ray source. In the production, gamma rays collide with electrons, causing a loss of energy for the gamma ray particle. Compton scattering was the name given by Tittman and Wahl (1965) to the interaction between the formation's electrons and the incoming gamma ray particles. Gamma rays that are scattered and reach the detector, which is positioned a fixed distance from the gamma ray source, are tallied as a measure of the formation density. The quantity of electrons in a formation directly affects the number of Compton Scattering collisions (electron density). As a result, the bulk density (gm/cc) of a formation can be connected to the electron density.

The matrix density, porosity, and fluid density in the pores all influence the formation bulk density (salt mud, fresh mud, or hydrocarbons). The matrix density (Table 2.3), as well as the type of fluid in the borehole, must be known in order to calculate density porosity using a chart or a formula.

$$\phi_{den} = \frac{\rho_{ma} - \rho_b}{\rho_{ma} - \rho_f} \qquad 2.14$$

Where:

ϕ_{den} = Density derived porosity

ρ_{ma} = matrix density (see Table 2)

ρ_b = formation bulk density

ρ_f = fluid density (1.1 salt mud, 1.0 fresh mud, and 0.7 gas)

Low density of the formation's hydrocarbons will increase density porosity where invasion is shallow. Gas has a greater impact on density porosity than oil does (gas effect). According to Hilchie (1978), if the fluid density (ρ_f) is uncertain, one should use a gas density of 0.7 gm/cc.

Table 2.3: Matrix Densities of Common Lithologies. The Density Porosity Formula uses the constants listed above (after Schlumberger, 1972).

	ρ_{ma} (gm/cc)
Sandstone	2.648
Limestone	2.71
Dolomite	2.876
Anhydrite	2.977
Salt	2.032

2.3.2.2.5 Neutron Logs

The concentration of hydrogen ions in a formation is determined by neutron logs, which are porosity logs. The neutron log detects liquid-filled porosity in clean formations (i.e., shale-free) with clean porosity (Figure 2.9). In the neutron logging device, neutrons are produced from a chemical source. Americium and beryllium may be the chemical source, and this mixture will continually emit neutrons. A neutron loses some of its energy when it collides with the nuclei of the forming material. Maximum energy loss happens when the neutron collides with a hydrogen atom since their masses are almost equal. As a result, the greatest quantity of energy loss depends on the concentration of hydrogen in a formation. Because hydrogen is concentrated in the fluid-filled pores of a porous formation, energy loss can be correlated with the formation's porosity. Neutron porosity will decrease whenever pores are occupied by gas as opposed to oil or water. This happens because gas has a lower proportion of hydrogen than oil or water. The gas effect refers to a reduction in neutron porosity caused by gas. Responses in the neutron log vary based on:

i. Variations in detector types
ii. Space between source and detector
iii. Lithology—i.e. sandstone, limestone, and dolomite.

A geologist should keep in mind that, unlike other logs, neutron logs must be read using a specific chart created for a particular log (i.e. Schlumberger charts for Schlumberger logs and Dresser Atlas charts for Dresser Atlas logs). This is because, unlike other logs, neutron logs are not calibrated in fundamental physical units (Dresser Atlas, 1975).

2.3.2.2.6 Neutron-Density Log

The Combination Neutron-Density Log is a combination porosity log. Besides its use as a porosity device, it is also used to determine lithology and to detect gas-bearing zones. Figure 2.9 presents the neutron-density log, which consists of neutron curves and neutron curves.True porosity can be obtained by, first, reading apparent limestone porosities from the neutron and density curves.

By identifying rock type from logs, a geologist can construct facies maps. The Neutron-Density Log also illustrates the change in neutron-density response between oil- or water-bearing sand and gas-bearing sand (Figure 2.9). The gas effect is when there is a decrease in neutron porosity and an increase in density and porosity in a gas-bearing zone. The gas effect occurs in a gas-bearing zone when neutron porosity decreases and density and porosity increase. The effect of gas on the Neutron-Density Log is a very important log response because it helps a geologist to detect gas-bearing zones.

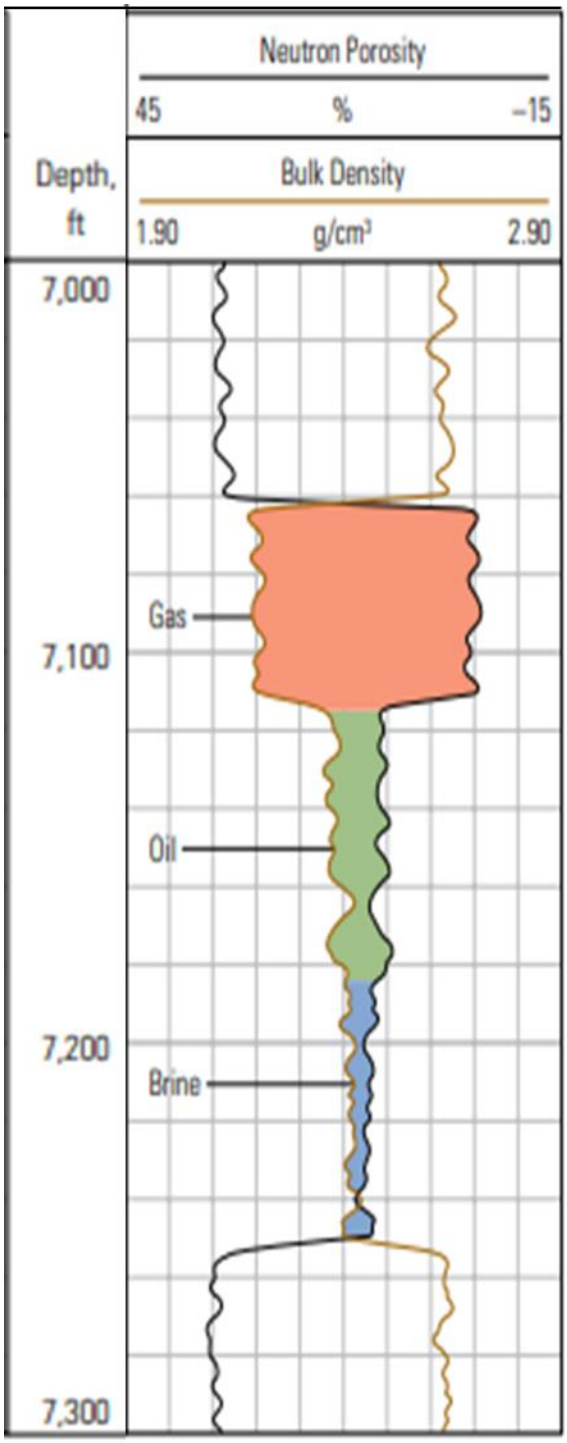

Figure 2.9: Typical Neutron-Density Log (Modified from Varhaug, 2016).

CHAPTER THREE

METHODOLOGY

3.1 Introduction

This chapter outlines the methods and materials employed in seismic reservoir characterization of the OY field, Niger Delta.

3.2 Processes and Workflow

The workflow and processes used in this research work are summarized in Figure 3.1.

3.3 Data Gathering

To achieve the objectives of this research integrated data set was used. The data collection includes 3D migrated seismic data that was acquired and processed by Chevron Nigeria Limited and its joint venture partners. Other data sets include wireline logs for four (4) wells (Figure 3.2). Table 3.1 shows the available suite of logs for the respective wells.

3.4 Data QC and Loading

The available data sets were quality checked and loaded into the Petrel software for interpretation.

3.4.1 Well Data

This contains cogent information as regards the individual wells used for interpretation. The well header used contained individual well names, Surface X and Y coordinates, Kelly Bushing (a well reference datum), and Total depth (TD). The well deviation data was provided and loaded into the software. A suit of well logs; which consist of the lithology logs, resistivity logs, and porosity logs.

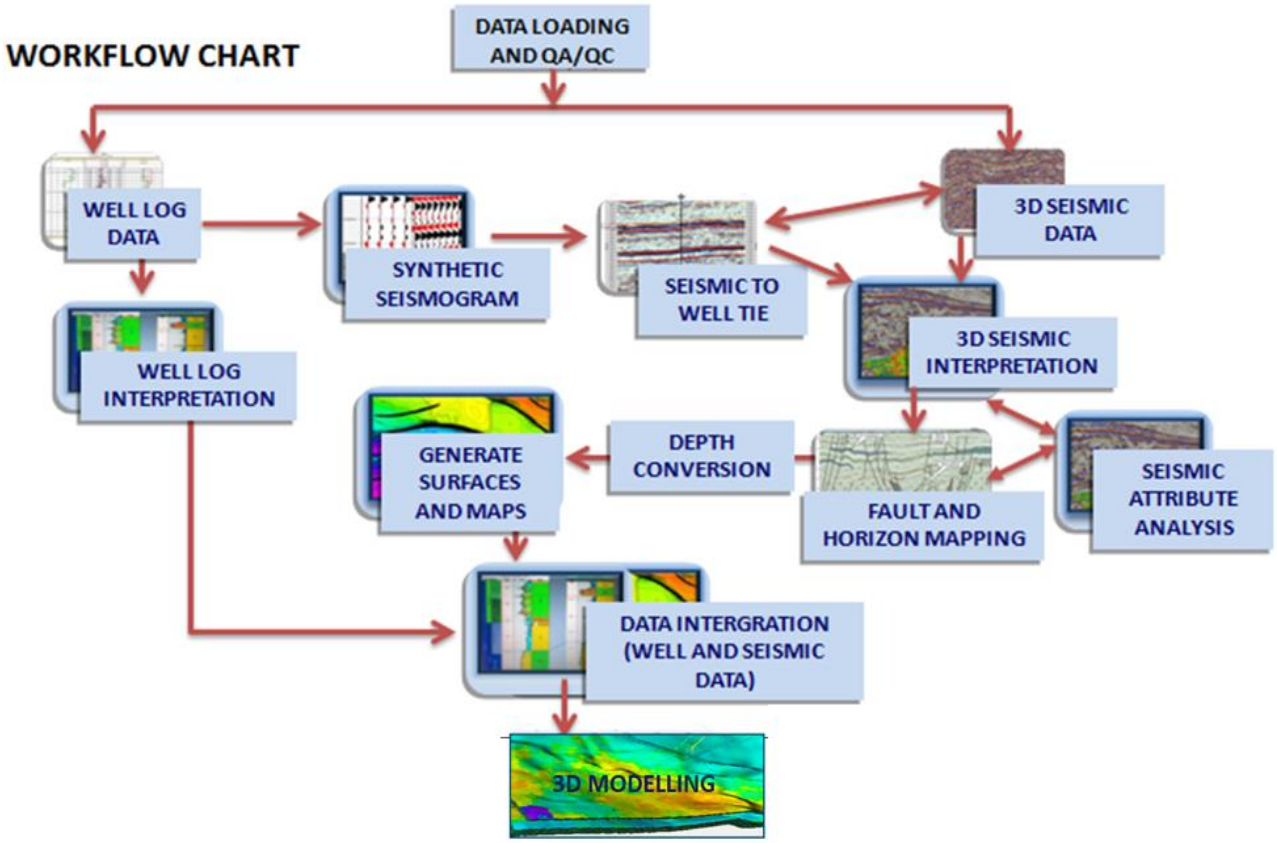

Figure 3.1: Workflow adopted to characterize OY field showing the methodology.

Table 3.1: Table showing all the available logs in the data set.

WELL NAME	GAMMA-RAY	RESISTIVITY	NEUTRON	DENSITY	SONIC	CALIPER
OY-01	+	+	+	+	+	+
OY-02	+	+	+	+	+	+
OY-03	+	+	+	+	-	+
OY-04	+	+	+	+	-	+

Available (+)

Not Available (–)

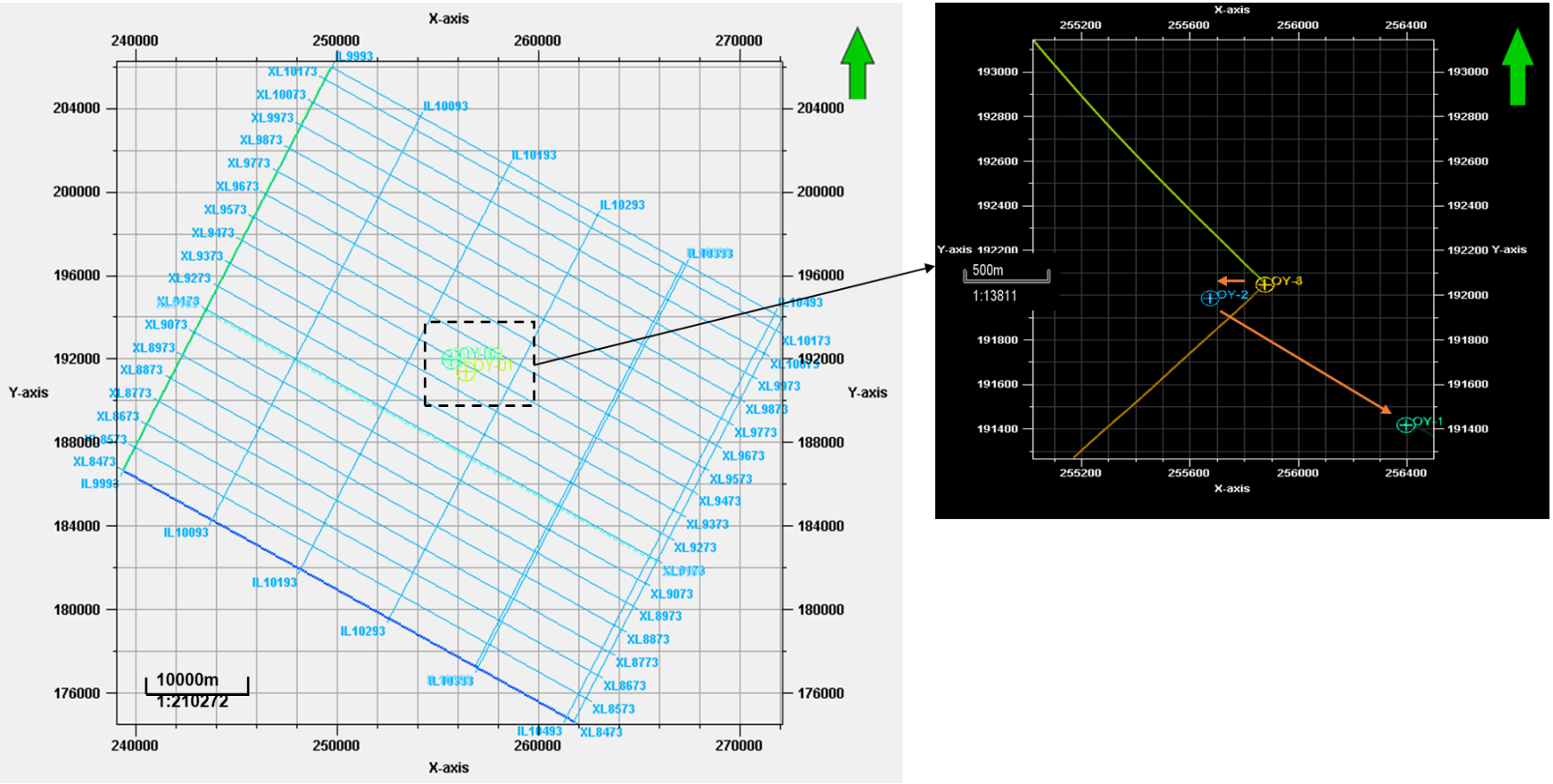

Figure 3.2: Base Map shows the 3D seismic coverage, Well locations for this study and the direction of Well Correlation. The annotated symbol OY-01, OY-02, OY-03 and OY-04 represents well locations.

The well data was first loaded into the petrel software which was in a LAS format. From the Data QC and loading, only four (4) of the wells have all the complete logs that were required for the project. Also, the well deviation data were loaded into the software. OY-02 was the only straight well while the remaining wells OY-01, OY-03 and OY-04 were all deviated (Figure 3.3).

3.4.2 Check-shot Data

The check-shot data was loaded into the software in the ASCII format. This data is used to create a relationship between the seismic (a function of time) and the well (a function of depth). It has a travel time that has been recorded at corresponding depths in a borehole environment.

3.3.3 3D Seismic Volume

This is a 3D migrated seismic data that was acquired after seismic reflection surveying was carried out. The use of an energy source allowed for the creation of several Inlines and crosslines. The seismic data was loaded into the petrel software which was in a SEGY format. The seismic volume acquired from the "OY" field, used for this research work has an inline ranging from 10000- 10500 (strike lines) and cross lines (dip lines) that range from 8500 - 10200 (Figure 3.4). From the Data QC it was found that parts of the data have already been muted. (Figure 3.5(a) and 3.5(b)). The seismic data loading was needed to map faults which could serve as a trap for hydrocarbon accumulation and also to map sand bodies identified from the well logs (seismic to well tie) and it will also be useful for hydrocarbon prospect identification.

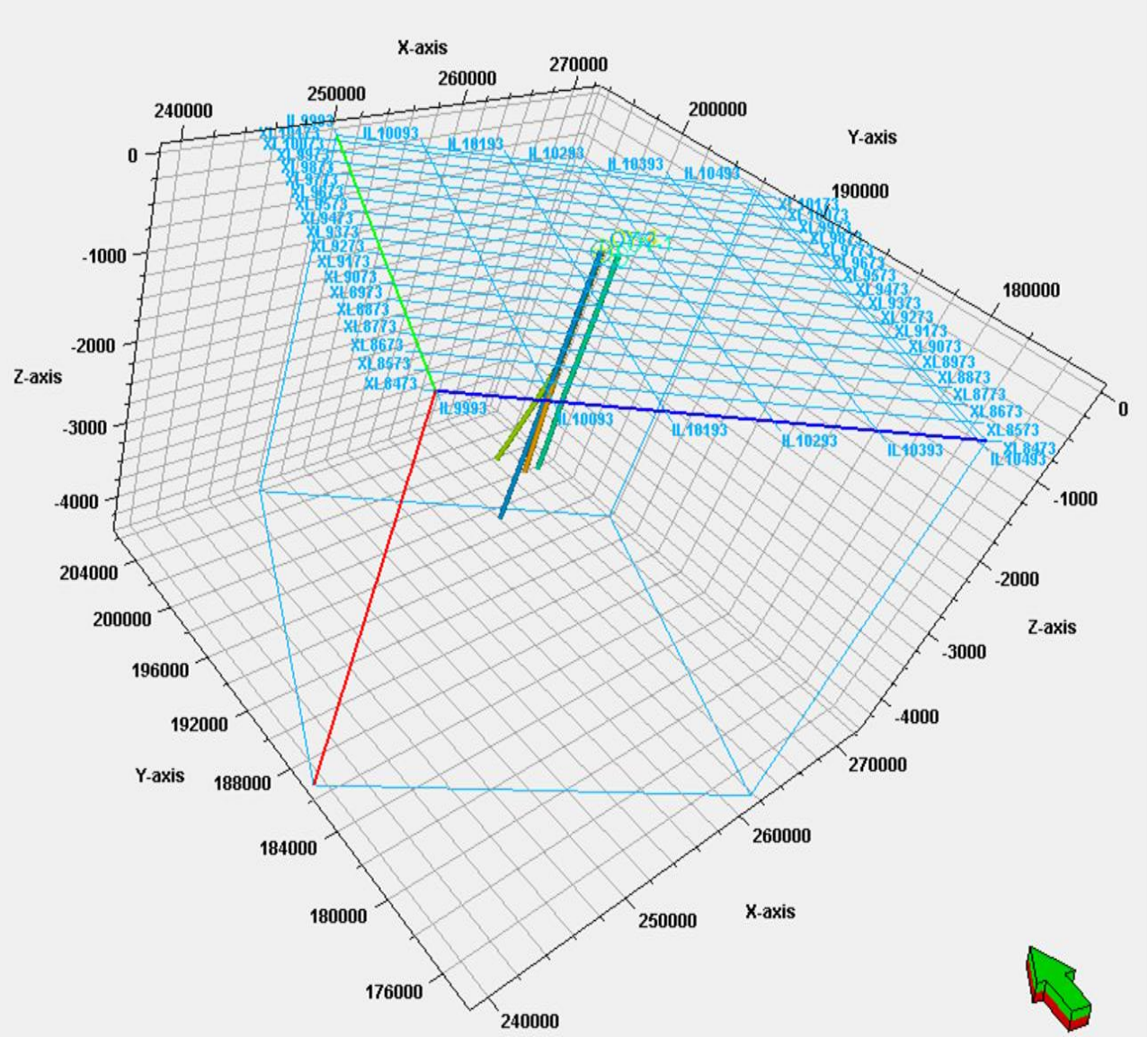

Figure 3.3: 3D view showing the well position and the well deviation.

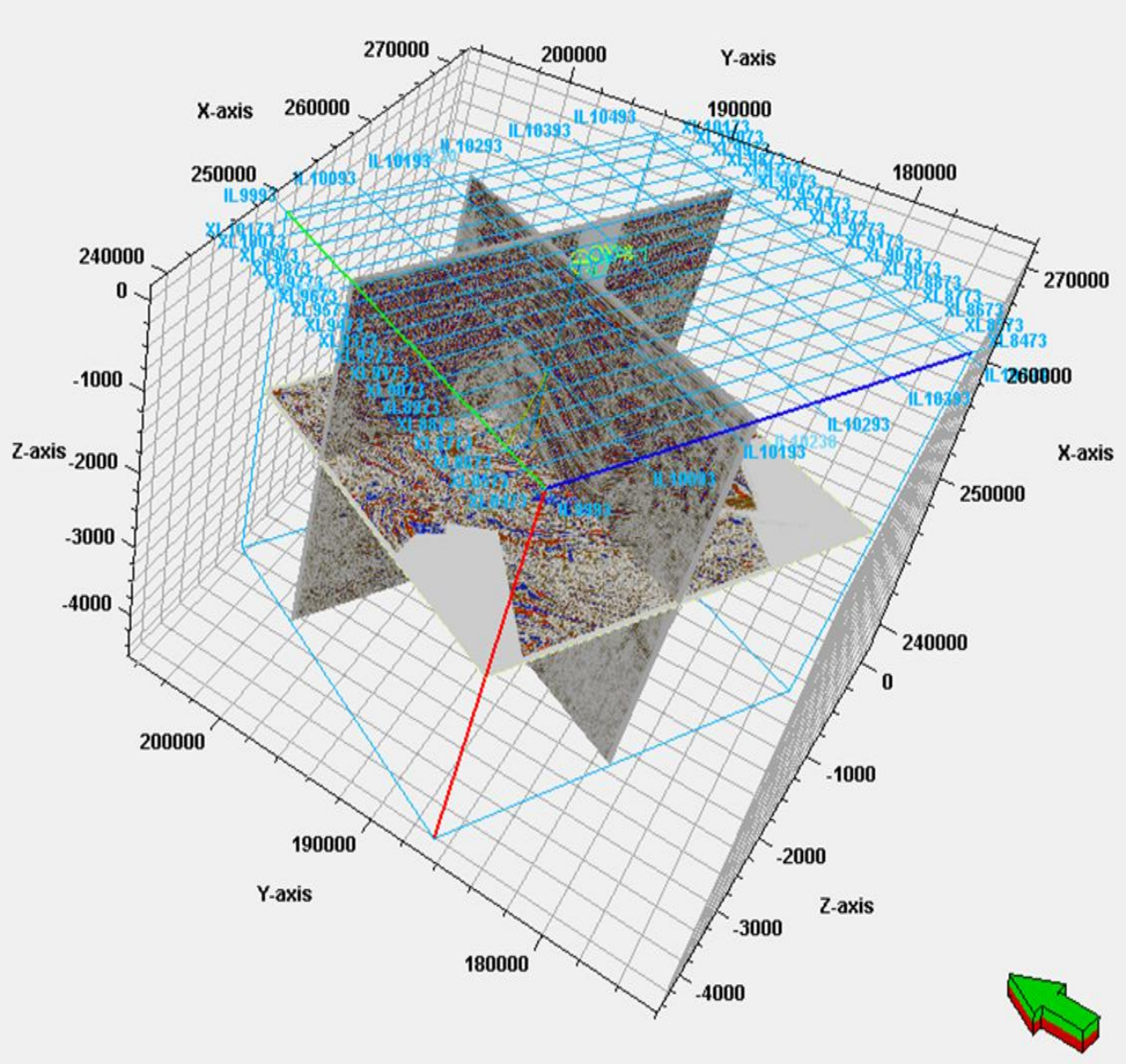

Figure 3.4: 3D Seismic volume and wells.

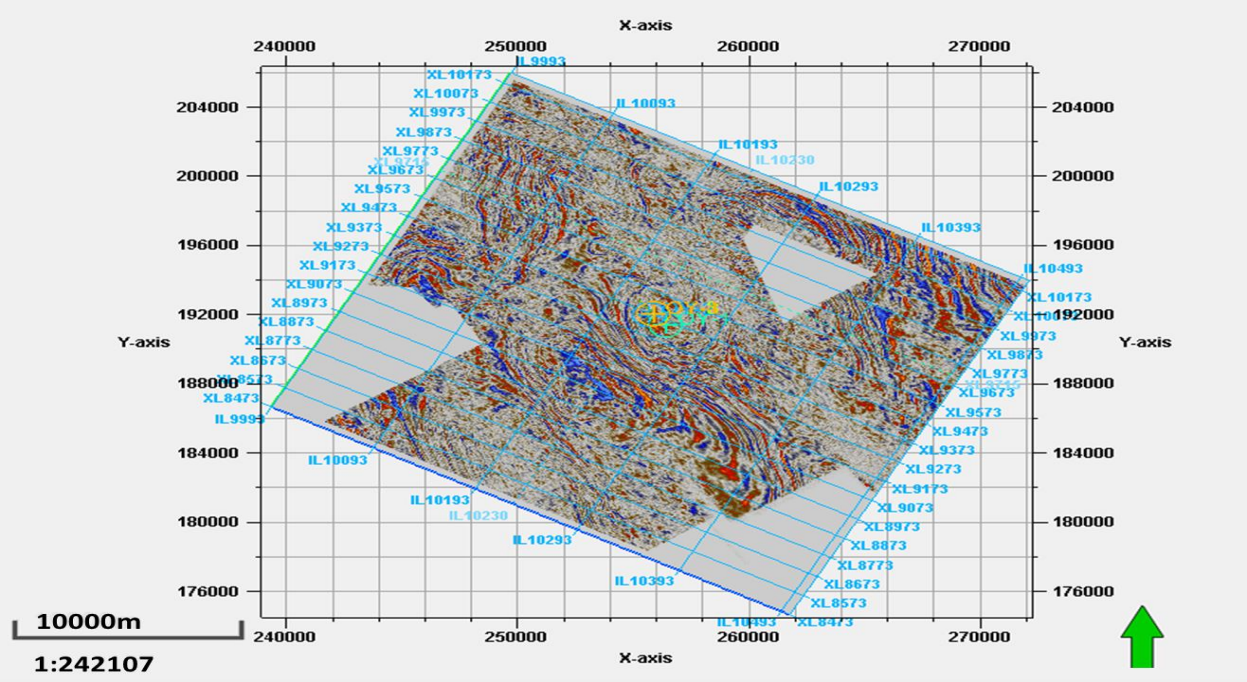

Figure 3.4(a): Time slice (-2144 ms) shows the position of the wells on 3D seismic cube.

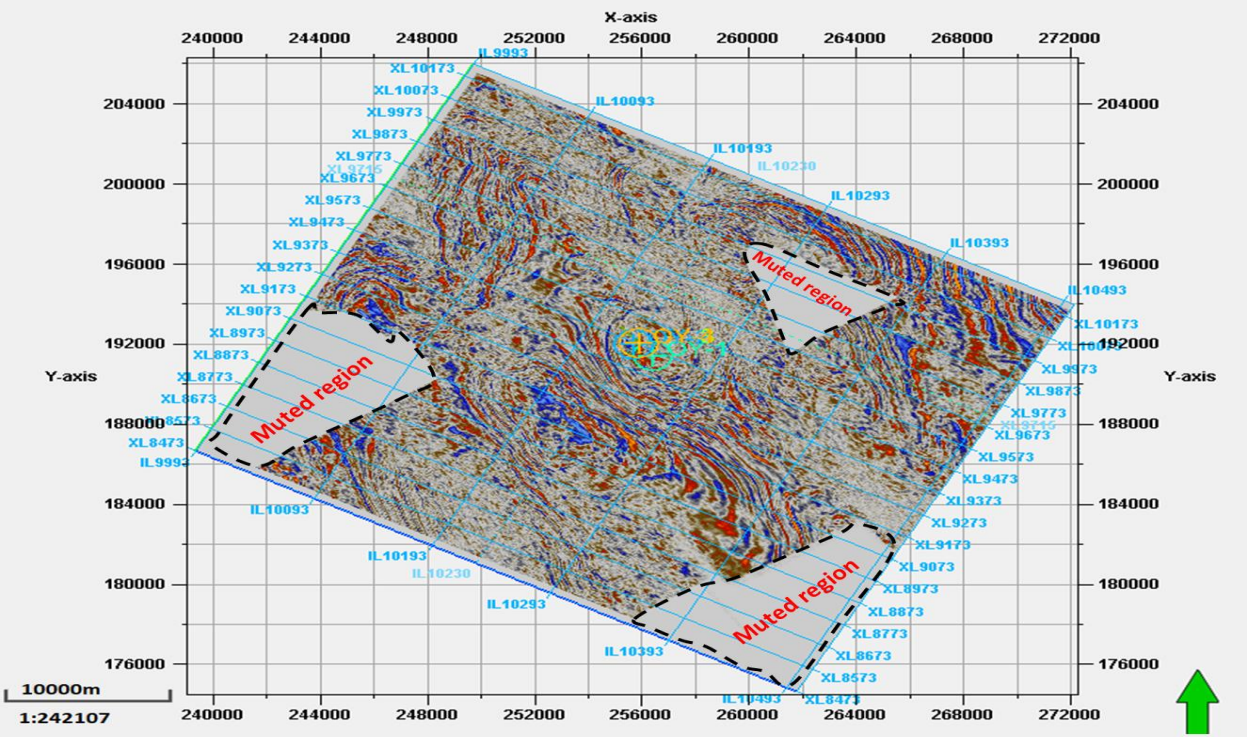

Figure 3.5(b): Time slice (-2144 ms) showing the muted regions on the 3D seismic cube.

3.5 Data Interpretation

The Petrel E&P software 2014 and 2017^{TM} was used to interpret the data provided for this research work.

3.5.1 Well Correlation

The orientation of the well log correlation was from North to South. Figure 3.6 shows the well correlation panel with the delineated reservoir unit on all the available wells. The gamma ray log was used for the lithology correlation. Determining the presence of hydrocarbon in the identified reservoir units required the use of the resistivity log. The hydrocarbon type was determined using the neutron and density log.

3.5.2 Petrophysical and Volumetric Estimation

Porosity estimation

Neutron and density logs were both used to estimate the porosity. A corrected porosity was produced from equation 3.1 by taking into account the fact that density logs will record very high estimate porosity and neutron logs will read very low neutron porosity in gas bearing zones.

$$\phi_{corr} = \sqrt{\frac{\phi^2{}_N + \phi^2{}_D}{2}} \qquad 3.1$$

Water Saturation

All water saturation methods are based on the standard Archie equation equ (3.2)

$$S_w = \sqrt[n]{\frac{a \times R_w}{\emptyset^m \times R_f}} \qquad 3.2$$

Where; $n =$ Saturation exponent (taken as 2)

$R_w =$ Formation water resistivity (Taken as 0.8)

$R_f =$ Resistivity of fluid (ILD)

$\emptyset =$ Porosity

a = Constant (0.62 for unconsolidated sands and 0.81 for consolidated sands)

m = Constant (2.0 for consolidated sands and 2.15 for unconsolidated sands)

Net to Gross Estimation

A closer examination of the gamma ray logs was done for each pay zone, and the thickness of the shale streaks within the reservoir interval was subtracted from the overall column. Also using a cut-off on the resistivity logs, water saturation and Volume of Shale (S_w and V_{shale} are derived logs computed using Petrel) the thickness of the reservoir was decreased by other reservoir portions that did not contain a significant amount of hydrocarbon. The ratio of the reservoir's total thickness to its hydrocarbon bearing thickness was used to calculate net to gross.

The volume of hydrocarbon oil was calculated using equation 3.3

$$STOIIP = GRV \times {}^{N}/_{G} \times \emptyset \times S_o \times {}^{1}/_{B_o}\ (stb) \qquad 3.3$$

The volume of hydrocarbon gas was calculated using equation 3.4

$$GIIP = GRV \times {}^{N}/_{G} \times \emptyset \times S_g \times {}^{1}/_{B_g}\ (scf) \qquad 3.4$$

Where $GRV = \text{Area} \times \text{Height}$

${}^{N}/_{G} = \text{Net To Gross.}$

$\emptyset = \text{Porosity.}$

$S_g = \text{Gas Saturation.}$

$B_g = \text{Gas formation factor (0.98 was the constant used).}$

$B_o = \text{Oil formation factor (1.17 was the constant used).}$

$S_o = \text{Oil Saturation.}$

3.5.3 Synthetic Seismogram and Well-to-Seismic Tie

To ensure that the horizons to be selected on the seismic sections are correct and really representative of the horizon picked on the well logs, this method (well-seismic tie) was carried out (based on good Petrophysical characteristics). It is employed to fix time shifts in the log signatures connected to the seismic data. Acoustic impedance was calculated using density and sonic velocity logs as the product of density and velocity, from which the reflection coefficient was derived. A synthetic seismogram was generated from the reference well by convolution of the reflection coefficient with a fundamental wavelet (Ricker wavelet) taken from the seismic volume. The fundamental input logs, the produced acoustic impedance log, the reflection coefficient, the synthetic seismogram, and the seismic trace are all displayed in Figure 3.7.

3.5.4 Fault Mapping

To understand the hydrocarbon-trapping mechanism in the structure, fault mapping is essential. The mapping of faults is most probably a severe problem in seismic exploration. Faults are mapped on the inlines across the seismic sections (Figures 3.8(a), 3.8(b), and 3.9). A total of twenty-nine faults including two major faults and 26 minor faults were discovered. To understand the pattern of faults in the area of study, the fault trends are selected on several seismic lines and mapped.

3.5.5 Horizon Mapping

It is much easier to display the wells on the seismic section and display the top of the mapped res ervoirs on seismic after the correlation of potential reservoirs from the qualitative interpretation f rom the well section and well to seismic tie. The seismic trough is traced in a grid pattern for the goal of horizon mapping over the entire 3D seismic volume without crossing into different cycles even though some of these horizons appear to have ended along certain chaotic reflections that were considered to be shale diapirs (Figures 3.9, 3.10(a), and 3.10(b) respectively).

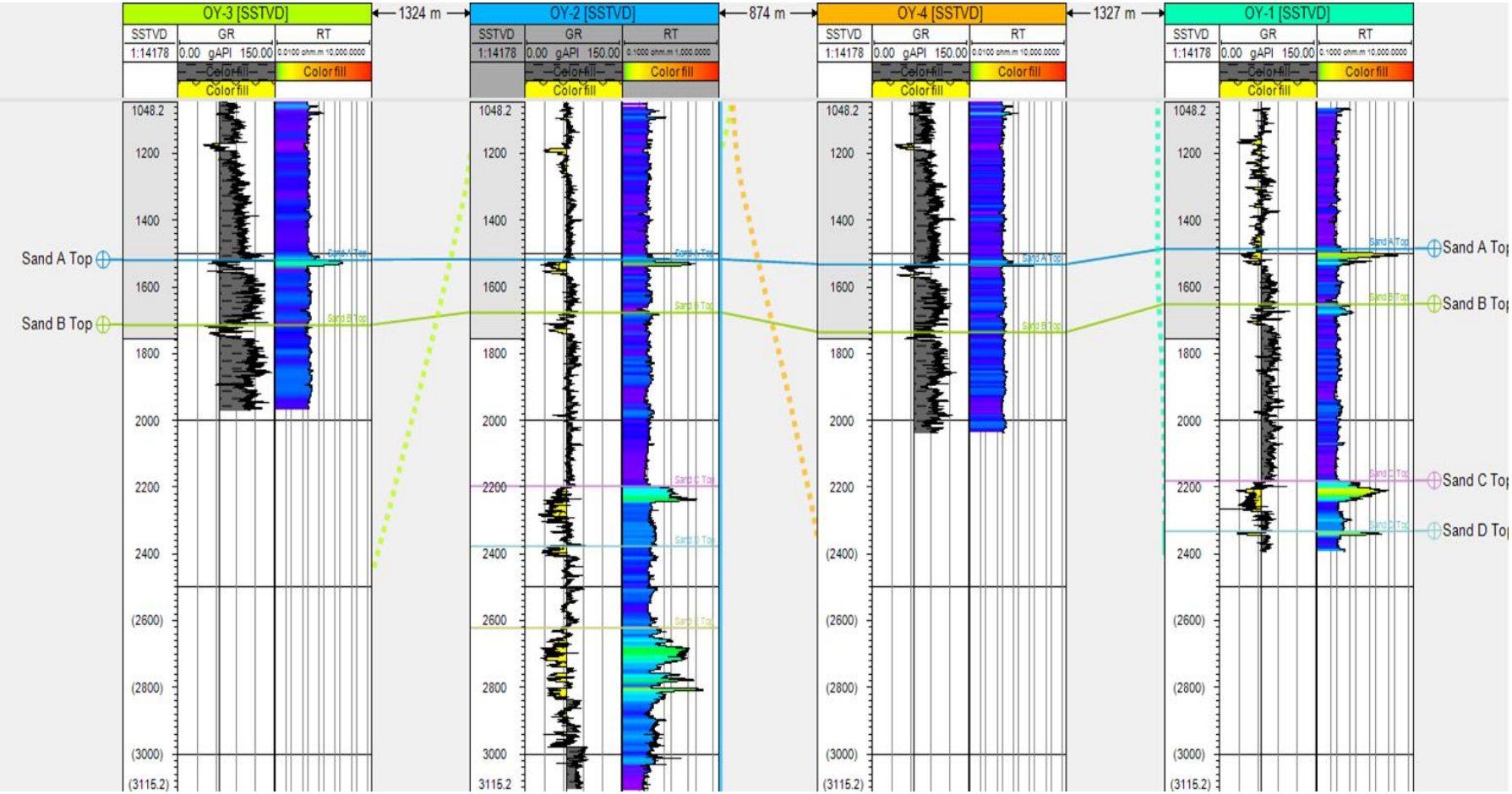

Figure 3.6: Well Section showing Lithological Correlation across all well.

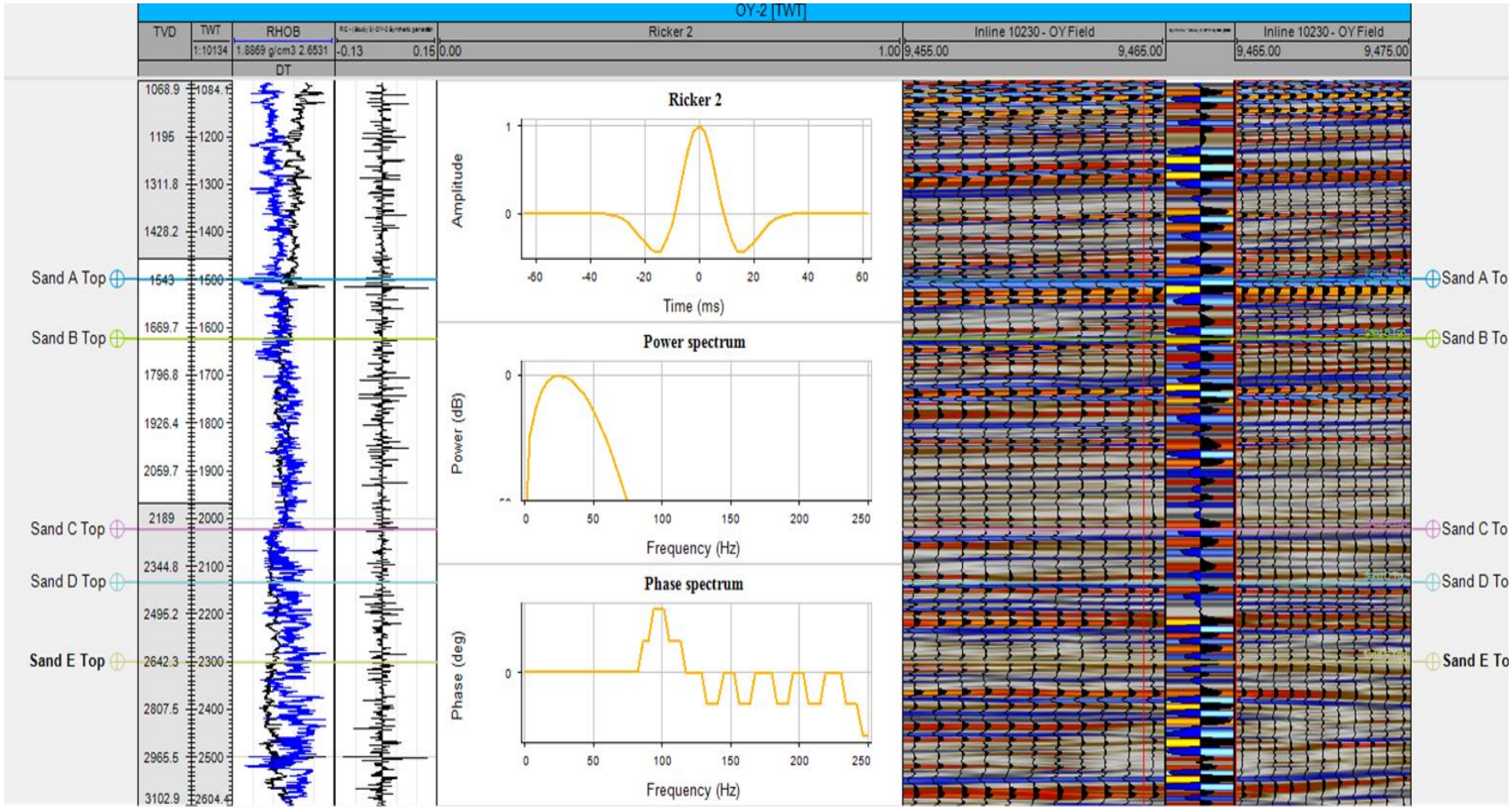

Figure 3.7**:** Synthetic Generation.

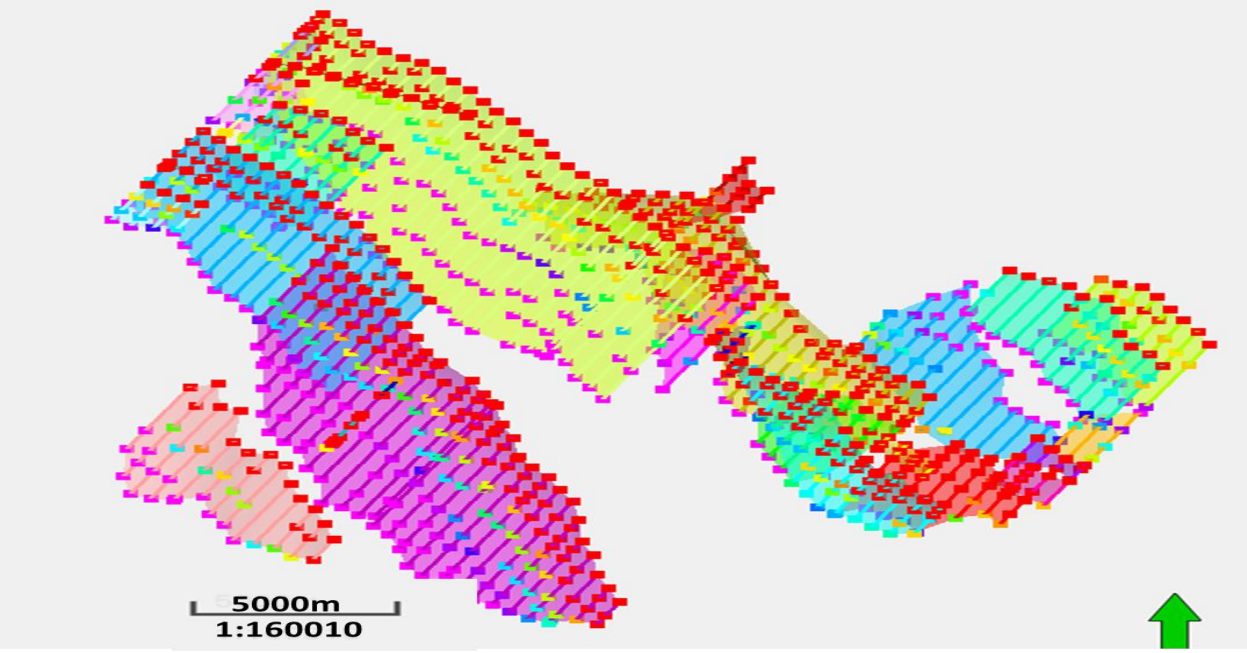

Figure 3.8(a): Interpreted Fault sticks in 2D view.

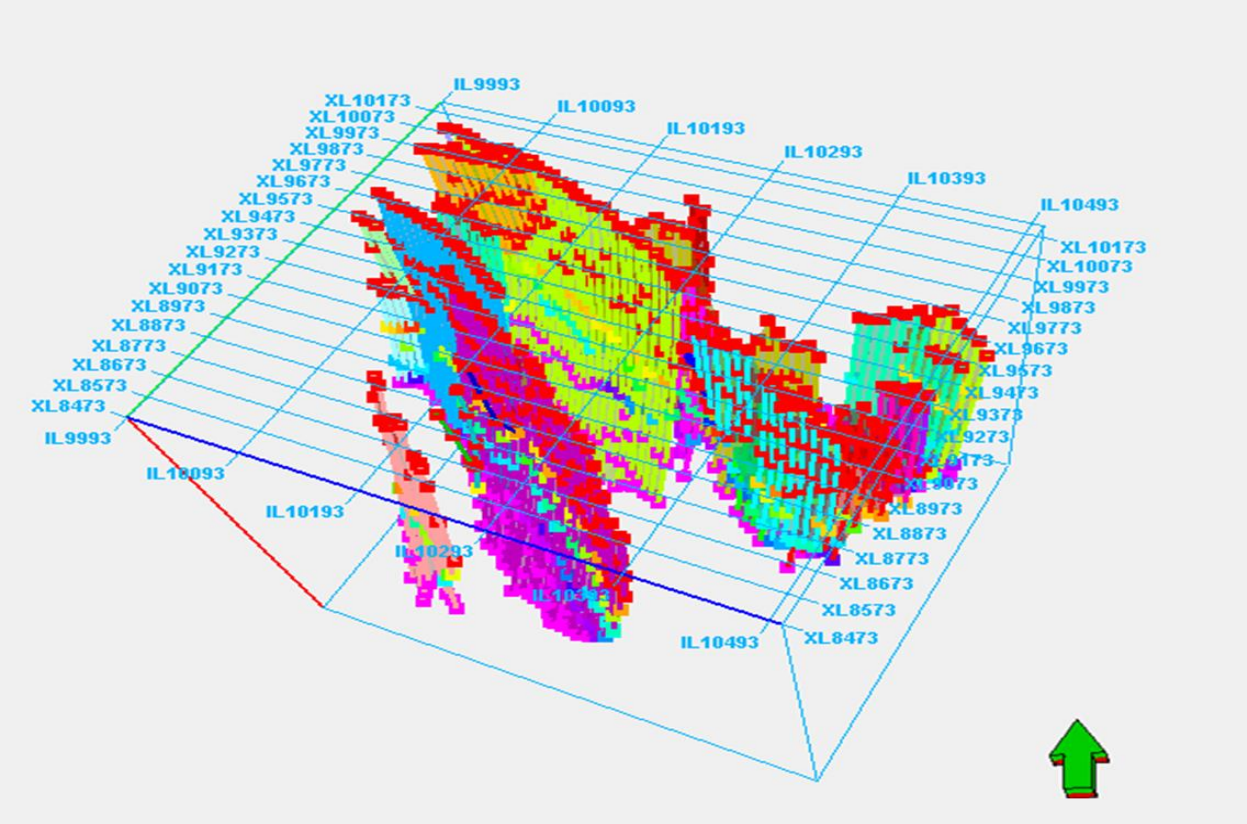

Figure 3.8(b): 3D view of the interpreted fault sticks showing their position in the survey area.

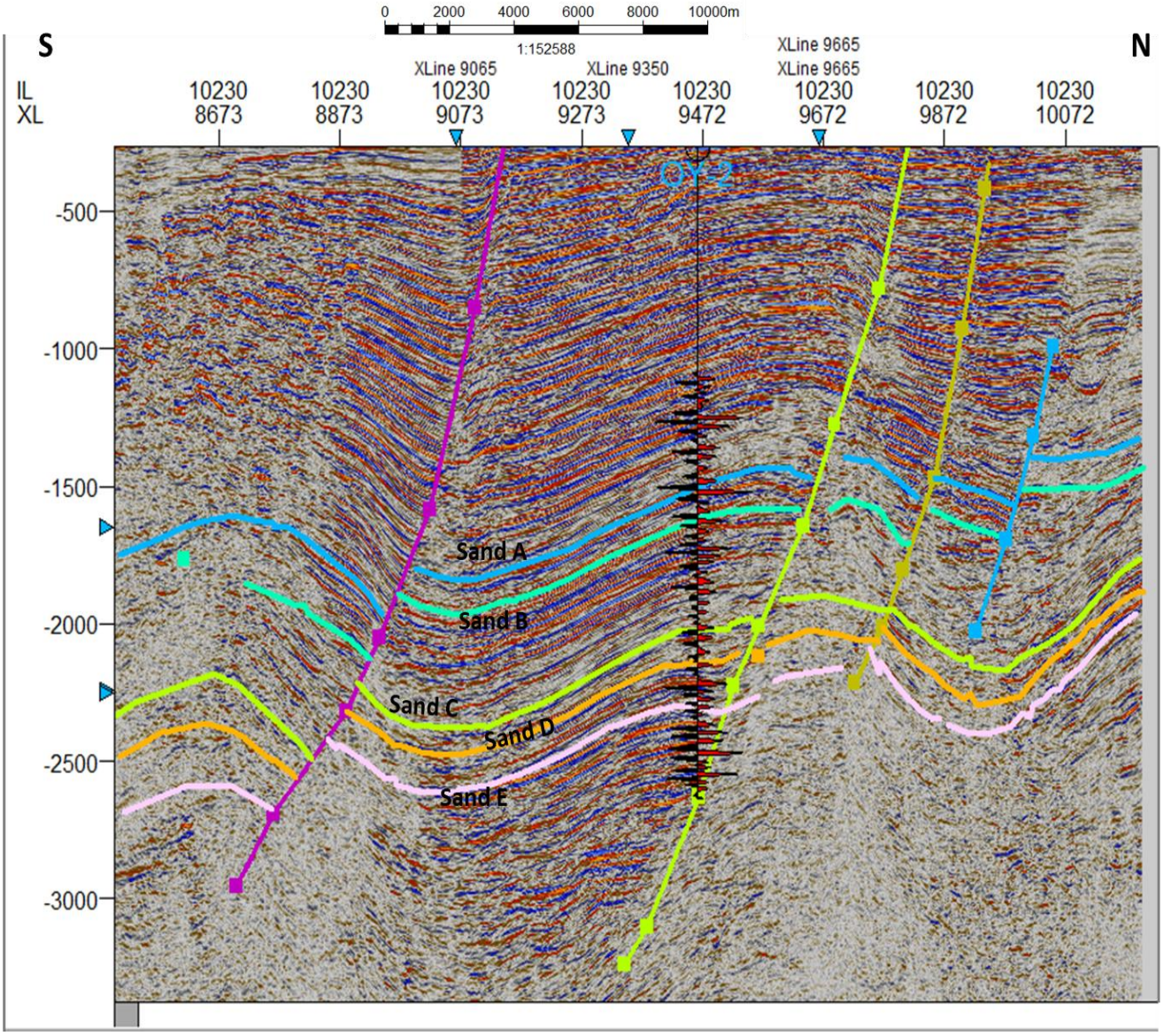

Figure 3.9: Seismic Section (inline 10230) showing the faults and horizons mapped across the seismic volume.

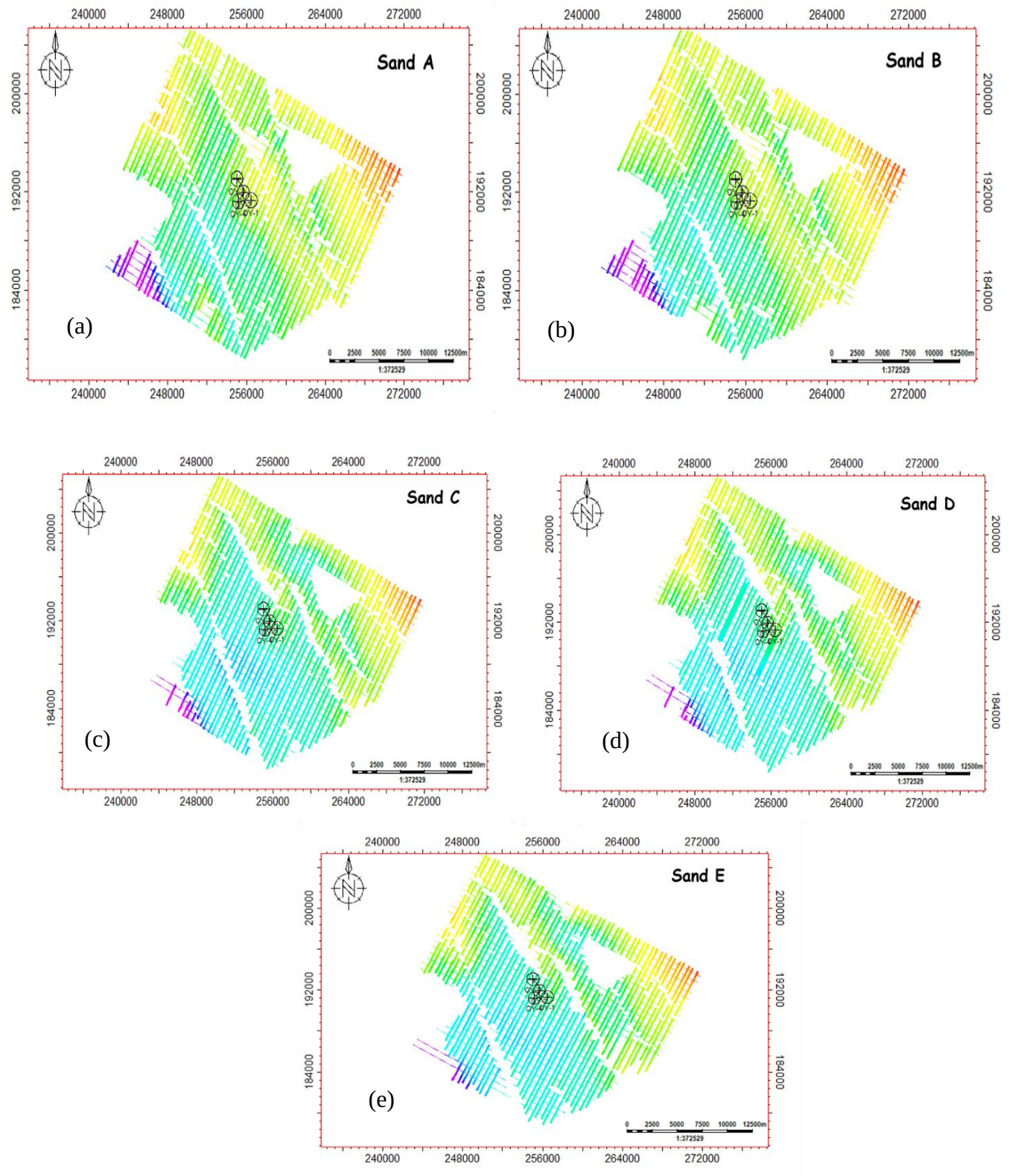

Figure 3.10(a) to 3.10(e): Showing the mapped OY Sand Top A, B C, D and E Horizons.

3.5.6 Time structural maps

Time structural maps (Figure 3.12(a)) were generated using the faults and horizons identified across the seismic. By connecting points of equal time (ms) separated by intervals of 25ms, contouring was created. The time value each colour represents is displayed in the colour legends in Figure 3.12(a), which was used to identify points with the same or equivalent times.

3.5.7 Depth structural maps

A velocity model derived from the checkshot data was used to generate depth maps (Figure 3.12 (a)). Using Microsoft Excel 2013, the time-depth conversion was done by plotting the depth (*ft*) against time (ms). Afterwards, an equation (Figure 3.11) was generated which was used for the conversion. Figure 3.5 shows the relationship between time (x axis) and depth (y axis).The time map was converted into depth structural map by entering the equation $y = 0.0001x^2 + 0.9675x + 113.95$ into the petrel software calculator. Different prospect was identified on the depth structural map. The trapping configuration of the prospects are fault dependent closure, fault supported closure and a four-way closure. The identified prospect that has not been drilled and may serve as new discoveries on OY field.

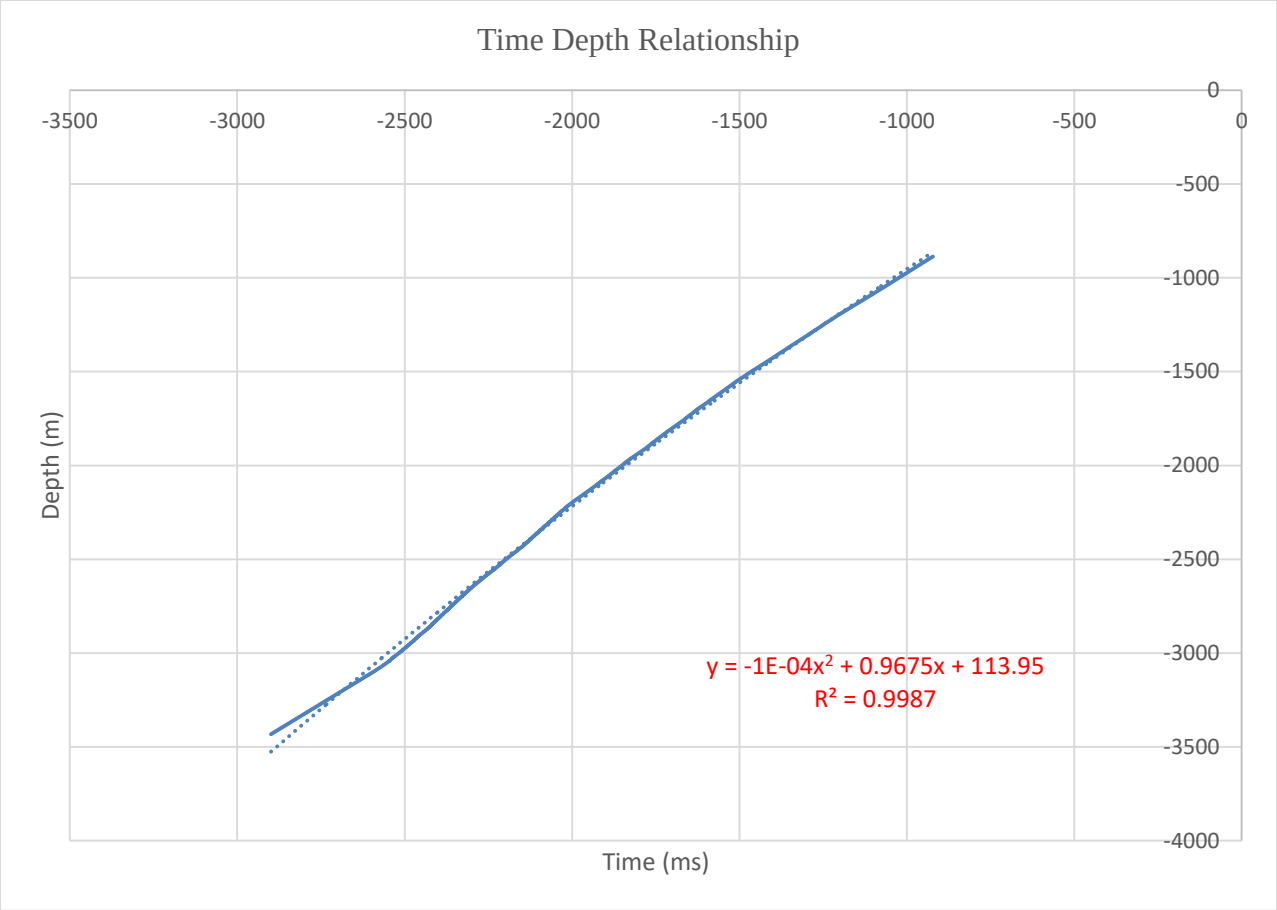

Figure 3.11: Graph showing the relationship between the time, x and the depth, y.

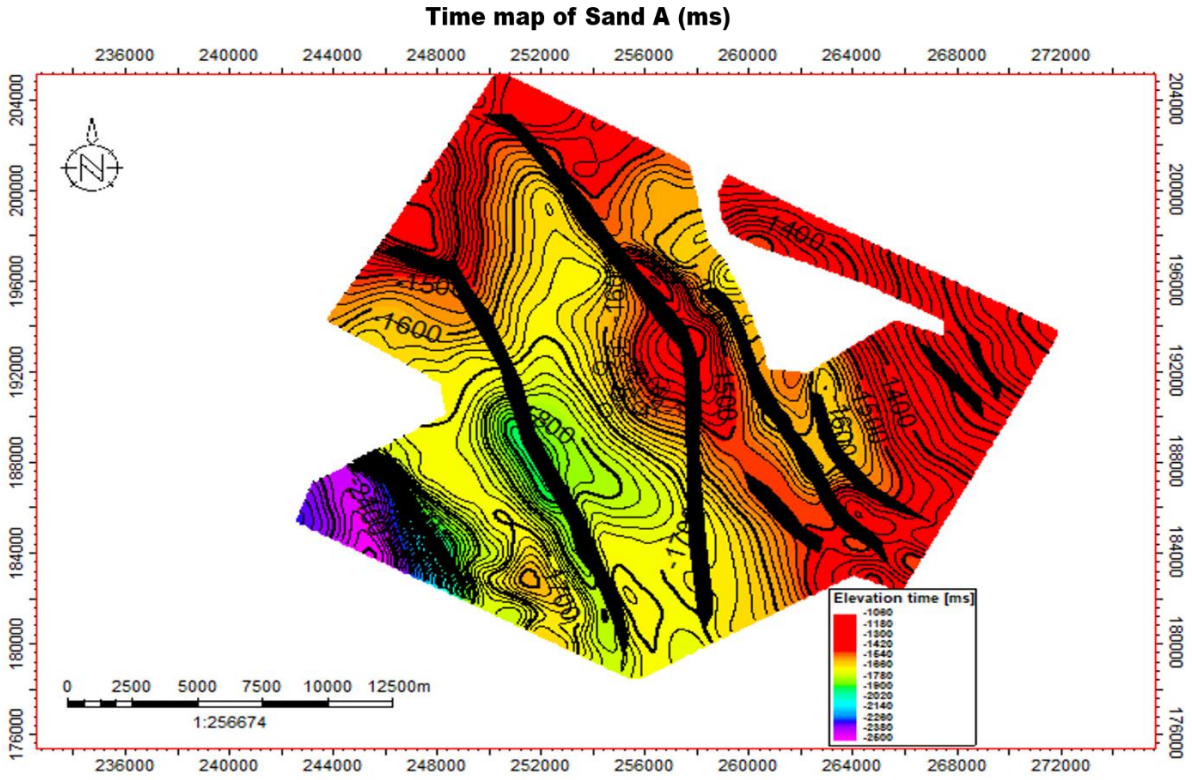

Figure 3.12(a): Time map generated from sand A.

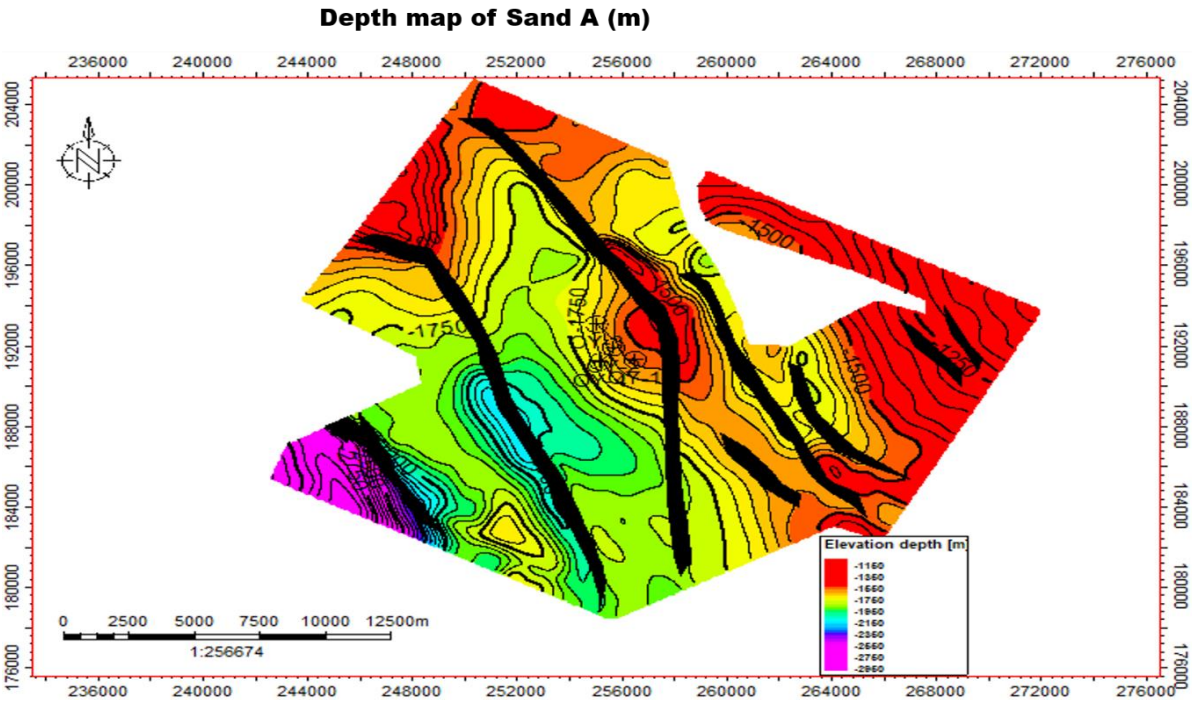

Figure 3.12(b): Depth map generated from sand A.

3.5.8 Seismic Attributes Analysis

The Seismic attributes which include the RMS amplitude, sum of energy, average energy and sum of amplitudes attribute were extracted from the time structural maps (Figure 3.13). The seismic attributes help in the enhancement of data for proper visualization of features of interest in this study and aided interpretation by acting as possible direct hydrocarbon indicator.

3.5.9 Reservoir modelling

The Schlumberger Petrel 2017^{TM} was used for the static reservoir modelling. The workflow and processes for the reservoir modelling are as follows;

3.5.9.1 QC of input parameters

The input consists of interpreted seismic horizons, faults, correlated stratigraphic tops and Petrophysical properties such as net to gross (NTG), porosity and water saturation.

3.5.9.2 Fault Modelling

This is a process whereby seismic interpreted faults are replicated in a 3D reservoir model. The fault modelling is required to carry out the structural modelling. Modelled faults are simple in geometry to reduce distortion to the cells (Figure 3.14).

3.5.9.3 Make External Grid Boundary

This is required to constrain the model's framework.

3.5.9.4 Pillar Gridding

Pillar gridding subdivides the area into cells. A typical areal cell size is 100 x 100 m. But in this project the cell size was reduced to 50 x 50 m to capture more of the heterogeneity within the reservoir. However, as the cell size gets smaller yet, the computer uses more memory. The pillar gridding was conducted in order to build a structural framework for the reservoir.

3.5.9.5 Make Horizons

This is the first subdivision of the stratigraphy. Make horizons subdivides the stratigraphy to the equivalent of a formation or Group. At least two interpreted seismic horizons are necessary to delimit the stratigraphic top and base.

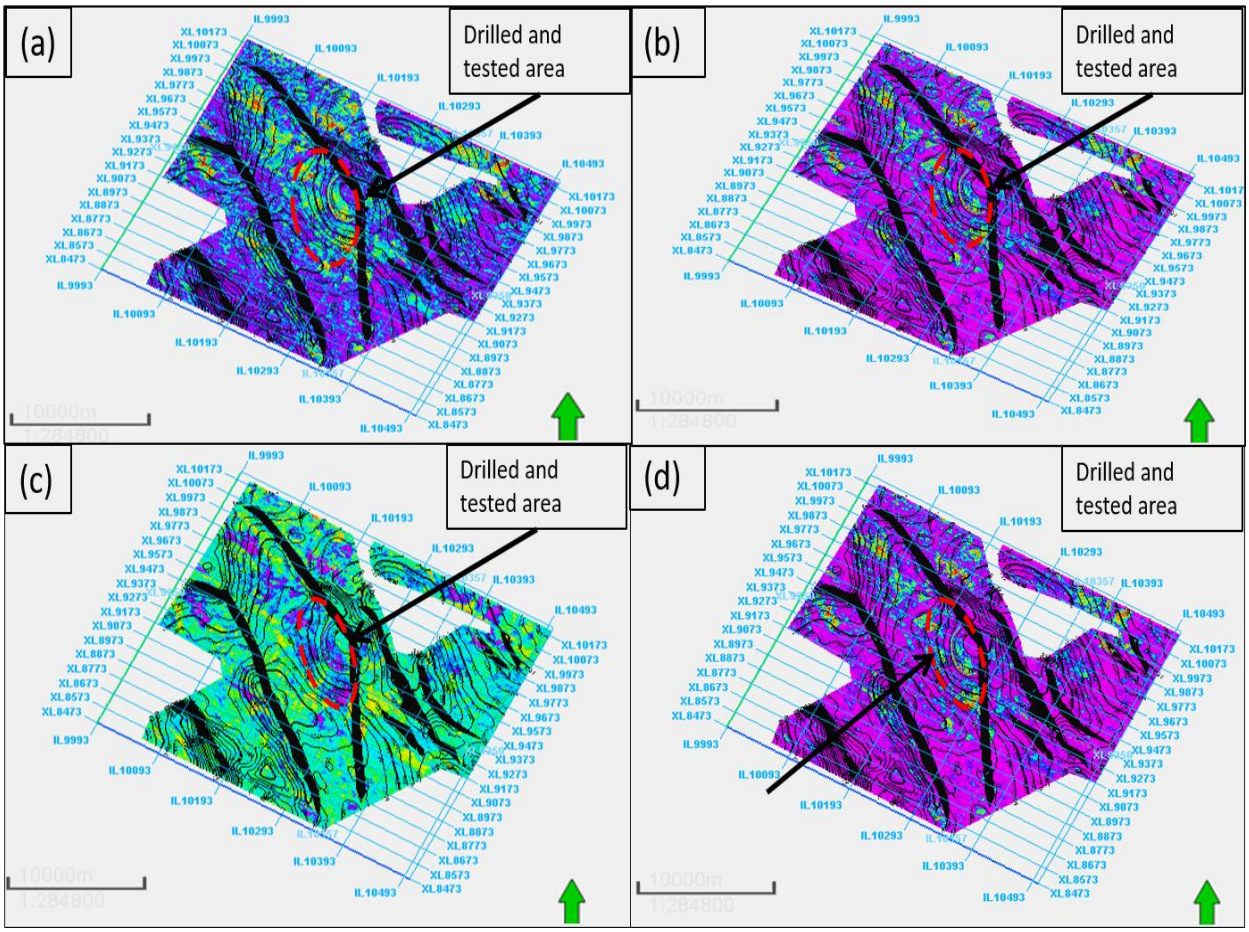

Figure 3.13: Seismic attributes extracted from the time structural map of Sand A characterized with high amplitude in the tested area. (a) RMS amplitude; (b) Sum of energies; (c) Sum of amplitudes; (d) Average energy.

3.5.9.6 Make Zones

Make zones further subdivides the horizons into zones. A zone could represent a reservoir level. Field that are stratigraphically complex requires many zones to control layering of Petrophysical properties. Where a reservoir has multiple contacts, every fluid interaction must be zoned separately.

3.5.9.7 Layering

This is the last subdivision of the stratigraphy. A typical layer height is about 5 ft. Fluid flow simulation demands granular layering. To capture stratigraphic heterogeneity better, fine layering is necessary. Layering could follow unconformities or a simple constant subdivision of a zone.

3.5.9.8 Upscale logs

Petrophysical logs were upscaled to be used for the modelling. The values from the upscaled log average are applied to the well-penetrated cells in the 3D grid, giving each cell a single value. Along the well path, these cells are present. Based on the well log values across the well path, the values are subsequently assigned to the cells.

3.5.9.8 3D petrophysical modelling

After the well logs have the upscaled the next process is the property modelling. For this research project the property distribution was done stochastically using the Sequential Gaussian Simulation (SGS). The spherical variogram was used to distribute properties across the 3D grid.

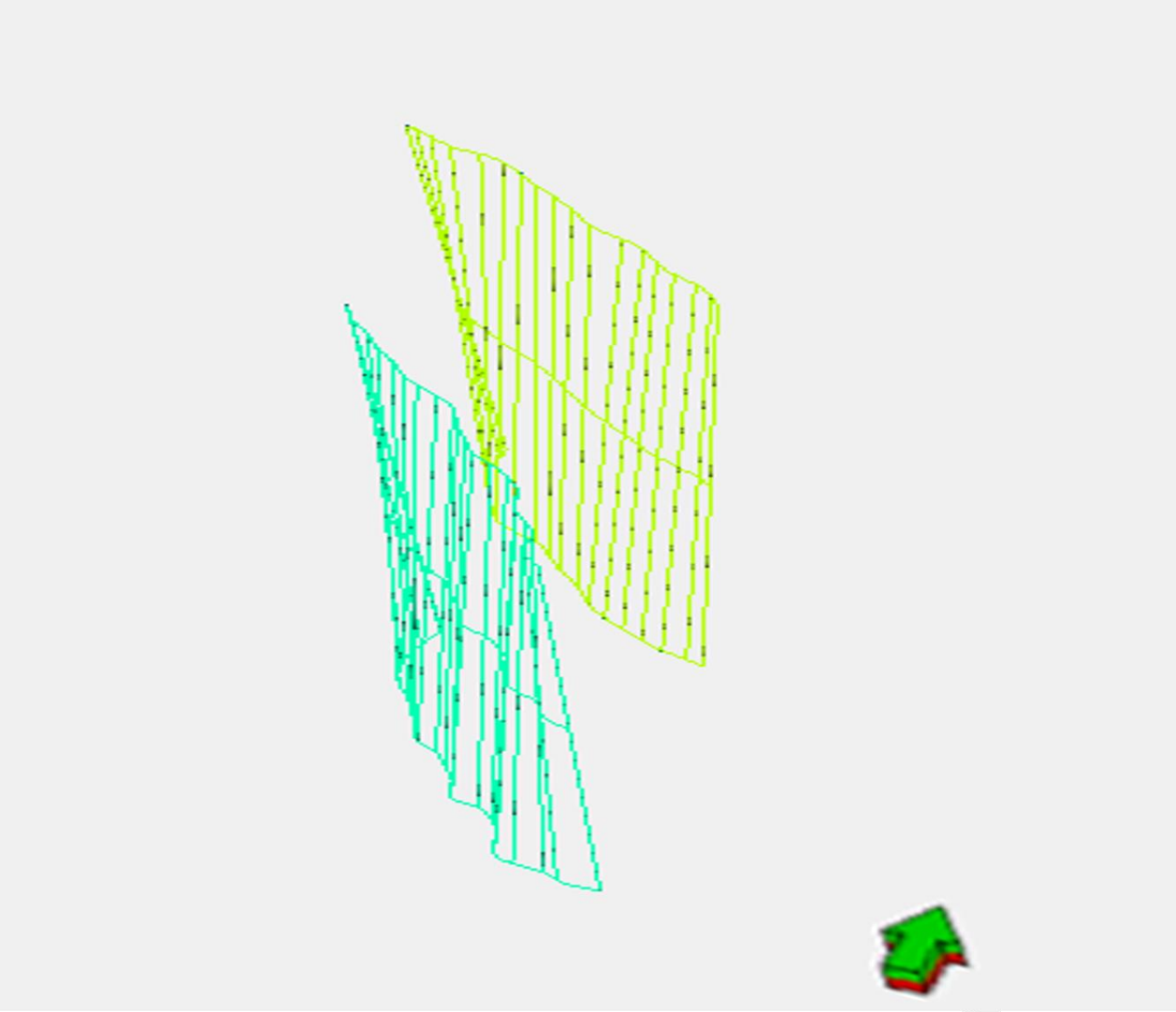

Figure 3.14: Modelled Fault.

CHAPTER FOUR

RESULTS AND DISCUSSION

4.1 Result and Discussion of interpreted Well logs

The results of the reservoir correlation are presented as a correlation panel in Figure 4.1. The results of the petrophysical analysis including porosity, NTG and Water saturation for Sand A to E are presented as a well section in Figures 4.2a to 4.2e respectively while the petrophysical summary is presented in Tables 4.1.

4.1.1 Discussion of Reservoir correlation

From the well log interpretation and knowledge of the geology of the area, the available suite of wireline logs shows two main lithological facies in the study area. The two main lithofacies are interpreted as sandstone and shale respectively. The gamma ray log, deep resistivity log and neutron-density logs reveal the sandstone facies to be hydrocarbon bearing. The hydrocarbon sands are characterized by low gamma ray, high resistivity, and negative separation of neutron-density logs. Figure 4.1 shows the delineated reservoir units (Sand A, B, C, D and E) were correlated across the well from North to South. It is evident that Sand A and B are continuous across all the wells and with relatively similar thickness. Wells OY-02 and 01 encountered Sand C and D while Well OY-02 is deep enough to encounter Sand E.

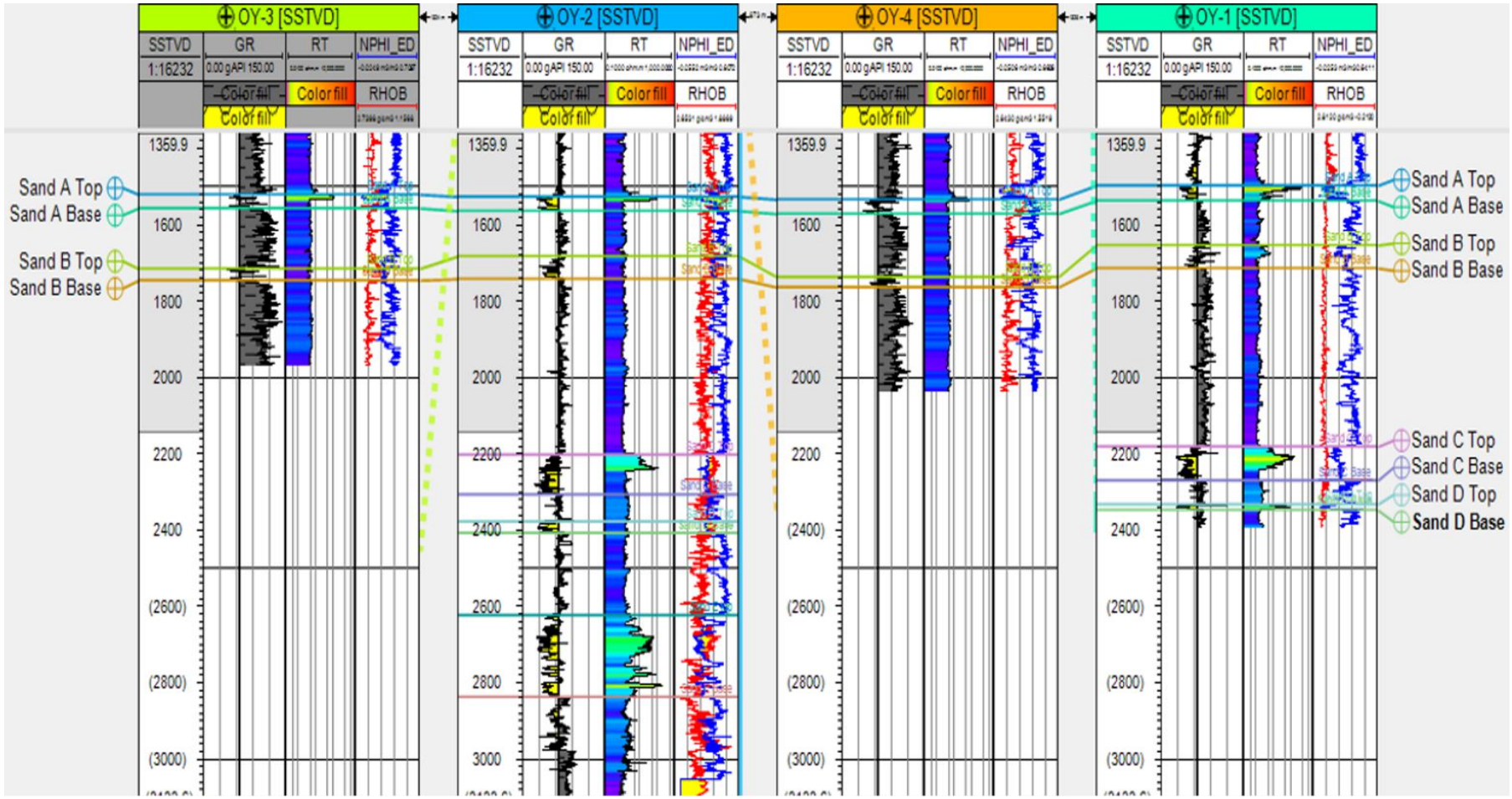

Figure 4.1: Lithostratigraphic correlation of wells arranged in N-S direction showing the top and base of the hydrocarbon bearing reservoirs.

4.1.2 Discussion of Petrophysical Results

The petrophysical properties were calculated for each reservoir in the five reservoirs of each well (Figure 4.2(a), 4.2(b), 4.2(c), 4.2(d) and 4.2(e)) is summarized in (Table 4.1). The results are presented and discussed as follows:

Sand A: Sand A was penetrated by all four (4) wells OY-01, OY-02, OY-03 and OY-04. The reservoir thickness ranges from about 33 – 42.54 m and GWC is at 1540 m. The average porosity of Sand A is 0.37 and net to gross is 0.72 which signifies very good reservoir properties. High resistivity signatures can be observed within this reservoir (Fig 4.2(a), Track 2) indicating presence of hydrocarbon. From the Neutron-Density overlay, (Fig 4.2(a), Track 3) it can be observed that the hydrocarbon within this reservoir section is mainly gas because of the "balloon effect". Sand A water saturation is estimated to be 0.40.

Sand B: is penetrated by well OY-01, OY-02 and OY-03. The reservoir thickness on Sand B ranges from 30.85 - 61.08 m. Sand B average porosity is 0.37 and net to gross is 0.62 which signifies good reservoir properties. High resistivity signatures can be observed within this reservoir (Fig 4.2(b), Track 2) indicating presence of hydrocarbon. From the Neutron-Density overlay (Fig 4.2(b), Track 3) it can be observed that the hydrocarbon within this reservoir section is mainly oil because the neutron-density log tracks on each other. The water saturation is estimated to be 0.65.

Sand C: Sand C was penetrated by only well OY-01 and OY-02. The reservoir thickness on Sand C ranges from 84.98 - 98.99 m and OWC is at 2245 m. The average porosity of Sand C is 0.34 and net to gross is 0.78 which signifies very good reservoir properties. High resistivity signatures can be observed within this reservoir (Fig 4.2(c), Track 2) indicating presence of hydrocarbon, From the Neutron-Density overlay, (Fig 4.2(c), Track 3). The hydrocarbon within this reservoir section is mainly oil. The water saturation is estimated to be 0.45.

Sand D: Sand D was penetrated by only well OY-01 and OY-02. The reservoir thickness on Sand D ranges from 15.94 - 29.29 m. Sand C average porosity is 0.31. The net to gross is 0.66 which signifies good reservoir properties. High resistivity signatures can be observed within this reservoir (Fig 4.2(d), Track 2) indicating presence of hydrocarbon. From the Neutron-Density overlay (Fig 4.29(d), Track 3) it can be observed that the hydrocarbon within this reservoir

section is mainly oil because the neutron-density log tracks on each other. The water saturation is estimated to be 0.362.

Sand E: Sand E was penetrated only by well OY-02 which is the deepest well. The reservoir thickness of Sand E is 213.9 m. Sand E porosity is 0.301. The net to gross is therefore 0.71 which signifies very good reservoir properties. High resistivity signatures can be observed within this reservoir (Fig 4.2e, Track 2) indicating presence of hydrocarbon. From the Neutron-Density overlay (Fig 4.2e, Track 3) it can be observed that the hydrocarbon within this reservoir section is also oil because the neutron-density log tracks on each other. Sand E water saturation is estimated to be about 0.42.

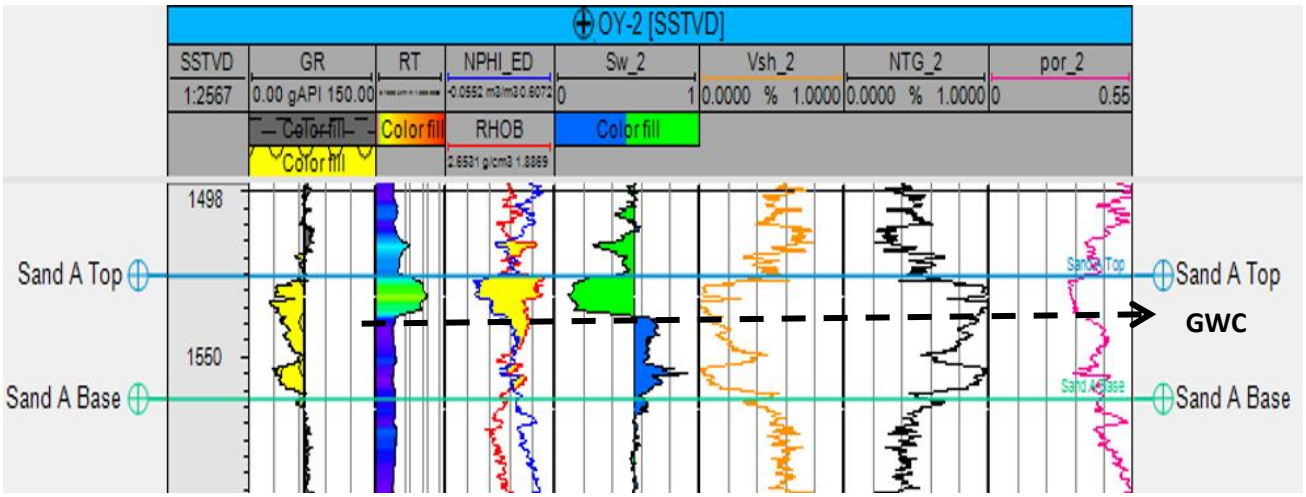

Figure 4.2(a): OY-02 well showing petrophysical properties for reservoirs Sand A.

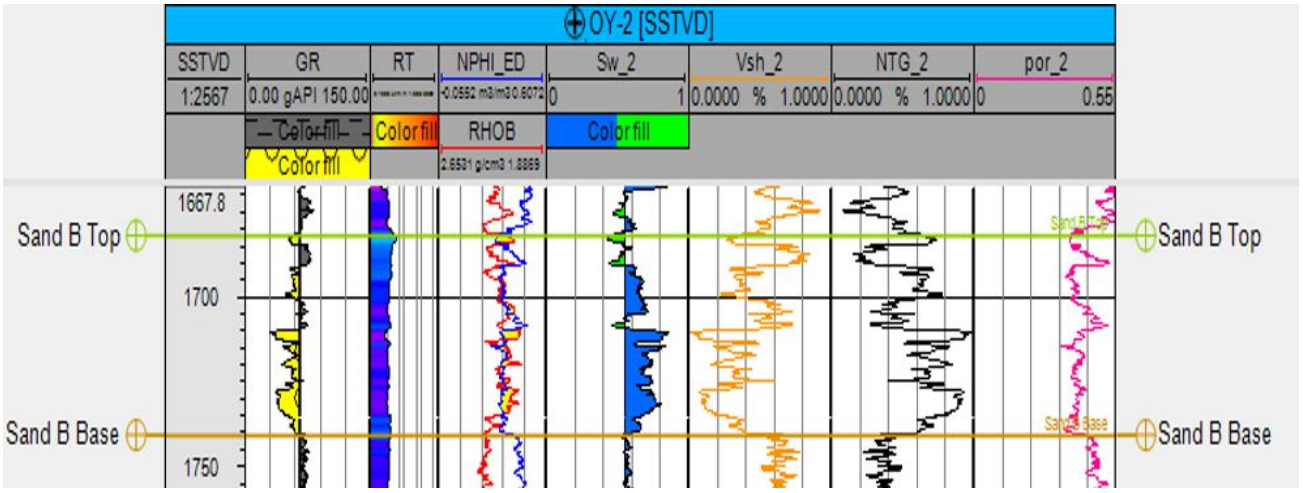

Figure 4.2(b): OY-02 well showing petrophysical properties for reservoirs Sand B

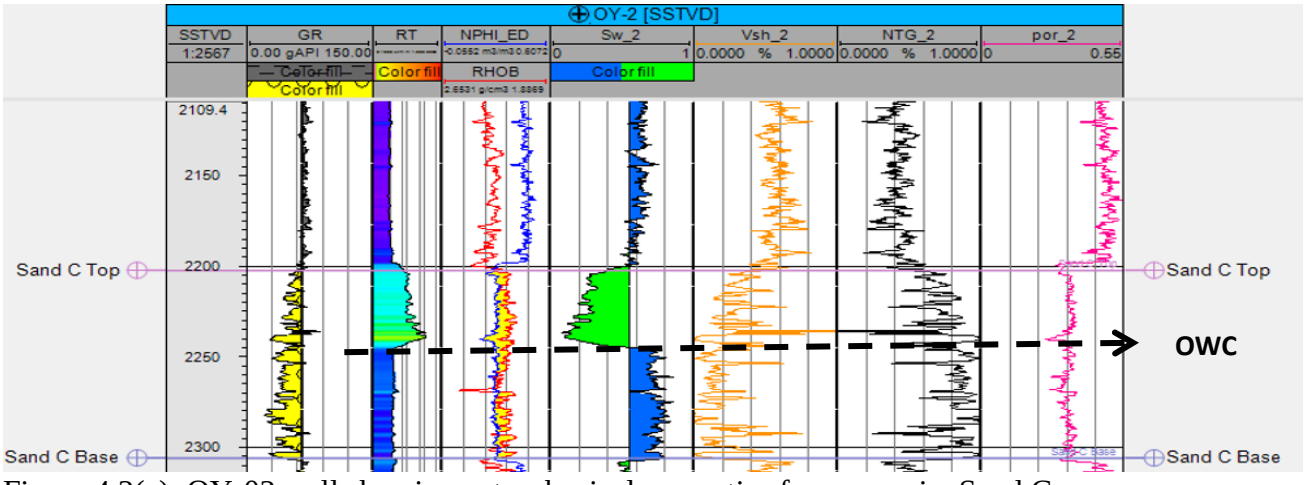

Figure 4.2(c): OY-02 well showing petrophysical properties for reservoirs Sand C.

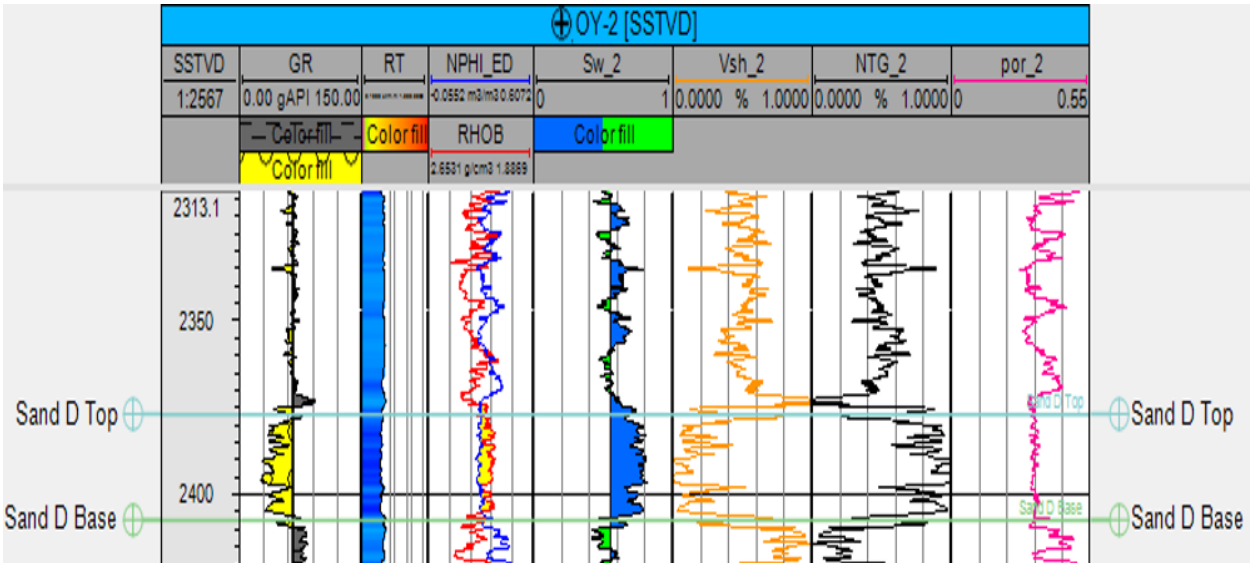

Figure 4.2(d): OY-02 well showing petrophysical properties for reservoirs Sand D.

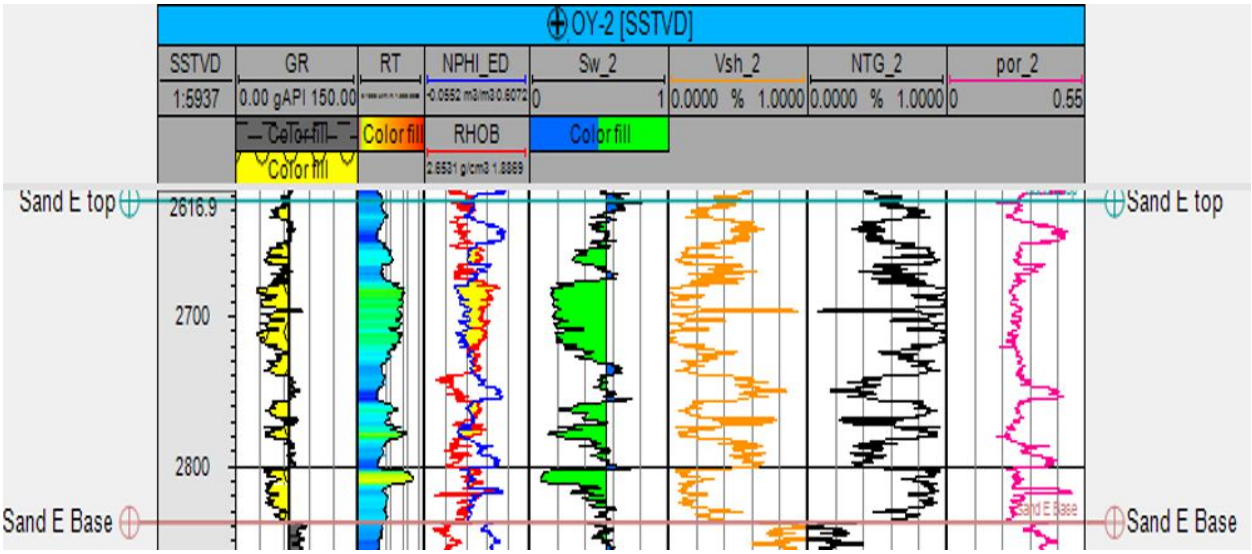

Figure 4.2(e): OY-02 well showing petrophysical properties for reservoirs Sand E.

Table 4.1: Summarized petrophysical properties of all the reservoirs for each well.

Reservoirs	**Top (m)**	**Base(m)**	**Gross Thickness(m)**	**NTG**	S_w	ϕ
Sand A	1496.95	1536.8	39.85	0.818	0.242	0.368
Sand B	1653.63	1714.71	61.08	0.59	0.574	0.369
Sand C	2182.09	2267.07	84.98	0.792	0.372	0.352
Sand D	2330.8	2346.74	15.94	0.58	0.307	0.286
			OY-02			
Reservoirs	**Top (m)**	**Base(m)**	**Gross Thickness(m)**	**NTG**	S_w	ϕ
Sand A	1521.09	1563.63	42.54	0.794	0.5132	0.387
Sand B	1682.85	1740.6	57.75	0.618	0.652	0.408
Sand C	2202.56	2301.55	98.99	0.775	0.524	0.333
Sand D	2377.78	2407.07	29.29	0.75.8	0.72	0.328
Sand E	2622.7	2836.6	213.9	0.707	0.417	0.301
			OY-03			
Reservoirs	**Top (m)**	**Base(m)**	**Gross Thickness(m)**	**NTG**	S_w	ϕ
Sand A	1521.66	1554.66	33	0.574	0.447	0.342
Sand B	1713.45	1744.3	30.85	0.649	0.749	0.374
			OY-04			
Reservoirs	**Top (m)**	**Base(m)**	**Gross Thickness(m)**	**NTG**	S_w	ϕ
Sand A	1532.77	1570.35	37.58	0.729	0.55	0.437

4.2 Result and Discussion of 3D Seismic Reservoir Characterization

The results of the gridded mapped horizons of the reservoir tops of Sand A, B, C, D, and E are presented as time structural maps in Figure 4.3(a),4.4(a),4.5(a),4.6(a), and 4.7(a) The results of the depth structural maps that were derived from time structural maps using the TDR are as presented in Figure 4.3(b),4.4(b),4.5(b),4.6(b), and 4.7(b). Meanwhile, the result of the seismic attribute analysis which includes RMS, sum of energies, sum of amplitudes and average energy carried out on each of the mapped horizons for possible anomalies that may be indicative of fluid or lithological distribution is presented in Figures 4.3(c),4.4(c),4.5(c),4.6(c), and 4.7(c)

4.2.1 Sand A

The structural time and depth map result for sand A is shown in figure 4.3(a) and figure 4.3(b) respectively. The depth structural map shows contour intervals of 30 m. The colour legend shows differences in elevation on the map. A drilled and tested area is identified on the map alongside five prospective traps (Figure 4.3(b)). The drilled and tested area on this reservoir can be classified as a fault dependent trap. Also, prospects one, two, three and four are classified to be a fault assisted trap (Fig 4.3b). While the prospect five is a four-way closure.

Meanwhile, the results of the seismic attribute analysis of Sand A have shown high amplitude anomalies around the tested prospect and this has further supported the presence and possible extent of hydrocarbon within the reservoir (Fig 4.3c). However, it can be observed that the identified prospects have displayed significant amplitude anomalies on the seismic attribute analysis.

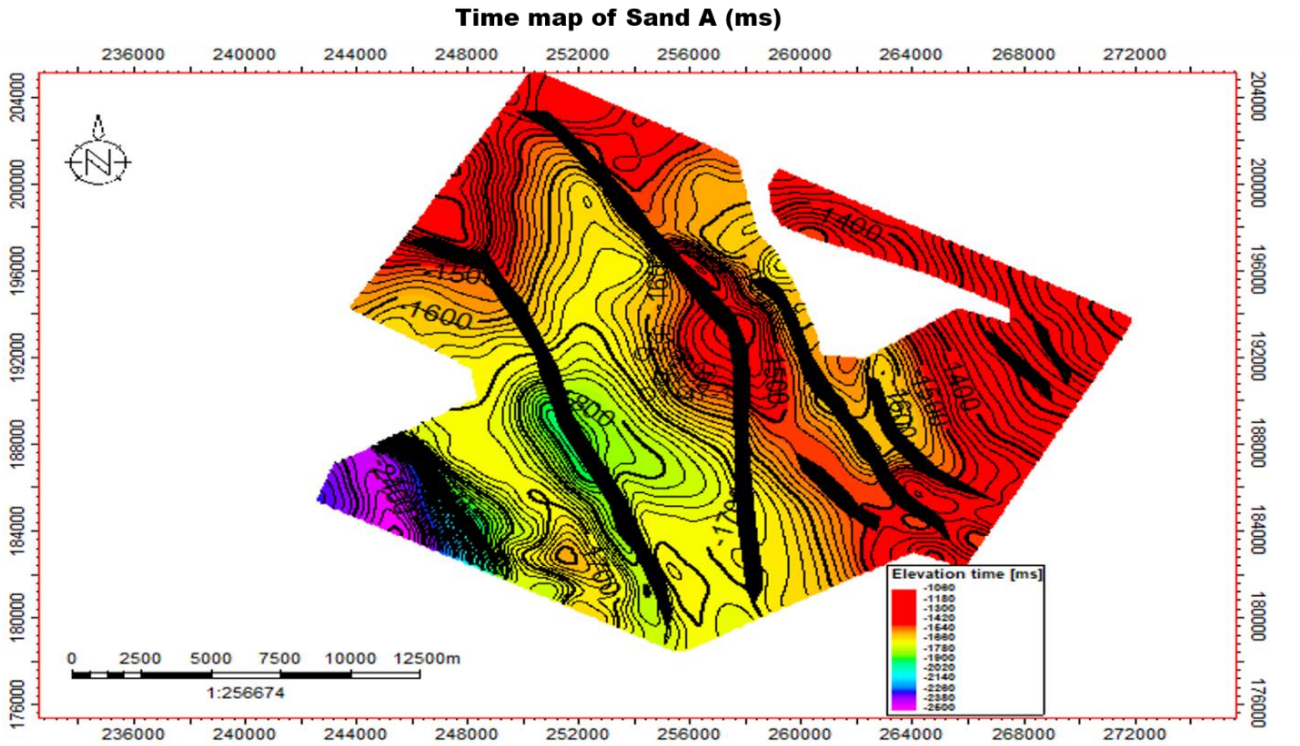

Figure 4.3(a): Time structure map for sand A.

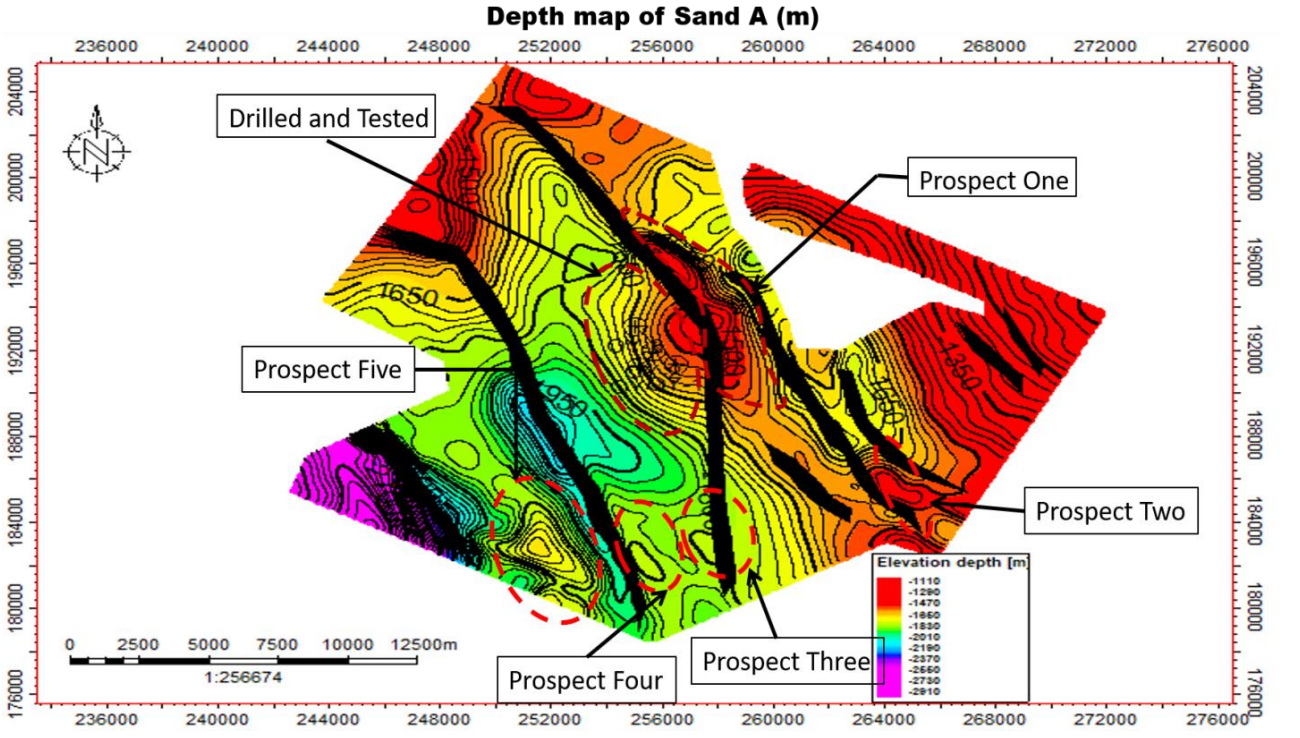

Figure 4.3(b): Depth structure map for sand A showing the showing the various prospects.

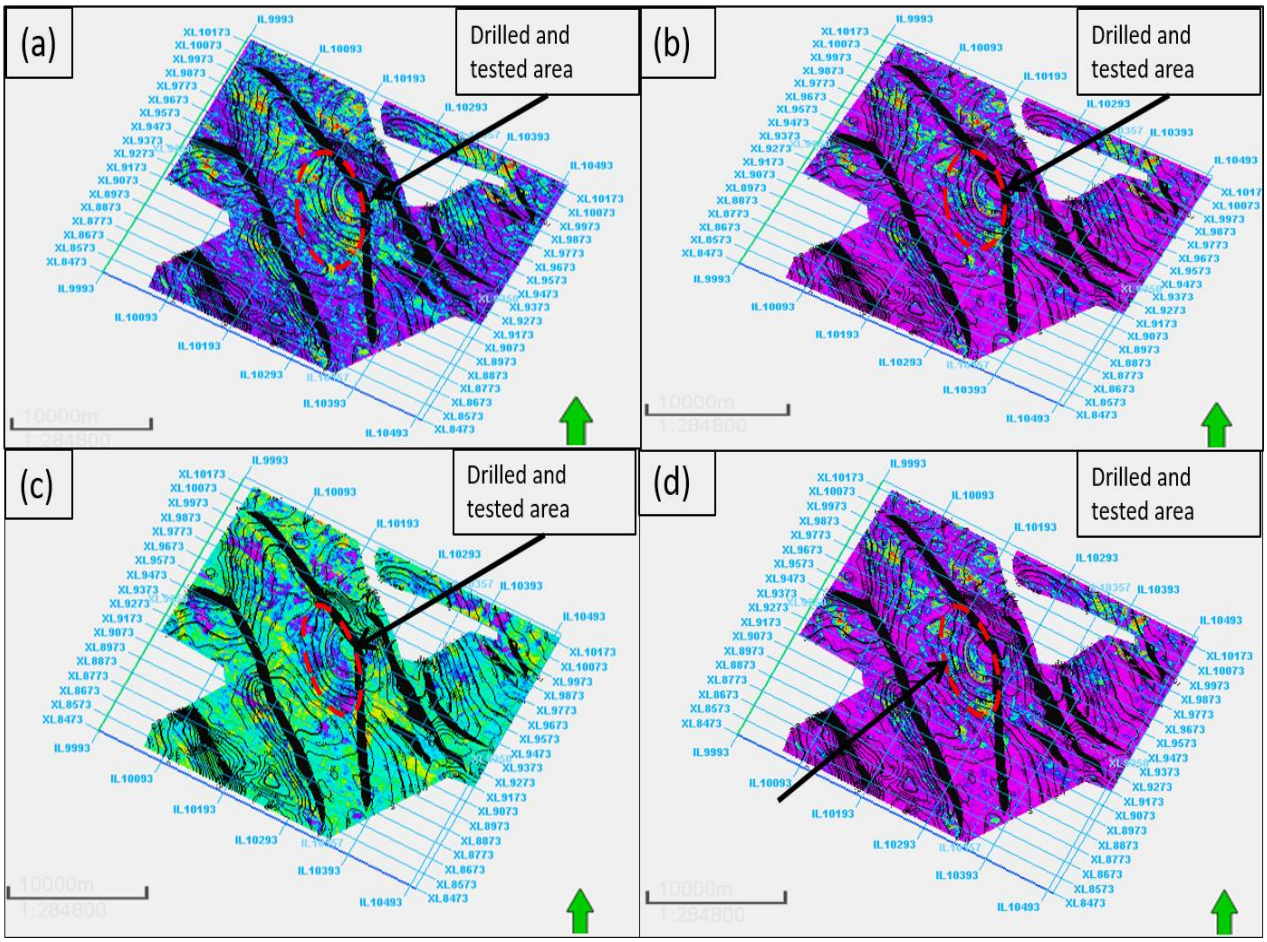

Figure 4.3(c): Seismic attributes of sand A characterized with high amplitude in the tested area. (a) RMS amplitude; (b) Sum of energies; (c) Sum of amplitudes; (d) Average energy.

4.2.2 Sand B

The structural time and depth map for sand B is shown in figure 4.4(a) and figure 4.4(b) respectively. The depth structural map shows contour intervals of 30 m. The colour legend shows differences in elevation on the map. A drilled and tested area is identified on the map alongside four prospective (Figure 4.4(b)). The drilled and tested area on this reservoir can be classified as a fault dependent trap. Also, prospects one, two and three are classified to be a fault assisted trap while prospect four is classified to be a four-way closures.

The results of the seismic attribute analysis have shown high amplitude anomalies around the tested prospect and this has further supported the presence and possible extent of hydrocarbon within the reservoir (Fig 4.4(c)). However, it can be observed that the identified prospects have displayed significant amplitude anomalies on the seismic attribute analysis.

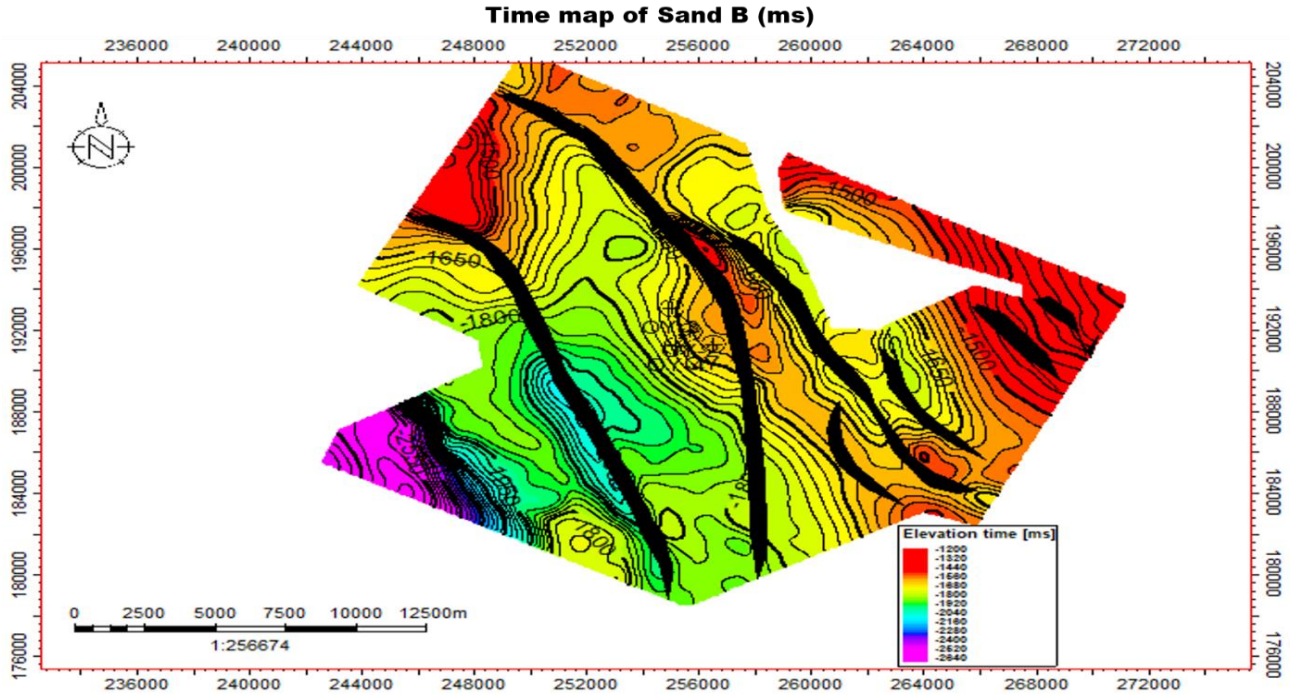

Figure 4.4(a): Time structure map for sand B.

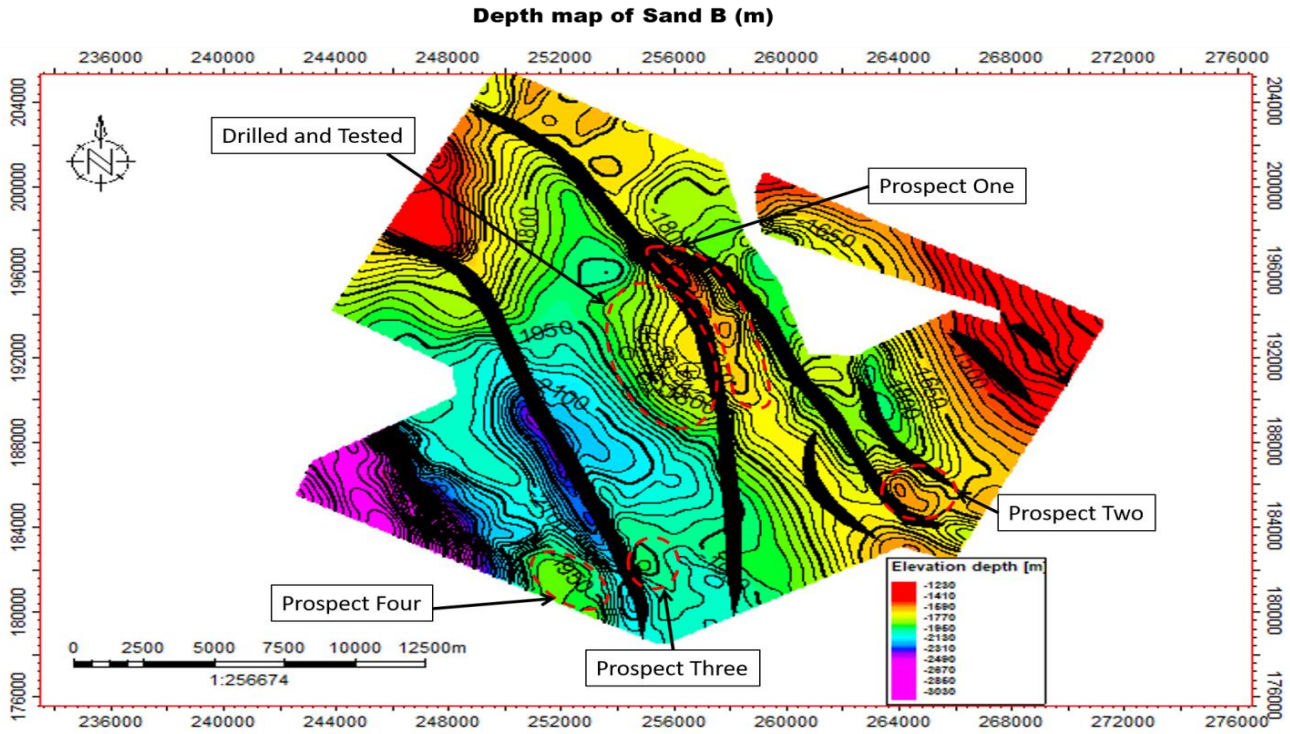

Figure 4.4(b): Depth structure map for sand B showing the showing the various prospects.

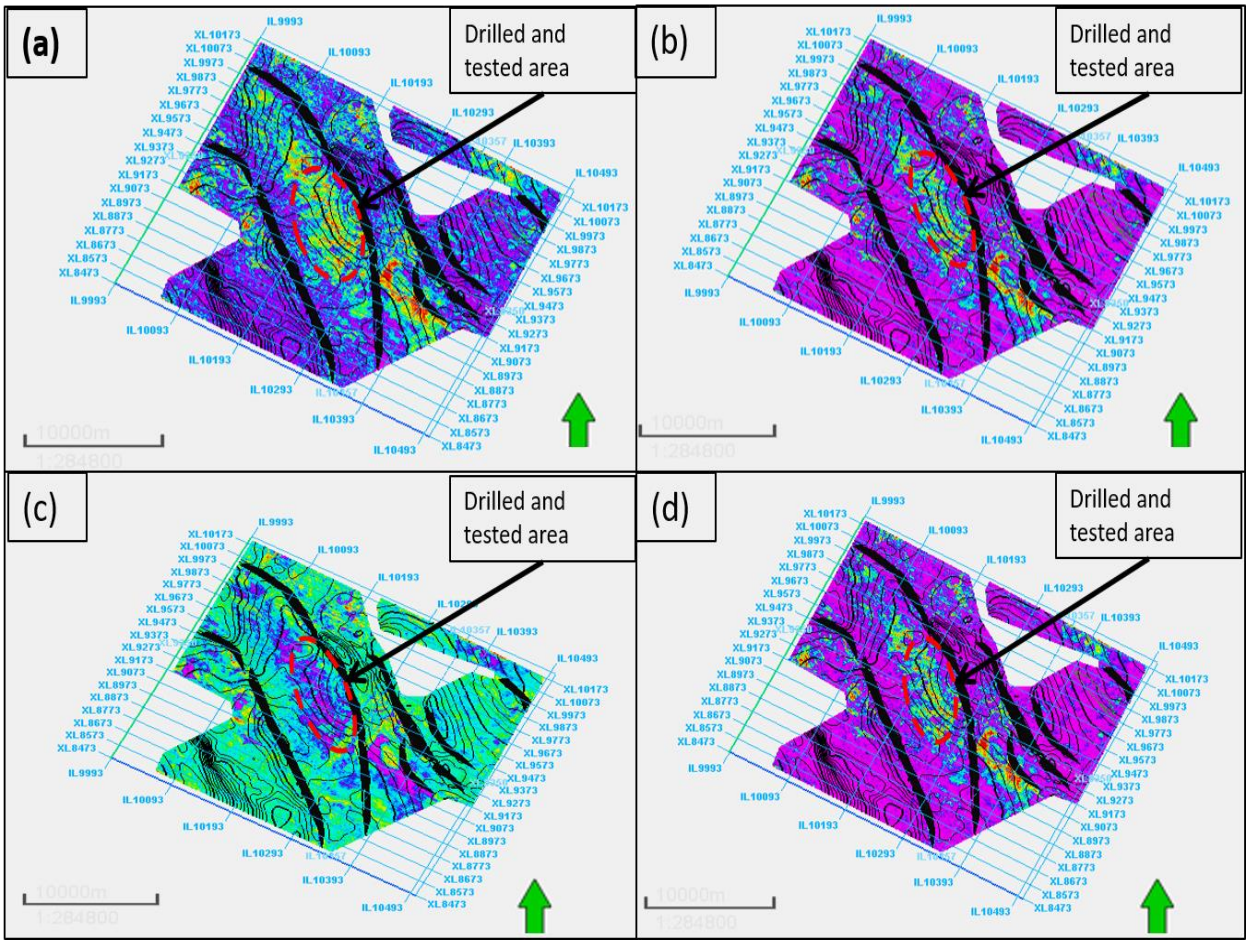

Figure 4.4(c): Seismic attributes of sand B characterized with high amplitude in the tested area. (a) RMS amplitude; (b) Sum of energies; (c) Sum of amplitudes; (d) Average energy.

4.2.3 Sand C

The structural time and depth map for sand C is shown in figure 4.5(a) and figure 4.5(b) respectively. The depth structural map shows contour intervals of 30 m. The colour legend shows differences in elevation on the map. The drilled and tested area is identified on the map alongside three prospective traps (Figure 4.5(b)). The drilled and tested area on this reservoir can be classified as a fault dependent trap. Also, prospects one and two are fault assisted traps while the prospect three is classified to be a four-way closures.

The results of the seismic attribute analysis have shown high amplitude anomalies around the tested prospect and this has further supported the presence and possible extent of hydrocarbon within the reservoir (Fig 4.5(d)). However, it can be observed that the identified prospects of Sand C have displayed significant amplitude anomalies on the seismic attribute analysis.

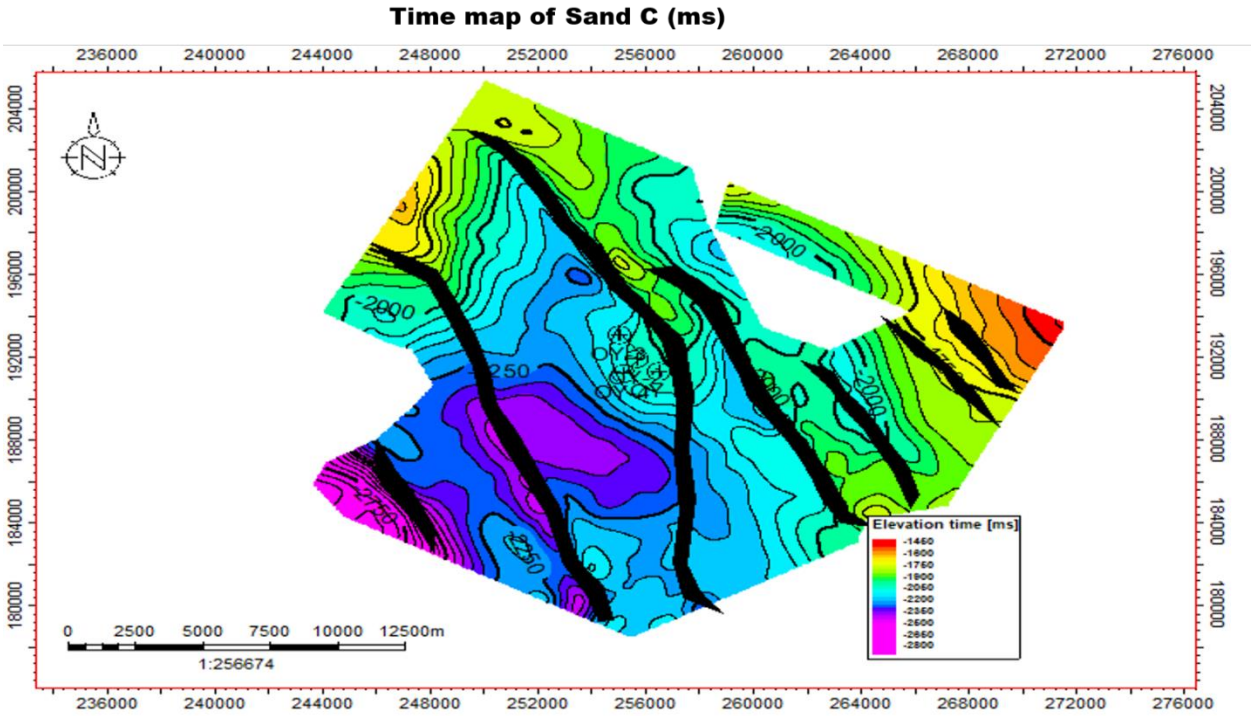

Figure 4.5(a): Time structure map for sand C.

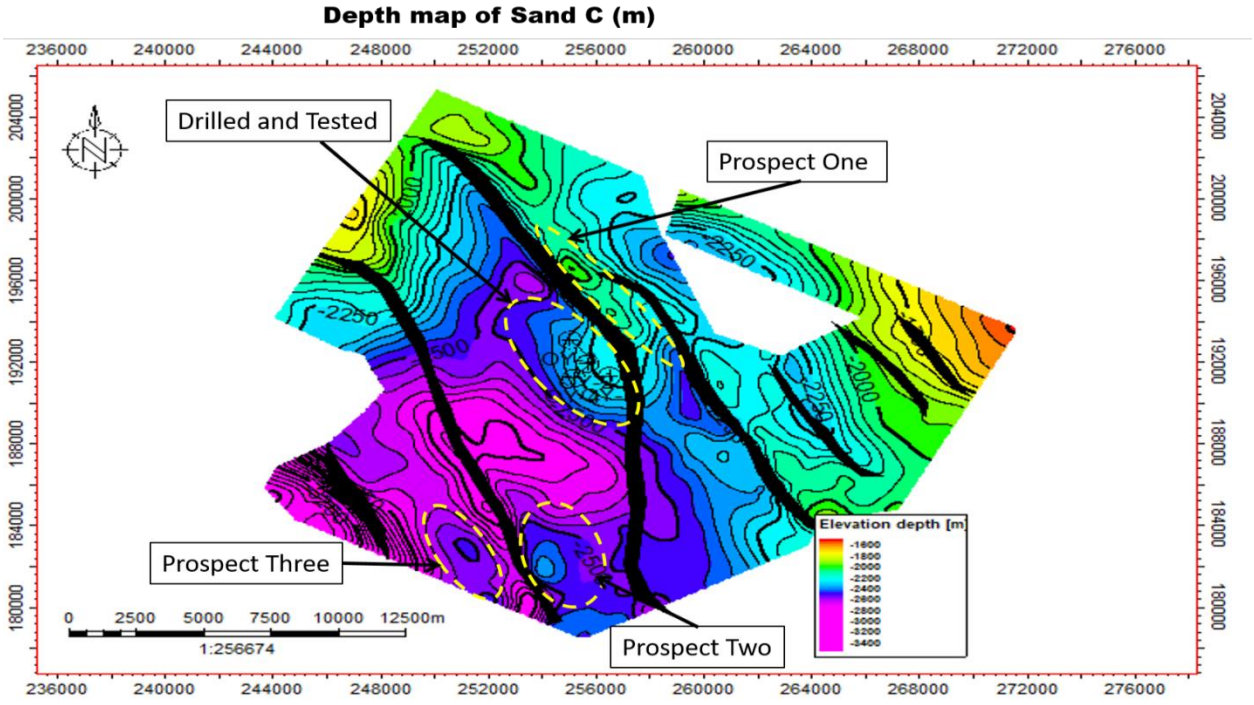

Figure 4.5(b): Depth structure map for sand C showing the showing the various prospects.

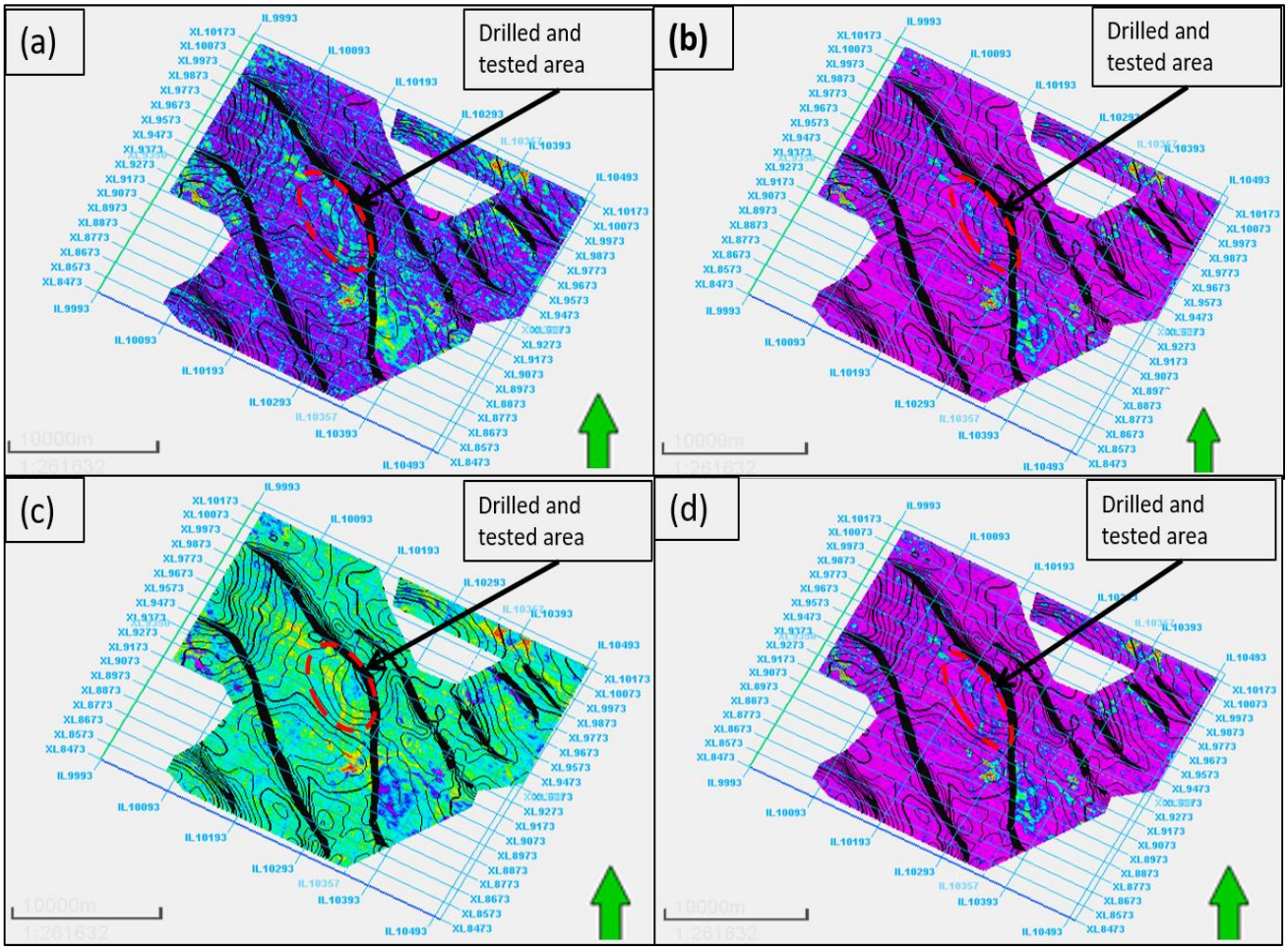

Figure 4.5(c): Seismic attributes of sand C characterized with high amplitude in the tested area. (a) RMS amplitude; (b) Sum of energies; (c) Sum of amplitudes; (d) Average energy.

4.2.4 Sand D

The structural time and depth map for sand D is shown in figure 4.6(a) and figure 4.6(b) respectively. The depth structural map shows contour intervals of 30 m. The colour legend shows differences in elevation on the map. A drilled and tested area is identified on the map alongside three prospective traps (Figure 4.6(b)). The drilled and tested area on this reservoir can be classified as a fault dependent trap. Prospects one and two are classified to be a fault assisted closure.

Meanwhile, the results of the seismic attribute analysis on sand D have shown high amplitude anomalies around the tested prospect and this has further supported the presence and possible extent of hydrocarbon within the reservoir (Fig 4.6(d)). However, it can be observed that the identified prospects have displayed significant amplitude anomalies on the seismic attribute analysis.

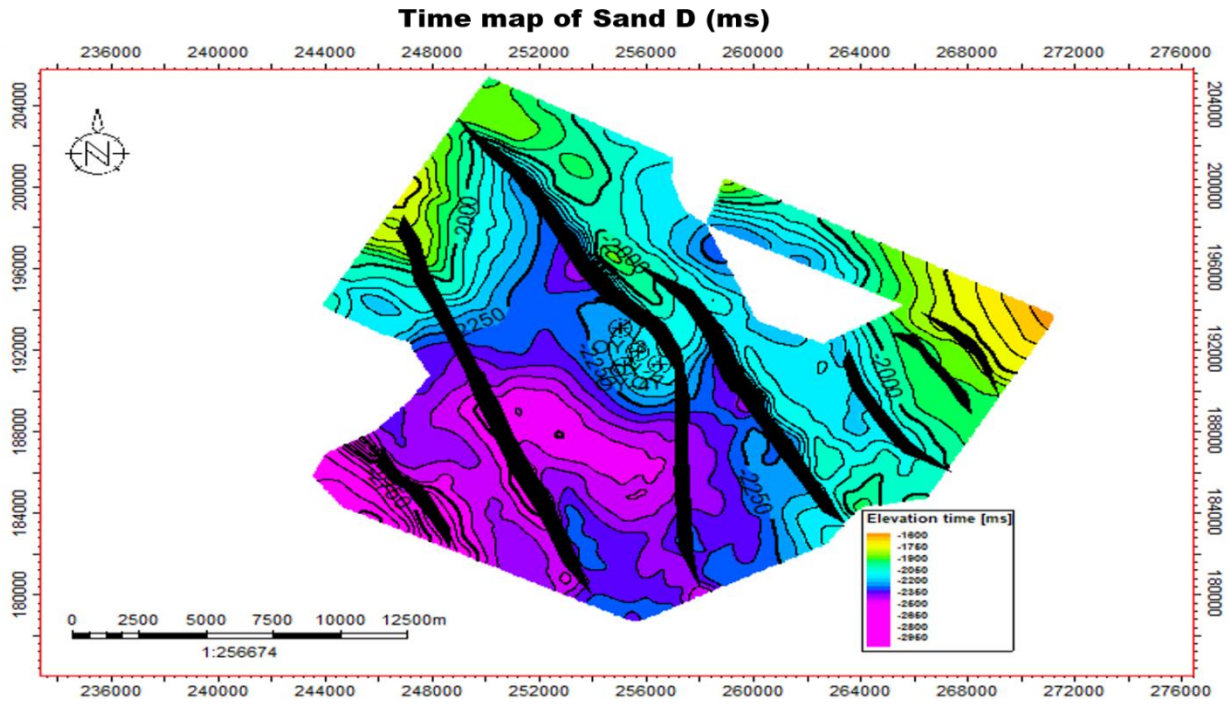

Figure 4.6(a): Time structure map for sand D.

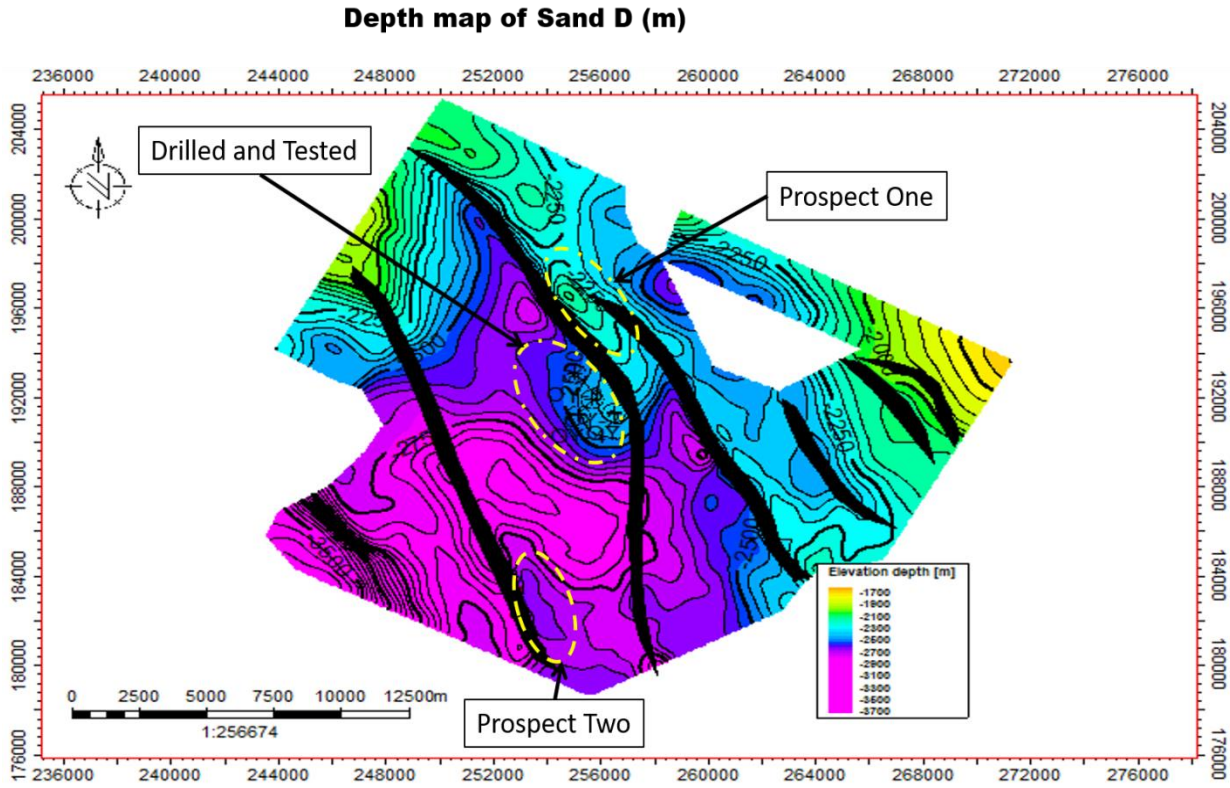

Figure 4.6(b): Depth structure map for sand D showing the showing the various prospects

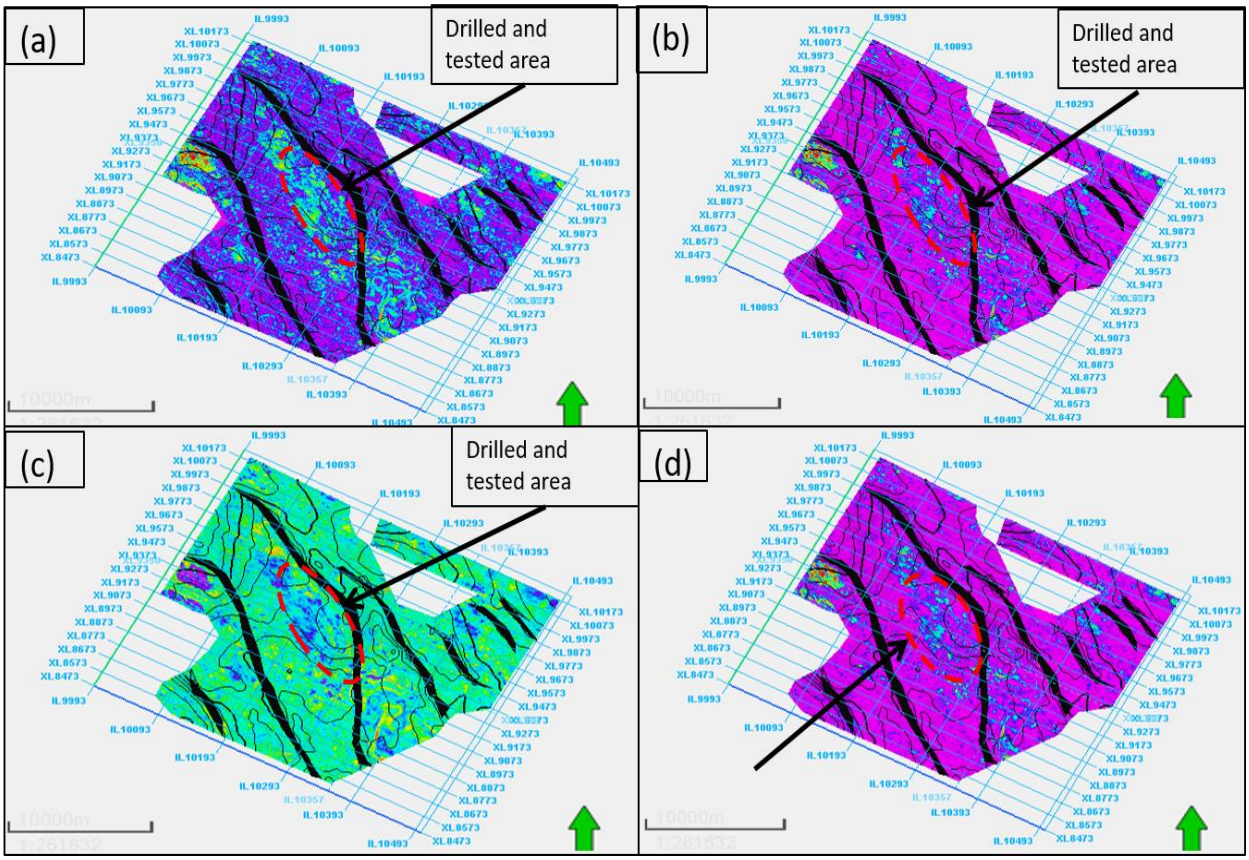

Figure 4.6(c): Seismic attributes of sand D characterized with high amplitude in the tested area. (a) RMS amplitude; (b) Sum of energies; (c) Sum of amplitudes; (d) Average energy.

4.2.5 Sand E

The results of the structural time and depth map for sand E is shown in figure 4.7(a) and figure 4.7(b) respectively. The depth structural map shows contour intervals of 30 m. The colour legend shows differences in elevation on the map. A drilled and tested area is identified on the map alongside two prospective traps (Figure 4.7(b)). The drilled and tested area on this reservoir can be classified as a fault dependent trap. Prospect one and two are classified to be a fault assisted trap.

Meanwhile, the results of the seismic attribute analysis have shown high amplitude anomalies around the tested prospect and this has further supported the presence and possible extent of hydrocarbon within the reservoir (Fig 4.7(e)). However, it can be observed that the identified prospects have displayed significant amplitude anomalies on the seismic attribute analysis.

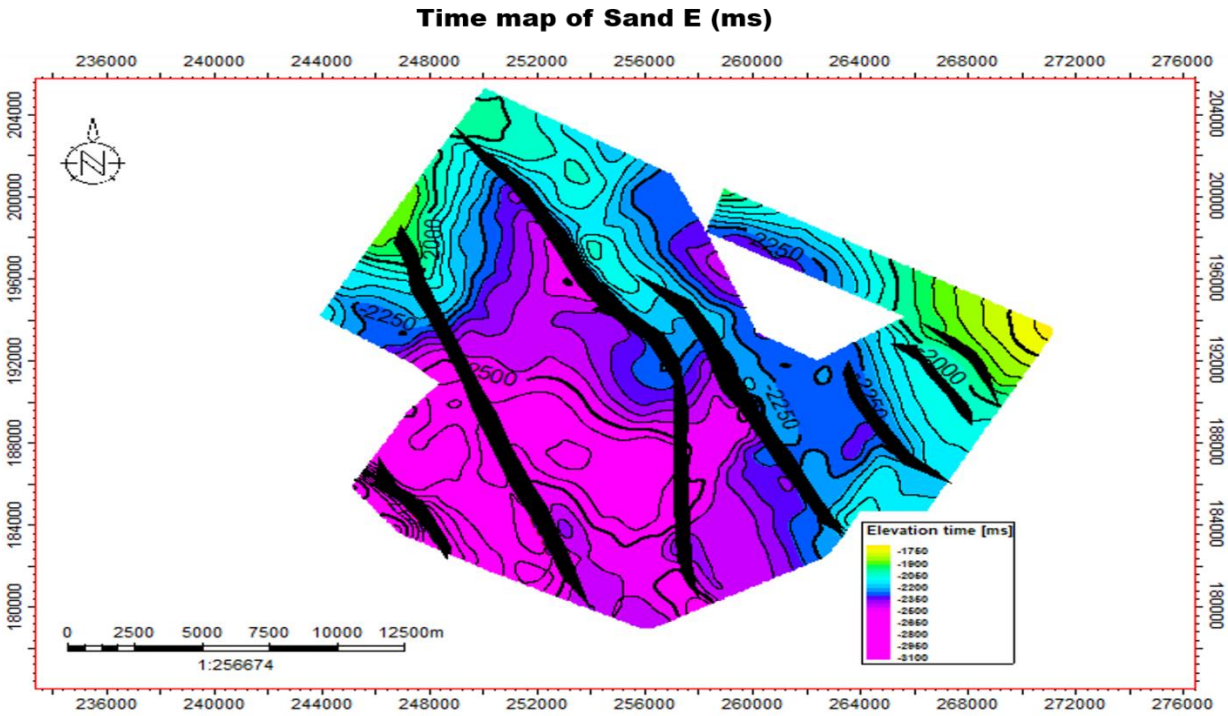

Figure 4.7(a): Time structure map for sand E.

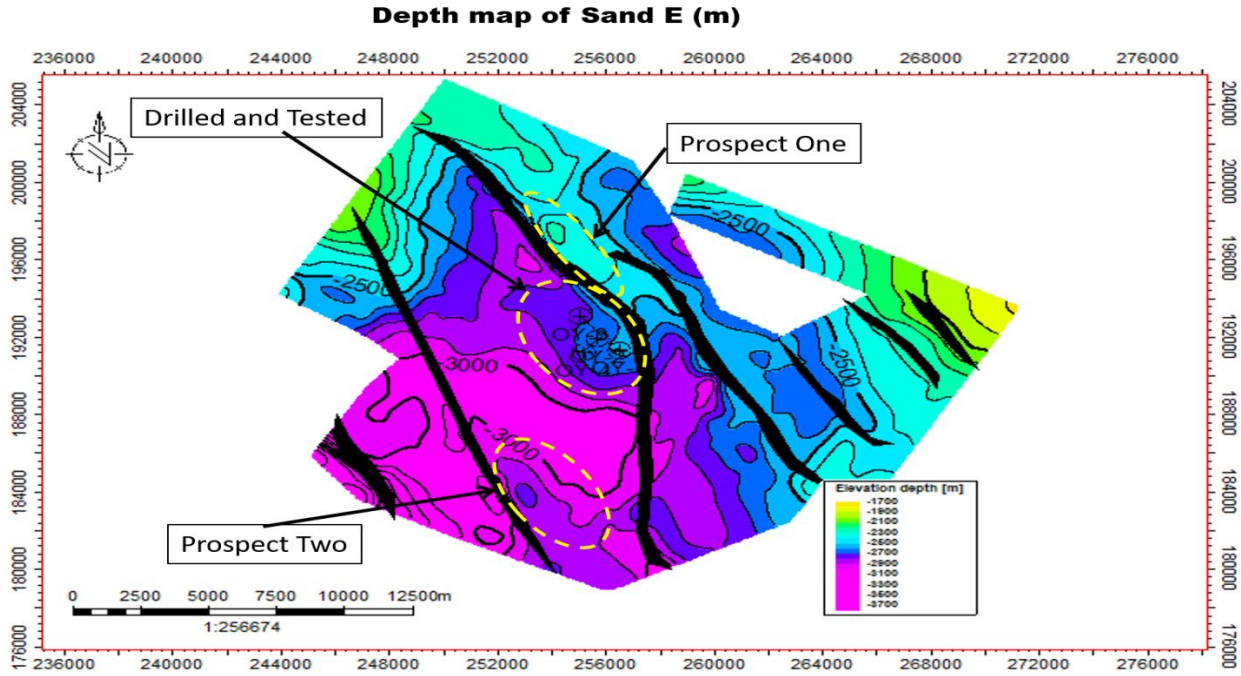

Figure 4.7(b): Depth structure map for sand E showing the showing the various prospects.

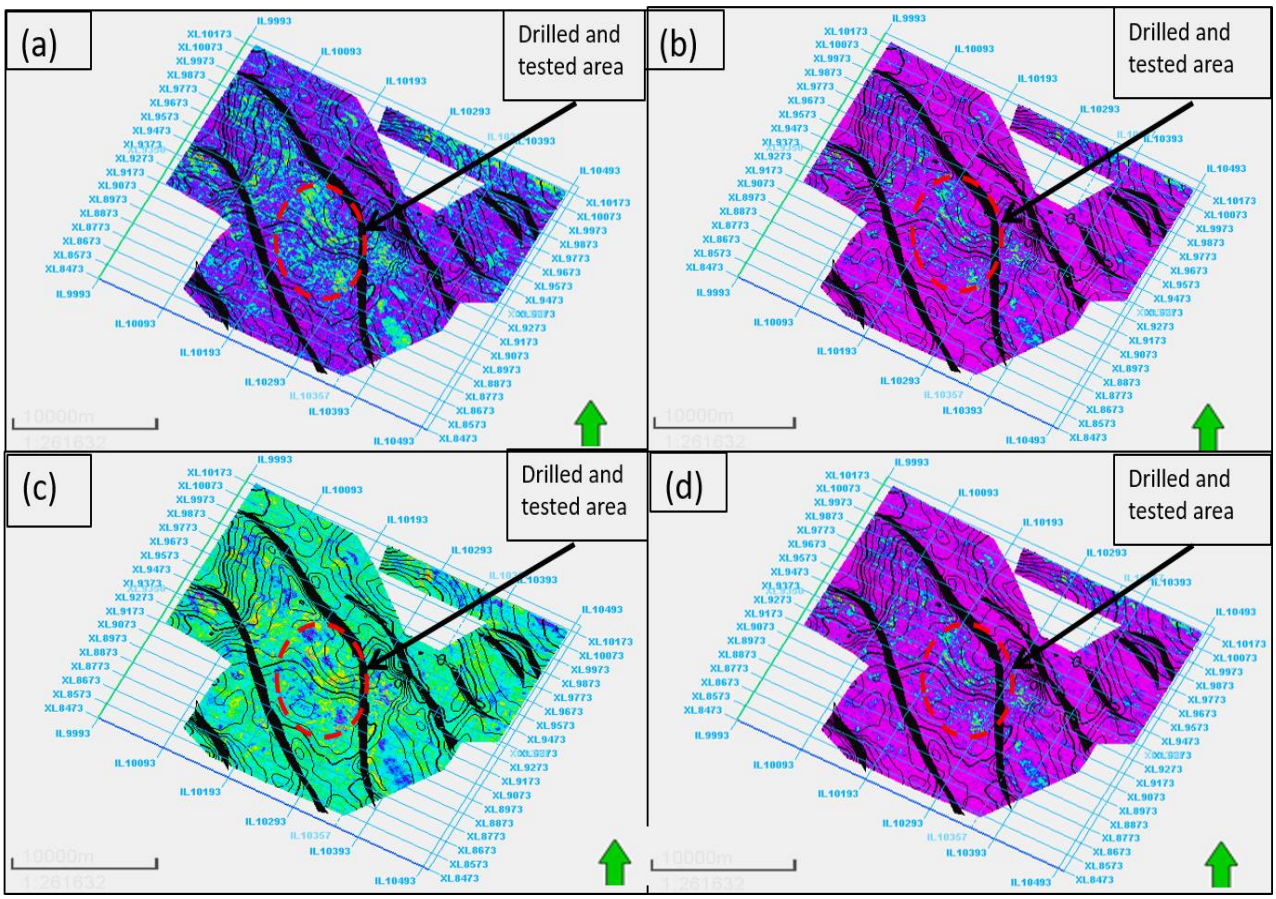

Figure 4.7(c): Seismic attributes of sand E characterized with high amplitude in the tested area. (a) RMS amplitude; (b) Sum of energies; (c) Sum of amplitudes; (d) Average energy.

4.3 Volumetric Estimations

The volumetric and area estimates of the tested area and the prospects of the reservoirs (Sand A, B, C, D and E) are calculated using the depth structural maps and the petrophysical properties of the particular reservoir.

Sand A: The volume of the hydrocarbon gas in place (GIIP) for the identified prospects ranges from 13,126,318.52 - 34,665,455.9 scf. The hydrocarbon gas in place for the tested area is 3,288,344.8 scf. The total hydrocarbon gas in place for this reservoir is 92,421,567.21 scf.

Sand B: The expected range for the volume of hydrocarbon in place for the identified prospects ranges from 5,983,702,495 - 6,292,582.9 stb. The volume of hydrocarbon in the tested area is 19,331,122.84 stb. The total hydrocarbon in place for this reservoir is 55,542,311.35 stb.

Sand C: The expected range for the volume of hydrocarbon in place for the identified prospects ranges from 59,832,013.01 - 86,401,652.75 stb. The volume of hydrocarbon in the tested area is 125,083,889.3 stb. The total hydrocarbon in place for this reservoir is 270,284,106.29 stb.

Sand D: The expected range for the volume of hydrocarbon in place for the identified prospects is 36,356,095.3 stb. The volume of hydrocarbon in the tested area is 46,127,500.59 stb. The total hydrocarbon in place for this reservoir is 85,483,595.9 stb.

Sand E: The expected range for the volume of hydrocarbon in place for the identified prospects ranges from 92,513,874.73 - 123,017,000.8 stb. The total hydrocarbon in place for this reservoir is 465,289,013.83 stb.

4.4 3D Static Reservoir Modelling

The result shows the 3D structural framework of the OY field which is presented in figure 4.8. The structural frame work shows a very good stratigraphic layering, reservoir geometry and reservoir thicknesses of the OY field. The result of the Petrophysical models of Sand A, B and D are presented in figure 4:9 - 4:14 showing the porosity, net to gross and water saturation model.

Table 4.2: Volumetric estimations of the various prospects for each map

		TESTED	PROSPECT ONE	PROSPECT TWO	PROSPECT THREE	PROSPECT FOUR	PROSPECT FIVE
Sand A	Area (m^2)	8,075,350	8,513,252	3,539,753	3,223,603	3,073,256	3,539,753
	GIIP (scf)	3,288,344	34,665,455	14,413,664	13,126,318	12,514,118	14,413,664
Sand B	Area (m^2)	7,143,080	3,049,147	2,211,049	-	2,325,184	5,795,083
	STOIIP (stb)	19,331,122	8,251,825	5,983,702	-	6,292,582	15,683,077
Sand C	Area (m^2)	10,718,178	5,126,880	-	-	5,038,321	7,403,577
	STOIIP (stb)	125,083,889	59,832,013	-	-	58,798,504	86,401,652
Sand D	Area (m^2)	5,167,922	4,073,177	-	-	4,073,177	-
	STOIIP (stb)	46,127,500	36,356,095	-	-	36,356,095	-
Sand E	Area (m^2)	11,009,785	5,422,809	-	-	4,078,176	-
	STOIIP (stb)	249,758,138	123,017,000	-	-	92,513,874	-

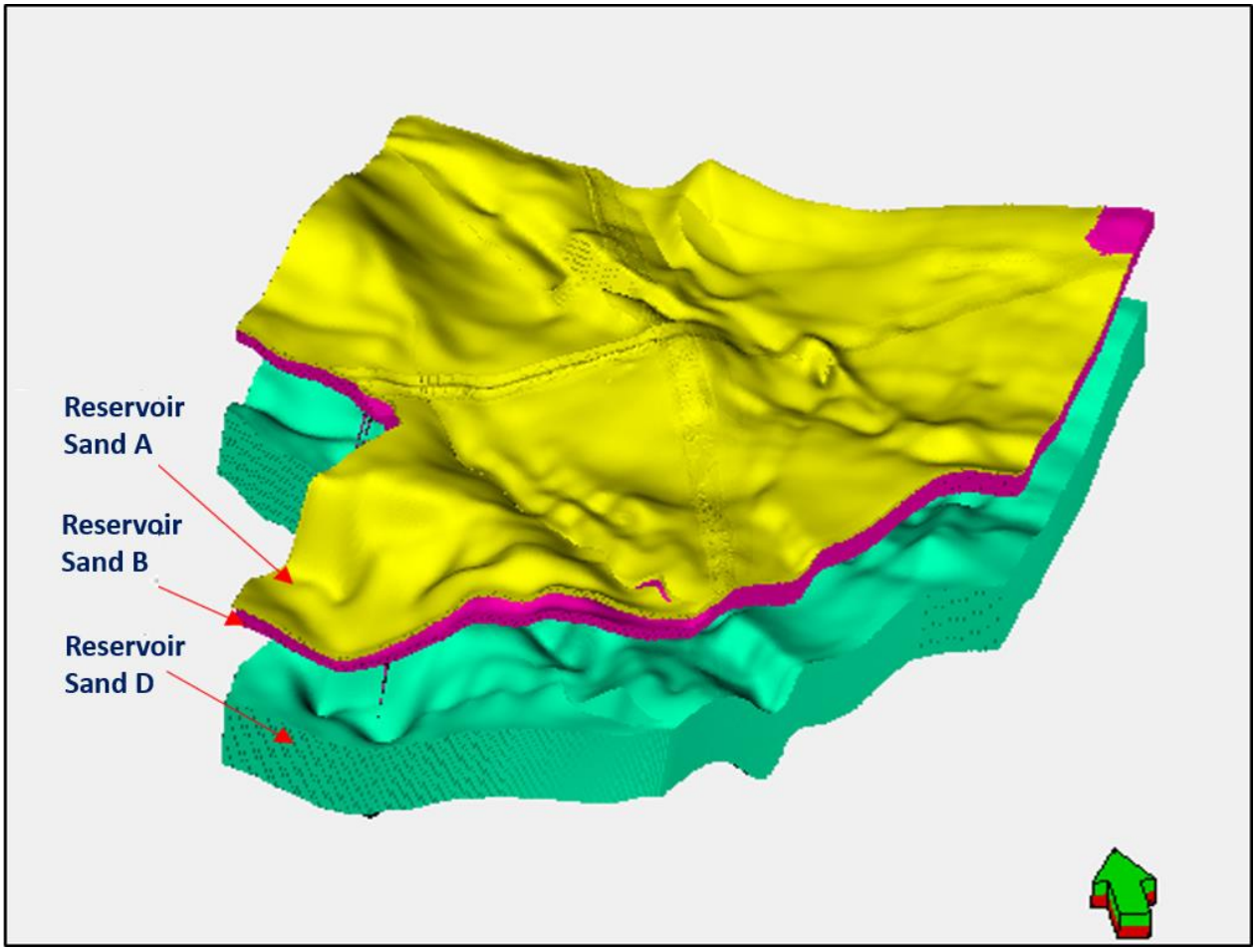

Figure 4.8: 3D structural frame work of OY field.

4.4.1 3D Porosity Model

Figure 4:9 and Figure 4:10 shows the results of the 3D models of the porosity distribution. The model shows the prominence of good porosity distribution which indicates that the pore spaces have enough space to accommodate fluid. The tested area shows a high porosity.

Sand A model shows the porosity distribution (Figure 4:9). Sand A porosity varies from 0.5 to 0.43. Sand A reservoir is porous.

Sand B model shows the porosity distribution (Figure 4:9). Sand B as a porosity range of 0.4-0.52. The southern part of the model shows very high porous region.

Sand C model shows the porosity distribution (Figure 4:9). Sand C model shows a porosity range of 0.3 – 0.5.

4.4.2 3D Net to Gross (NTG) Model

Figure 4:11 and Figure 4:12 shows the result of the net to gross model which reveals good net to gross values within the well area.

Sand A model shows the NTG distribution (Figure 4:11). Sand A net to gross varies from 0.5 to 0.8.

Sand B model shows the NTG distribution (Figure 4:11). Sand B net to gross values varies from 0.4 - 0.52.

Sand D model shows the NTG distribution (Figure 4:11). Sand D net to gross values varies from 0.5 -1.0.

4.4.3 3D Water Saturation Model

Figure 4:13 and Figure 4:14 show the result of the 3D perspective view of the water saturation distribution. The model shows the hydrocarbon zone region. The tested areas have high hydrocarbon saturation.

Sand A model shows the water saturation distribution (Figure 4:13). Sand A shows abundant hydrocarbon saturation than water saturation. The water saturation varies from 0.1 to 0.4. Sand A has abundance of hydrocarbon saturation.

Sand B model shows the water saturation distribution (Figure 4:13). Sand B model shows abundant water than hydrocarbon with the water saturation varying from 0.3 to 0.5. The hydrocarbon saturation is more abundant in the northern part and some parts in the south-west direction

Sand C model shows the water saturation distribution (Figure 4:13). Sand C model shows abundant hydrocarbon than water. The water saturation varies from 0.1 to 0.4.

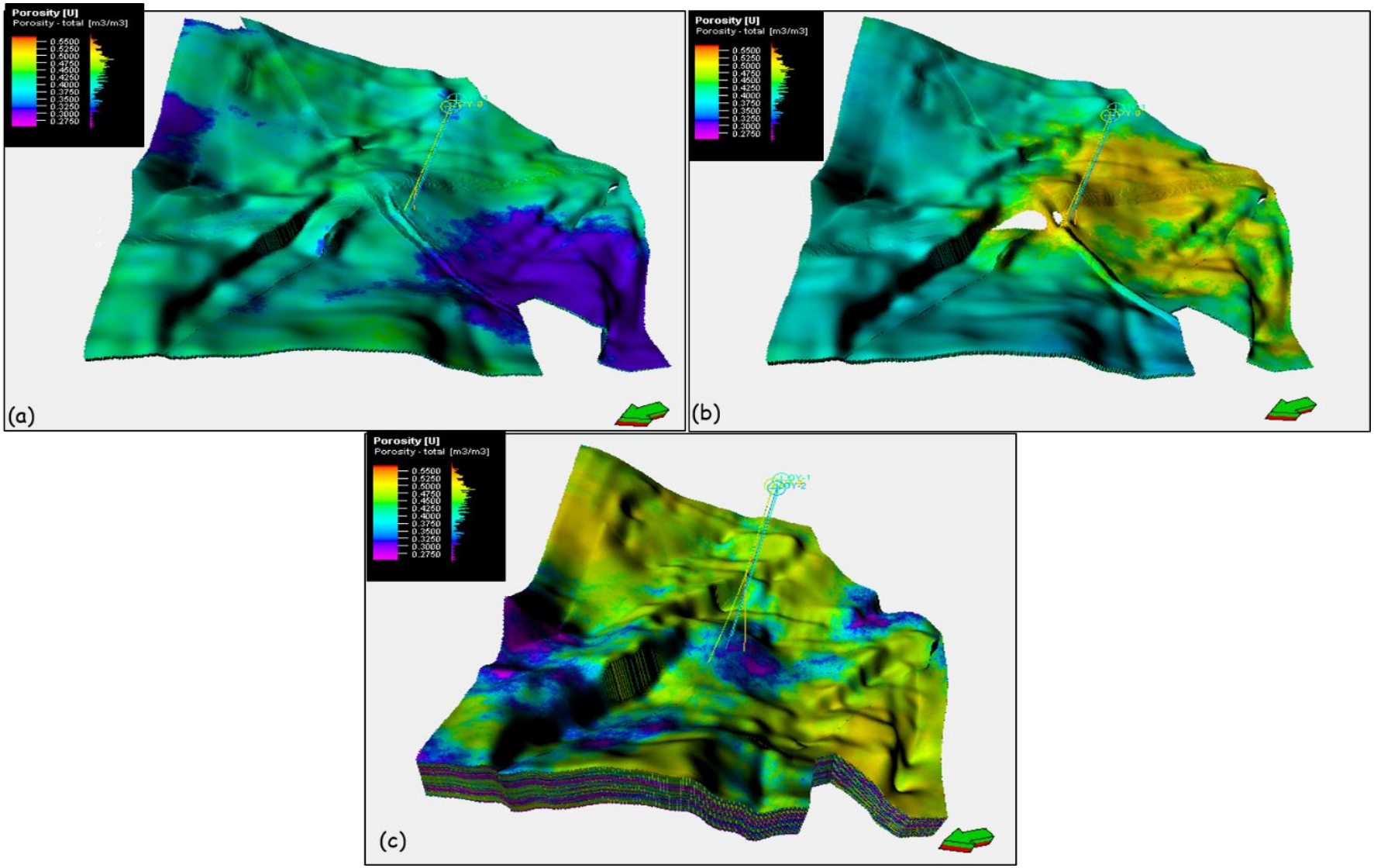

Figure 4.9: 3D porosity model showing the reservoirs (a) Sand A (b) Sand B (c) Sand D**.**

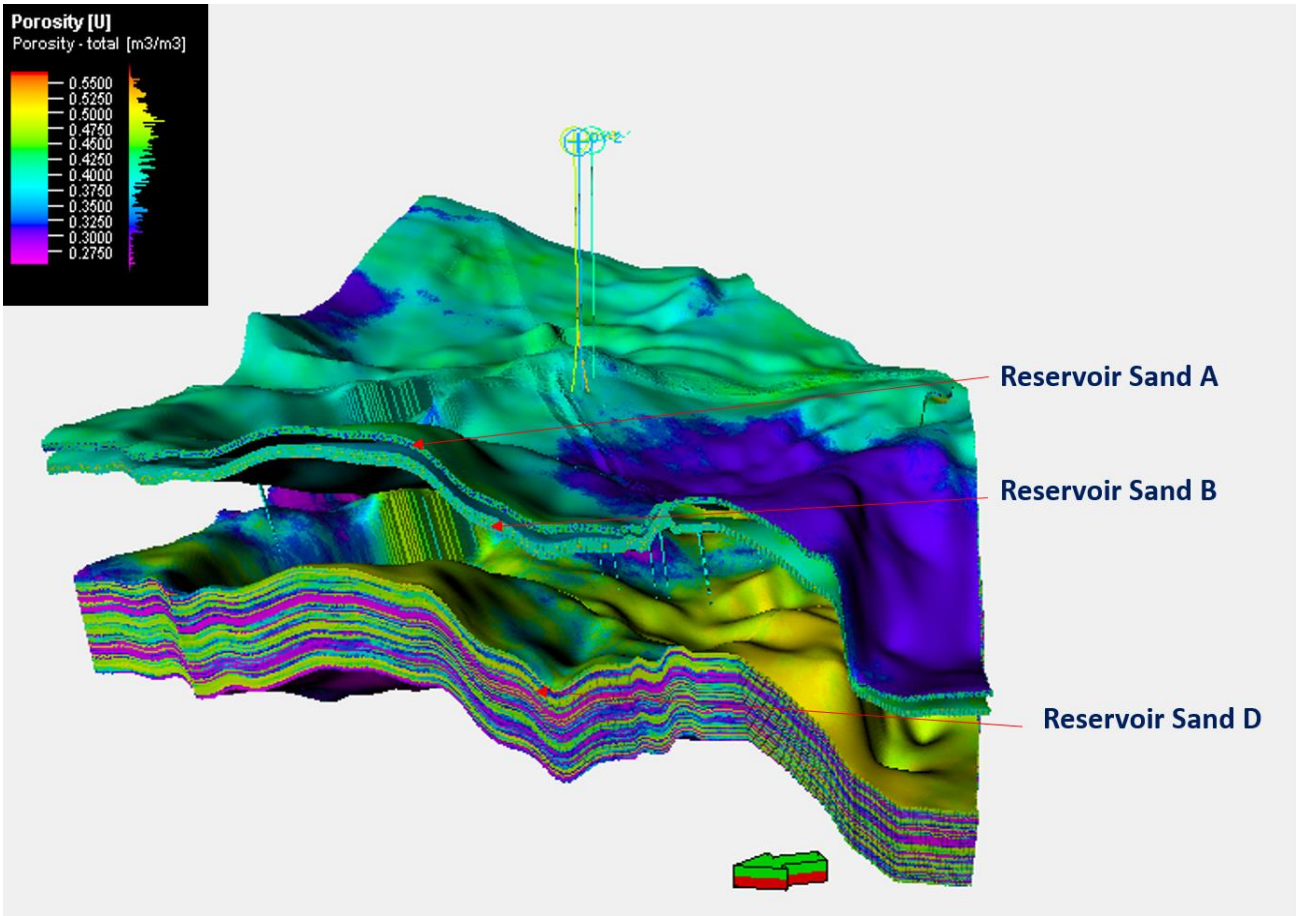

Figure 4.10: 3D Window showing the porosity model for the reservoirs Sand A, B and D.

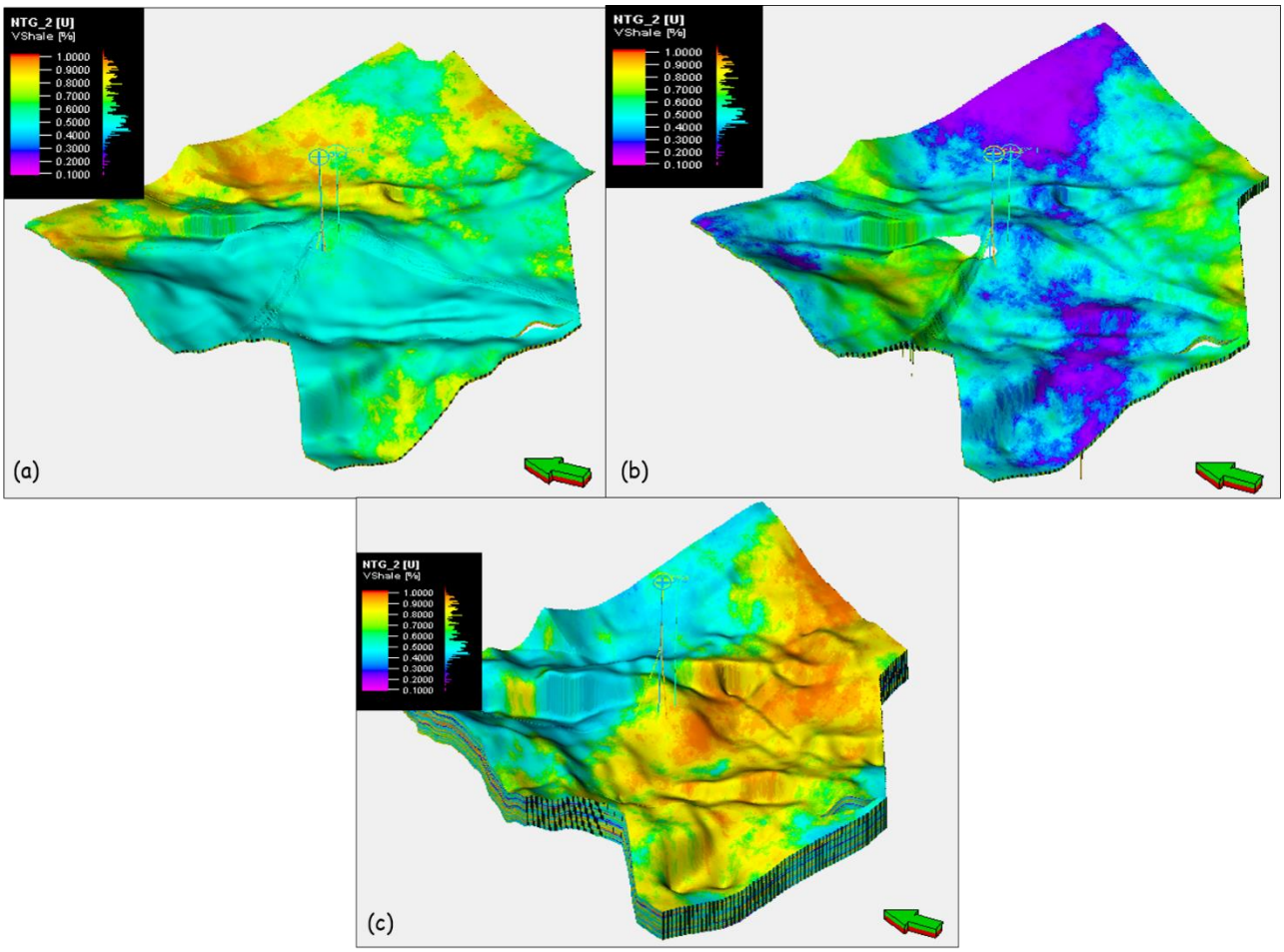

Figure 4.11: 3D Net to gross model showing the reservoirs (a) Sand A (b) Sand B (c) Sand D

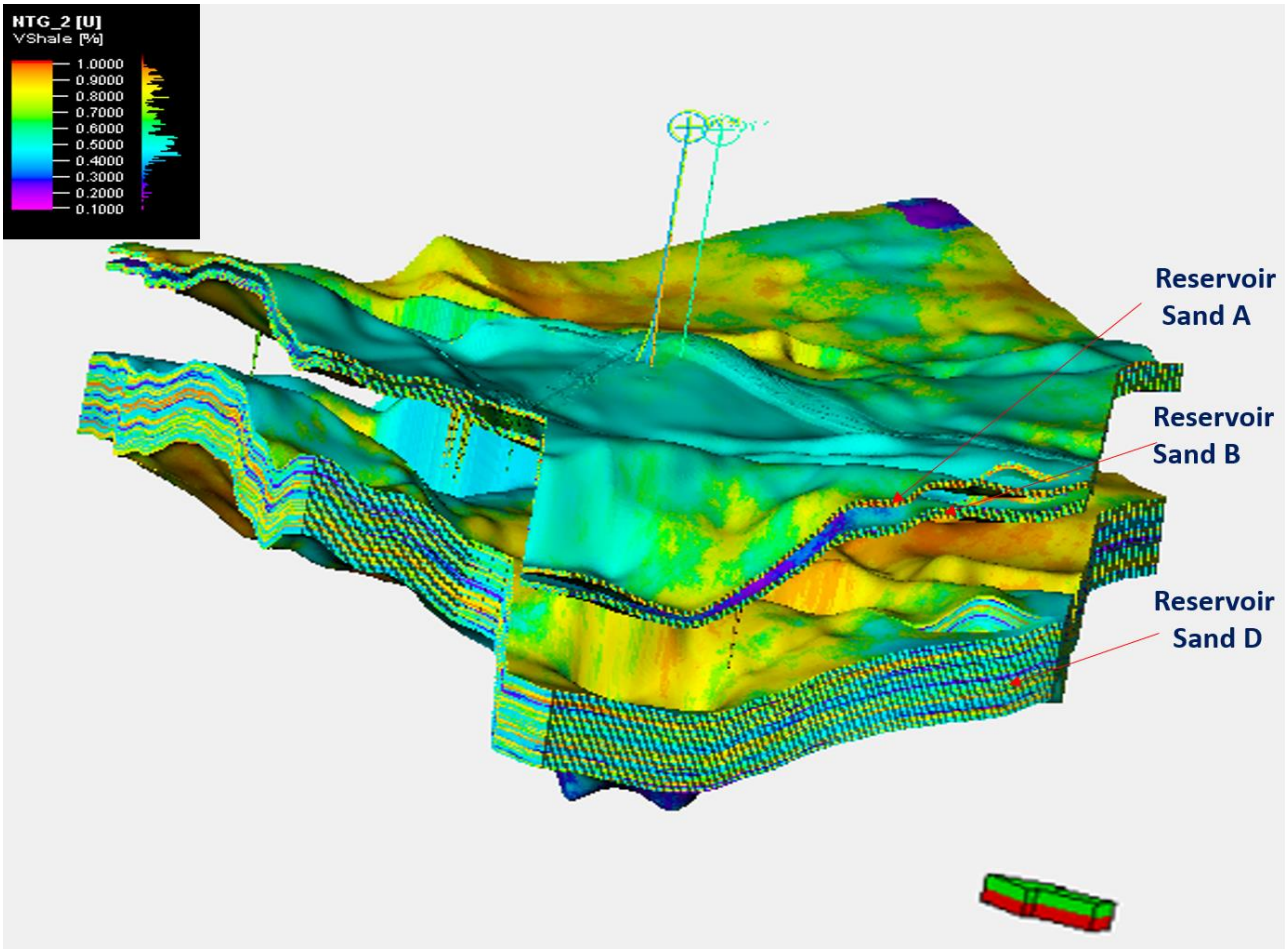

Figure 4.12: 3D Window showing the Net to gross model for the reservoirs Sand A, B and D.

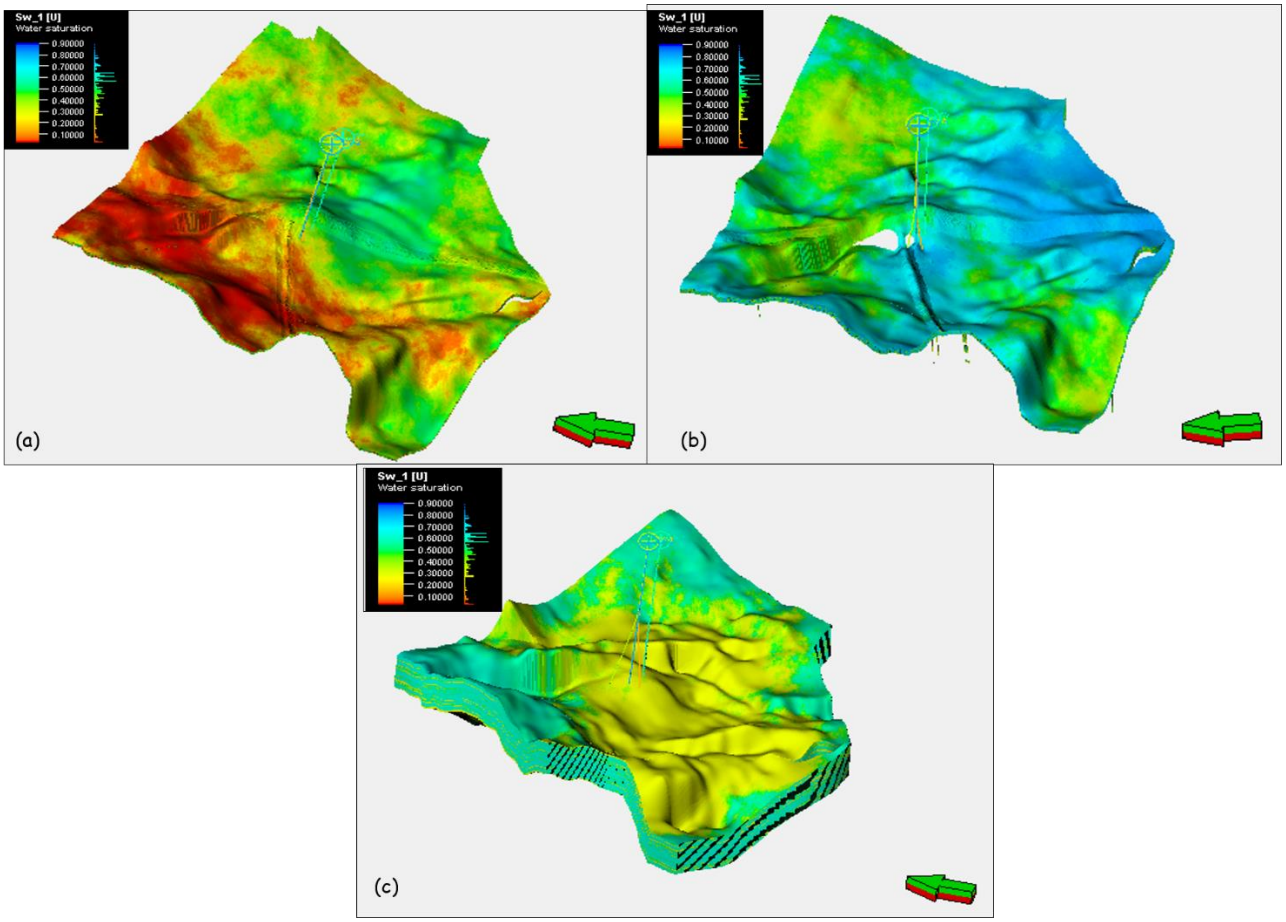

Figure 4.13: 3D water saturation model showing the reservoirs (a) Sand A (b) Sand B (c) Sand D.

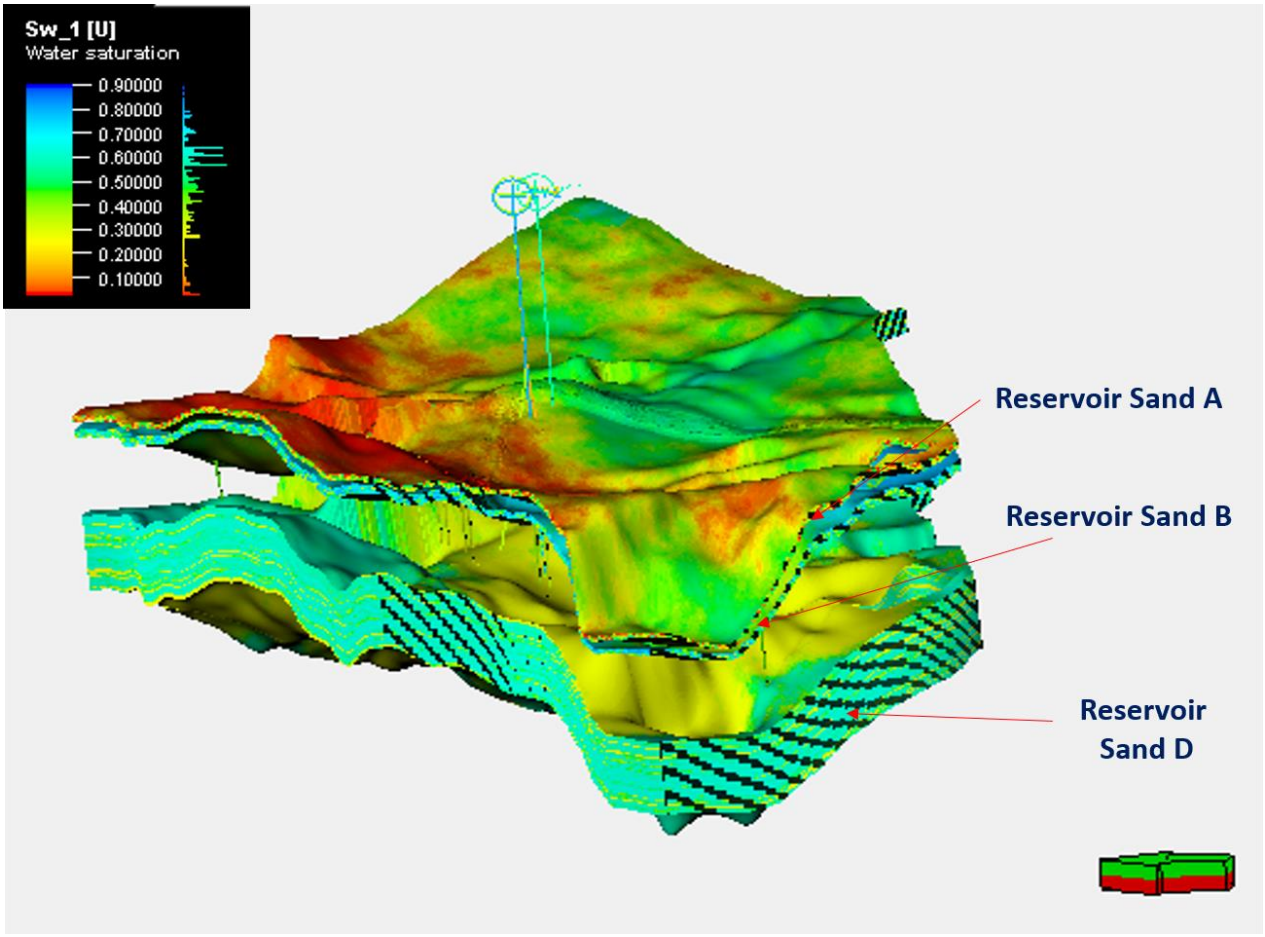

Figure 4.14: 3D Window showing the water saturation model for the reservoirs Sand A, B and D.

CHAPTER FIVE

CONCLUSION AND RECOMMENDATION

5.1 Conclusion

3D migrated seismic and well log data of OY Field, Offshore, Niger Delta has been integrated for Seismic reservoir characterization and 3D Modelling in order to evaluate the petrophysical properties and its distribution across the 3D reservoir.

From the well correlation five hydrocarbon bearing reservoirs (Sand A, Sand B, Sand C, Sand D and Sand E) were delineated. The reservoirs gross thickness ranges from between 15.94 and 213.9 m. The neutron-density log overlay was used in determining the hydrocarbon type and it can be observed that Sand A is mainly gas and Sand B, C, D and E are mainly oil. The petrophysical analysis have shown that the net to gross of OY field ranges from 0.57 to 0.82 and the porosity ranges from to 0.27 to 0.38 which depicts good to very good reservoir properties. The estimated water saturation ranges from 0.2 to 0.7.

From the basic input logs of sonic and density logs, the synthetic seismogram for the reference well (OY-02) was generated and had a relatively precise correlation of peak to peak and trough to trough on the 3D seismic. The reservoir tops of Sand Top A, B, C, D and E falls on the trough. It can be concluded that the well to seismic have a good tie and the event corresponding to the reservoir tops are mappable across the 3D seismic cube.

For this study all mapped faults are normal faults. Two major growth faults were identified and other faults are either synthetic or antithetic to these major faults on the OY field, shallow offshore Niger Delta. Five selected horizons corresponding to the reservoir tops were mapped out across the 3D seismic cube namely; Sand A, Sand B, Sand C, Sand D and Sand E. The depth structural maps generated from the time structural map using the velocity models have structural highs. The mapped horizons and faults configuration form fault traps for the accumulation of hydrocarbon in the field. From the structural maps, it was observed that the hydrocarbon accumulations are associated with anticlines, fault assisted closures and fault dependent closures. The seismic attributes such as RMS, average energy, sum of energy, sum of amplitude were extracted from the time map and have enhanced data interpretation. High anomalies were

observed around regions with the drilled trap and have shown possible extent of the hydrocarbon accumulation.

Volumetric estimations were calculated for all the reservoirs. The total hydrocarbon gas in place for Sand A is 92,421,567.21 scf. The total hydrocarbon in place for Sand B is 55,542,311.35 stb. The total hydrocarbon in place for this Sand C is 270,284,106.29 stb. The total hydrocarbon in place for Sand D is 85,483,595.9 stb. The total hydrocarbon in place Sand E is 465,289,013.83 stb. Sand E have the largest hydrocarbon zone while Sand B have the smallest hydrocarbon zone.

The 3D static modelling of the OY field has given insight to the spatial distribution of the petrophysical properties (porosity, water saturation and Net to gross) in the investigated field. A 3D structural framework was generated which have shown the reservoir thicknesses variation and also the faults compartments. The 3D modelling has helped in populating petrophysical properties into the 3D structural framework and has shown a layer-cake model and it shows the reservoir heterogeneity. 3D reservoir models of the porosity, Net to Gross and water saturation was generated and has shown the 3D distribution of the petrophysical properties. Generally, the model shows the prominence of good porosity distribution with porosity varying from 0.3 - 0.5. The net to gross model reveals good net to gross within the well area varying from 0.5 - 1.0. The 3D water saturation model shows the hydrocarbon zone region with water saturation value varying from 0.1 - 0.5. The 3D static models can be used for informed field development plan (FDP), well planning, production and Enhanced Recovery towards the depletion of the hydrocarbon accumulation.

5.2 Recommendations

It is recommended that the identified prospects should be drilled and tested for possible hydrocarbon accumulation. The 3D static model can be used as an input by reservoir and petroleum engineers for dynamic flow simulations and projected production behaviours of the reservoir under different conditions.

REFERENCES

Abdullah, E. A., Abdelmaksoud, A., & Hassan, M. A. (2022). Application of 3D Static Modelling in Reservoir Characterization: A Case Study from the Qishn Formation in Sharyoof Oil Field, Masila Basin, Yemen. *Acta Geologica Sinica-English Edition*, *96*(1), 348-368.

Adagunodo, T. A., Bayowa, O. G., Alatise, O. E., Oshonaiye, A. O., Adewoyin, O. O., & Opadele, V. O. (2022). Characterization of reservoirs and depositional study of JP Field, shallow offshore of Niger Delta Basin, Nigeria. *Scientific African*, *15*, e01064.

Allen, J. R. L. (1965). Late Quaternary Niger Delta and Adjacent areas: sedimentary environment and lithofacies. *American Association of Petroleum Geologists*, Vol. 49, 549-600.

Ashcroft, W. (2011). *A petroleum geologist's guide to seismic reflection*. John Wiley & Sons.

Beka, F. T., & Oti, M. N. (1995). The distal offshore Niger Delta: frontier prospects of a mature petroleum province. In *Geology of deltas* (pp. 237-241).

Burke, K. C., Dessauvagie, T. F. J., & Whiteman, A. J. (1972). Geological history of the Benue valley and adjacent areas. *African geology*, *1*(8), 7-2.

Daukoru, J. W. (1975). PD 4 (1) petroleum geology of the Niger Delta. In *9th World Petroleum Congress*. OnePetro.

Doust, H., Omatsola, E., Edwards, J. D., & Santogrossi, P. A. (1990). Divergent/passive margin basins. *AAPG memoir*, *48*, 239-248.

Dresser Atlas, (1979). Log Interpretation Charts. Dresser Industries, Houston, TX. 107 pp.

Ebong, E. D., Akpan, A. E., Emeka, C. N., & Urang, J. G. (2017). Groundwater quality assessment using geoelectrical and geochemical approaches: case study of Abi area, southeastern Nigeria. *Applied Water Science*, *7*(5), 2463-2478.

Edigbue, P. I., Komolafe, A. A., Adesida, A. A., & Itamuko, O. J. (2014). Hydrocarbon reservoir characterization of "Keke" field, Niger Delta using 3D seismic and petrophysical data. *Standard Global Journal of Geology and Explorational Research*, *2*(1), 043-052.

Edwards, J. D., & Santogrossi, P. A. (Eds.). (1990). *Divergent/passive margin basins* (pp. 201-238). Tulsa, Oklahoma, USA: American Association of Petroleum Geologists.

Ejedawe, J. E. (1981). Patterns of incidence of oil reserves in Niger Delta Basin. *AAPG Bulletin*, *65*(9), 1574-1585.

Ejedawe, J. E., Coker, S. J. L., Lambert-Aikhionbare, D. O., Alofe, K. B., & Adoh, F. O. (1984). Evolution of oil-generative window and oil and gas occurrence in Tertiary Niger Delta Basin. *AAPG bulletin*, *68*(11), 1744-1751.

Evamy, B. D., Haremboure, J., Kamerling, P., Knaap, W. A., Molloy, F. A., & Rowlands, P. H. (1978). Hydrocarbon habitat of Tertiary Niger delta. *AAPG bulletin*, *62*(1), 1-39.

Haack, R. C., Sundararaman, P., & Dahl, J. (1997). Niger Delta petroleum system. In *Extended abstracts, AAPG/ABGP Hedberg research symposium, petroleum systems of the South Atlantic margin* (Vol. 1619).

Hilchie, D. W. (1978). *Applied Openhole Log Interpretation for Geologists and Engineers: Charts*. DW Hilchie.

Hossain, M., Sohel, I., Woobaidullah, A. S. M., & Rahman, M. (2021). Reservoir characterization and identification of new prospect in Srikail gas field using wireline and seismic data. *Journal of Petroleum Exploration and Production Technology*, *11*(6), 2481-2495.

Hunt, J. M. (1990). Generation and migration of petroleum from abnormally pressured fluid compartments. *AAPG bulletin*, *74*(1), 1-12.

Kobesh, F. P., & Blizard, R. B. (1959). Geometrical factors in sonic logging. *Geophysics*, *24*(1), 64-76.

Kulke, H., 1995, Nigeria, in, Kulke, H., ed., Regional Petroleum Geology of the World. Part II: Africa, America, Australia and Antarctica: Berlin, Gebrüder Borntraeger, p. 143-172.

Lehner, P., & De Ruiter, P. A. C. (1977). Structural history of Atlantic margin of Africa. *AAPG Bulletin*, *61*(7), 961-981.

Nwachukwu, J. I., and Chukwurah, P. I., (1986), Organic matter of Agbada Formation, Niger Delta, Nigeria: American Association of Petroleum Geologists Bulletin, v. 70, p. 48-55.

Nwajide, C. S. (2013). *Geology of Nigeria's sedimentary basins*. CSS Bookshop Limited.

Odai, L. A. (2010). *Building and Ranking of Geostatistical Petroleum Reservoir Models* (Doctoral dissertation).

Okpogo, E. U., Abbey, C. P., & Atueyi, I. O. (2018). Reservoir characterization and volumetric estimation of Orok Field, Niger Delta hydrocarbon province. Egyptian journal of petroleum, 27(4), 1087-1094.

Osinowo, O. O., Ayorinde, J. O., Nwankwo, C. P., Ekeng, O. M., & Taiwo, O. B. (2018). Reservoir description and characterization of Eni field Offshore Niger Delta, southern Nigeria. *Journal of Petroleum Exploration and Production Technology*, *8*(2), 381-397.

Reijers, T. J. A. (1996). Selected Chapters on Geology: with notes on Sedimentary Geology, Sequence Stratigraphy and three case studies and a field guide. *SPDC Corporate Reprographic Services, Warri, Nigeria*, *197*.

Schlumberger (1972). Log Interpretation: Volume 1—Principles. Schlumberger Well Services, Houston.

Shannon, P. M., & Naylor, D. (1989). Petroleum basin studies.

Shofiqul, I. M., & Nusrat, J. L. (2013). Reservoir characterization of Habiganj gas field. *International Journal of Oil, Gas and Coal Engineering*, *1*(1), 7-15.

Short, K. C., & Stable, A. J. (1967). Outline of geology of Niger Delta. *AAPG bulletin*, *51*(5), 761-779.

Stacher, P. (1995). Present understanding of the Niger Delta hydrocarbon habitat. In *Geology of deltas* (pp. 257-267).

Tittman, J., & Wahl, J. S. (1965). The physical foundations of formation density logging (gamma-gamma). *Geophysics*, *30*(2), 284-294.

Varhaug, M. (2016). Basic Well Log Interpretation: *Oilfield Review.*

Weber, K. J., 1987, Hydrocarbon distribution patterns in Nigerian growth fault structures controlled by structural style and stratigraphy: Journal of Petroleum Science and Engineering, v. 1, p. 91-104.

Wikipedia, (2022). Niger Delta. https://en.wikipedia.org/wiki/Niger_Delta. Retrieved on 6th August, 2022.

Wyllie, M. R. J., Gregory, A. R., & Gardner, G. H. F. (1958). An experimental investigation of factors affecting elastic wave velocities in porous media. *Geophysics*, *23*(3), 459-493.

Xiao, H., & Suppe, J. (1992). Origin of rollover (1). *AAPG bulletin*, *76*(4), 509-529.